

UNDERSTANDING AND FINE TUNING MOLECULAR RECOGNITION

by

KANISHKA NAVODH EPA

B.S., University of Peradeniya, 2006

AN ABSTRACT OF A DISSERTATION

submitted in partial fulfillment of the requirements for the degree

DOCTOR OF PHILOSOPHY

Department of Chemistry  
College of Arts and Sciences

KANSAS STATE UNIVERSITY  
Manhattan, Kansas

2013

## Abstract

Co-crystallization allows the manipulation of physical properties of a given compound without affecting its chemical behavior. The ability to predict hydrogen bonding interactions, provides means to the rational design of supramolecular architectures. It also makes it possible to select with a degree of accuracy, a few co-formers that have a high probability of forming co-crystals with a compound of interest, instead of blindly screening against a large number of candidates.

To study the effects of changing electronic environment on the ability to form co-crystals, five symmetric dioximes of different hydrogen bond donating ability were synthesized with different functional groups on the carbon  $\alpha$  to the oxime moiety. It was shown that the supramolecular yield increase with the positive MEP value on the donor site.

In order to further explore this relationship between calculated MEP values and supramolecular selectivity three asymmetric ditopic donors containing phenol carboxylic acid and aldoxime groups were screened against a series of asymmetric ditopic acceptors. Nine crystal structures show that the supramolecular outcome can be predicted according to Etter's rules by ranking donors and acceptors according to calculated MEP values.

To explore the possibility of using the same approach with other hydrogen bond donors, three asymmetric ditopic donor ligands containing cyanooxime groups were synthesized and screened against a series of asymmetric ditopic acceptors. Nine out of ten times the supramolecular outcome could be predicted by MEP calculations

1-deazapurine exists in two tautomeric forms (1H and 3H) in aqueous solution, which have very different hydrogen bonding environments. The 3H tautomer forms a self-complementary dimer involving a donor and an acceptor site leaving a second acceptor site vacant. In order to stabilize this tautomer the molecule was screened against a of series hydrogen and halogen bond donors. Four out of five structures obtained showed 3H tautomer. The 1H tautomer is the geometric complement of urea. Therefore the molecule was screened against a series of N,N-diphenylureas and all five structures showed the 1H tautomer.

UNDERSTANDING AND FINE TUNING MOLECULAR RECOGNITION

by

KANISHKA NAVODH EPA

B.S., University of Peradeniya, 2006

A DISSERTATION

submitted in partial fulfillment of the requirements for the degree

DOCTOR OF PHILOSOPHY

Department of Chemistry  
College of Arts and Sciences

KANSAS STATE UNIVERSITY  
Manhattan, Kansas

2013

Approved by:

Major Professor  
Christer B. Aakeröy

# **Copyright**

KANISHKA NAVODH EPA

2013

## Abstract

Co-crystallization allows the manipulation of physical properties of a given compound without affecting its chemical behavior. The ability to predict hydrogen bonding interactions, provides means to the rational design of supramolecular architectures. It also makes it possible to select with a degree of accuracy, a few co-formers that have a high probability of forming co-crystals with a compound of interest, instead of blindly screening against a large number of candidates.

To study the effects of changing electronic environment on the ability to form co-crystals, five symmetric dioximes of different hydrogen bond donating ability were synthesized with different functional groups on the carbon  $\alpha$  to the oxime moiety. It was shown that the supramolecular yield increase with the positive MEP value on the donor site.

In order to further explore this relationship between calculated MEP values and supramolecular selectivity three asymmetric ditopic donors containing phenol carboxylic acid and aldoxime groups were screened against a series of asymmetric ditopic acceptors. Nine crystal structures show that the supramolecular outcome can be predicted according to Etter's rules by ranking donors and acceptors according to calculated MEP values.

To explore the possibility of using the same approach with other hydrogen bond donors, three asymmetric ditopic donor ligands containing cyanooxime groups were synthesized and screened against a series of asymmetric ditopic acceptors. Nine out of ten times the supramolecular outcome could be predicted by MEP calculations

1-deazapurine exists in two tautomeric forms (1H and 3H) in aqueous solution, which have very different hydrogen bonding environments. The 3H tautomer forms a self-complementary dimer involving a donor and an acceptor site leaving a second acceptor site vacant. In order to stabilize this tautomer the molecule was screened against a of series hydrogen and halogen bond donors. Four out of five structures obtained showed 3H tautomer. The 1H tautomer is the geometric complement of urea. Therefore the molecule was screened against a series of N,N-diphenylureas and all five structures showed the 1H tautomer.

# Table of Contents

List of Figures .....	xiii
List of Tables .....	xviii
Acknowledgements.....	xix
Chapter 1. Introduction.....	1
1.1. Supramolecular chemistry .....	1
1.1.1. Self-assembly.....	2
1.1.2. Molecular recognition.....	2
1.2. The Hydrogen bond .....	4
1.2.1. Selectivity in hydrogen bonding and Etter's rules.....	6
1.3. Co-crystals .....	7
1.3.1. Importance in industry .....	8
1.3.2. Visualizing molecular interactions .....	9
1.4. Predicting molecular recognition.....	10
1.5. Predicting hydrogen bonding through calculated molecular electrostatic potential surfaces.....	11
1.6. Goals .....	12
Chapter 2. Fine-tuning the hydrogen bond donor ability of oximes .....	15
2.1. Introduction.....	15
2.1.1. Oximes .....	15
2.1.2. Predicting the supramolecular outcome.....	18
2.1.3. Hypothesis.....	18
2.2. Experimental .....	21
2.2.1. Synthesis of dioximes .....	21
2.2.1.1. Synthesis of 1,4-benzenedicarboxaldehyde dioxime, di(H)ox .....	21
2.2.1.2. Synthesis of 1,4-diacetylbenzene dioxime, di(CH <sub>3</sub> )ox.....	22
2.2.1.3. Synthesis of N'1,N'4-dihydroxyterephthalimidoyl dichloride, di(Cl)ox.....	22
2.2.1.4. Synthesis of 2,2'-(1,4-phenylene)diacetonitrile .....	23
2.2.1.5. Synthesis of N'1,N'4-dihydroxyterephthalimidoyl cyanide, di(CN)ox.....	23

2.2.1.6.	Synthesis of N'1,N'4-dihydroxyterephthalimidamide, di(NH <sub>2</sub> )ox .....	24
2.2.2.	Conditions used in the co-crystallization.....	24
2.2.2.1.	Synthesis of 1,4-benzenedicarboxaldehyde, 1,4-dioxime 4-picolyl-N-oxide(1:2), di(H)ox:4po .....	24
2.2.2.2.	Synthesis of N'1,N'4-dihydroxyterephthalimidoyl cyanide 4-picolyl-N-oxide(1:1), di(CN)ox:4po .....	24
2.2.2.3.	Synthesis of N'1,N'4-dihydroxyterephthalimidoyl cyanide 4-benzoylpyridine (1:2), di(CN)ox:4bp .....	25
2.2.2.4.	Synthesis of N'1,N'4-dihydroxyterephthalimidoyl cyanide 4-benzoylpyridine (1:2), di(CN)ox:3bp .....	25
2.2.2.5.	Synthesis of N'1,N'4-dihydroxyterephthalimidamide DMSO (1:2), di(NH <sub>2</sub> )ox:DMSO.....	25
2.2.3.	Semi empirical AM1 calculations.....	25
2.2.4.	Solvent drop grinding experiments.....	25
2.3.	Results.....	26
2.3.1.	Molecular electrostatic potential calculations.....	26
2.3.2.	Solvent drop grinding experiments.....	27
2.3.2.1.	Crystal structure of 1,4-Benzenedicarboxaldehyde dioxime 4-picolyl-N-oxide(1:2), di(H)ox:4po .....	29
2.3.2.2.	Crystal structure of N'1,N'4-dihydroxyterephthalimidoyl cyanide, 1,4-dioxime 4-picolyl-N-oxide(1:1), di(CN)ox:4po .....	29
2.3.2.3.	Crystal structure of N'1,N'4-dihydroxyterephthalimidoyl cyanide, 1,4-dioxime 4-benzoylpyridine (1:2), di(CN)ox:4bp .....	30
2.3.2.4.	Crystal structure of N'1,N'4-dihydroxyterephthalimidoyl cyanide, 1,4-dioxime 3-benzoylpyridine (1:2), di(CN)ox:3bp .....	30
2.3.2.5.	Crystal structure of N'1,N'4-dihydroxyterephthalimidamide, DMSO (1:2), di(NH <sub>2</sub> )ox:DMSO.....	31
2.4.	Discussion.....	32
2.4.1.	Synthesis .....	32
2.4.2.	Infra-red spectroscopy .....	32
2.4.3.	The effect of the MEP values and pKa on supramolecular yield .....	33

2.5. Conclusions.....	35
Chapter 3. pK <sub>a</sub> vs calculated molecular electrostatic potential values: which is better at predicting molecular recognition? .....	38
3.1. Introduction.....	38
3.2. Experimental.....	44
3.2.1. Synthesis .....	44
1.1.1.1. Synthesis of 4-((hydroxyimino)methyl)benzoic acid, 4ABA.....	45
1.1.1.2. Synthesis of 1-(pyridin-4-ylmethyl)-1H-benzo[d]imidazole,.....	45
3.2.2. Synthesis of co-crystals.....	46
3.2.2.1. Synthesis of 4-hydroxybenzoic acid, 3PB (1:1), 4HBA:3PB.....	46
3.2.2.2. Synthesis of 3-hydroxybenzoic acid, 3PB (1:1), 3HBA:3PB.....	46
3.2.2.3. Synthesis of 4-hydroxybenzoic acid, 4PMB (1:1), 4HBA:4PMB.....	46
3.2.2.4. Synthesis of 3-hydroxybenzoic acid, 3PMB (1:1), 3HBA:3PMB.....	46
3.2.2.5. Synthesis of 4-((hydroxyimino)methyl)benzoic acid, 1PB (1:1), 4ABA:1PB.....	46
3.2.2.6. Synthesis of 4-((hydroxyimino)methyl)benzoic acid, 4PMB (1:1), 4ABA:4PMB.....	46
3.3. Results.....	47
3.3.1. Calculations.....	47
3.3.1.1. Molecular electrostatic potential (MEP) calculations.....	47
3.3.2. Identification on co-crystals.....	48
3.3.3. Description of crystal structures .....	49
3.3.3.1. Crystal structure of 4-hydroxybenzoic acid, 3PB (1:1), 4HBA:3PB.....	49
3.3.3.2. Crystal structure of 3-hydroxybenzoic acid, 3PB (1:1), 3HBA:3PB.....	49
3.3.3.3. Crystal structure of 4-hydroxybenzoic acid, 4PMB (1:1), 4HBA:4PMB.....	50
3.3.3.4. Crystal structure of 3-hydroxybenzoic acid, 3PMB (1:1), 3HBA:3PMB:CH <sub>3</sub> CN.H <sub>2</sub> O.....	50
3.3.3.5. Crystal structure of 4-((hydroxyimino)methyl)benzoic acid, 4PMB (1:1), 4ABA:4PMB.....	51
3.3.3.6. Crystal structure of 4-((hydroxyimino)methyl)benzoic acid, 1PB (2:1), 4ABA:1PB.....	51
3.4. Discussion.....	52



3.4.1.	Evaluation of co-crystals.....	52
3.4.2.	Predicting molecular recognition based on pKa and MEP values .....	53
3.4.3.	Conclusions.....	55
Chapter 4.	Establishing the place of cyanooximes in the hierarchy of hydrogen-bond donors	
	57	
4.1.	Introduction.....	57
4.1.1.	Cyanooximes.....	57
4.1.2.	Towards a unified theory for predicting selectivity in hydrogen-bonding .....	58
4.1.3.	Virtual co-crystal screening .....	59
4.1.4.	Hypothesis.....	60
4.2.	Experimental .....	62
4.2.1.	Molecular electrostatic potential calculations.....	62
4.2.2.	Synthesis of asymmetric ditopic donors .....	63
4.2.2.1.	Synthesis of (Z)-N,4-dihydroxybenzimidoyl cyanide, PhOx .....	63
4.2.2.2.	(Z)-4-(cyano(hydroxyimino)methyl)benzoic acid, 4BaOx.....	64
4.2.2.2.1.	Synthesis of 4-(bromomethyl)benzoic acid.....	64
4.2.2.2.2.	Synthesis of 4-(cyanomethyl)benzoic acid .....	64
4.2.2.2.3.	(Z)-4-(cyano(hydroxyimino)methyl)benzoic acid, 4BaOx .....	64
4.2.2.3.	(Z)-3-(cyano(hydroxyimino)methyl)benzoic acid, 3BaOx.....	65
4.2.2.3.1.	Synthesis of 3-(bromomethyl)benzoic acid,.....	65
	Synthesis of 3-(cyanomethyl)benzoic acid, .....	65
	(Z)-3-(cyano(hydroxyimino)methyl)benzoic acid, 3BaOx.....	66
4.2.3.	Synthesis of co-crystals.....	66
4.2.3.1.	Synthesis of PhOx:MPzO (1:1) .....	66
4.2.3.2.	Synthesis of 4-hydroxycyanooxime, BPO (1:1) PhOx:BPO .....	66
4.2.3.3.	Synthesis of 4-hydroxycyanooxime, 4PI (1:1) PhOx:4PI.....	67
4.2.3.4.	Synthesis of 4-hydroxycyanooxime, 3PMB (1:1) PhOx: 3PMB.....	67
4.2.3.5.	Synthesis of 4-hydroxycyanooxime, 4PMB (1:1) PhOx: 4PMB.....	67
4.2.3.6.	Synthesis of 4-acidcyanooxime, PzO (1:1) 4BAOx:PzO .....	67
4.2.3.7.	Synthesis of 4-acidcyanooxime, MPzO (1:1) 4BAOx:MPzO .....	67
4.2.3.8.	Synthesis of 3-acidcyanooxime, 4PMB (1:1) 3BAOx:4PMB .....	67

4.2.3.9.	Synthesis of 3-acidcyanooxime, 4PB (1:1) 3BAOx:4PB .....	68
4.3.	Results.....	68
4.3.1.	Description of crystal structures .....	68
4.3.1.1.	Crystal structure of PhOx:MPzO .....	68
4.3.1.2.	Crystal structure of PhOx:BPO.....	69
4.3.1.3.	Crystal structure of PhOx:3PI.....	69
4.3.1.4.	Crystal structure of PhOx:3PMB .....	70
4.3.1.5.	Crystal structure of PhOx:4PMB .....	70
4.3.1.6.	Crystal structure of 3BAOx:4PB .....	71
4.3.1.7.	Crystal structure of 3BAOx:4PMB.....	72
4.3.1.8.	Crystal structure of 4BAOx:PzO .....	72
4.3.1.9.	Crystal structure of 4BAOx:MPzO.....	73
4.3.2.	Calculation of pairing energies for possible supramolecular outcomes .....	74
4.4.	Discussion.....	75
Chapter 5.	Exploring the structural landscape of 1-deazapurine.....	80
5.1.	Tautomerism .....	80
5.2.	Purines and deazapurines .....	81
5.3.	Supramolecular control of tautomerism.....	82
5.4.	Experimental.....	85
5.4.1.	Synthesis .....	85
5.4.1.1.	Synthesis of 2-amino-5-bromopyridine .....	85
5.4.1.2.	Synthesis of 2-amino-3-nitro-5-bromopyridine.....	86
5.4.1.3.	Synthesis of 2,3-diaminopyridine .....	86
5.4.1.4.	Synthesis of 1-deazapurine .....	86
5.4.2.	MEP calculations on the donors and acceptors.....	87
5.4.2.1.	Calculated MEP values for the 1H and 3H tautomers of 1-Deazapurine .....	87
5.4.2.2.	Calculated MEP values for the hydrogen-bond and halogen bond donors.....	87
5.4.3.	Solvent-drop grinding experiments.....	88
5.4.4.	Determination of the tautomer based on IR spectroscopy .....	89
5.4.5.	Syntheses for obtained co-crystals.....	90
5.4.5.1.	Synthesis of 1-deazapurine, 1,2-diiodotetrafluorobenzene (1:1), DP:II .....	90

5.4.5.2.	Synthesis of 1-deazapurine, 1,4-diiidotetrafluorobenzene (1:1), DP:I2 .....	90
5.4.5.3.	Synthesis of 1-deazapurine, adipic acid (1:1), DP:DA1 .....	90
5.4.5.4.	Synthesis of 1-deazapurine, sebacic acid (1:1), DP:DA4.....	90
5.4.5.5.	Synthesis of 1-deazapurine, 4-hydroxybenzoic acid (1:1), DP:A4.....	90
5.4.6.	Structure descriptions.....	91
5.4.6.1.	Crystal structure of 1-deazapurine , 1,2-diiidotetrafluorobenzene (1:1), DP:I1	91
5.4.6.2.	Crystal structure of 1-deazapurine , 1,4-diiidotetrafluorobenzene (1:1), DP:I2	91
5.4.6.3.	Crystal structure of 1-deazapurine , adipic acid (1:1), DP:DA1 .....	92
5.4.6.4.	Crystal structure of 1-deazapurine , sebacic acid (2:1), DP:DA4.....	92
5.4.6.5.	Crystal structure of 1-deazapurine , 4-hydroxybenzoic acid (1:1), DP:A4 .....	93
5.5.	Discussion .....	94
5.6.	Conclusions.....	96
Chapter 6.	Can urea be used to isolate the 1H tautomer of 1-deazapurine?.....	99
6.1.	Introduction.....	99
6.1.1.	Deazapurines.....	99
6.1.2.	Urea.....	99
6.1.3.	Hypothesis.....	101
6.2.	Experimental .....	103
6.2.1.	Synthesis of ureas .....	103
6.2.1.1.	Synthesis of diphenylurea U1 .....	103
6.2.2.	MEP calculations .....	103
6.2.3.	Solvent-drop grinding experiments.....	105
6.2.4.	IR data from solvent drop grinding experiments .....	105
6.2.5.	Syntheses of co-crystals .....	107
6.2.5.1.	Synthesis of 1-deazapurine diphenylurea (1:1), DP:U1 .....	107
6.2.5.2.	Synthesis of 1-deazapurine 1-(2-cyanophenyl)-3-phenylurea (1:1), DP:U3 ..	107
6.2.5.3.	Synthesis of 1-deazapurine 1-(4-bromophenyl)-3-phenylurea (1:1), DP:U4 .	108
6.2.5.4.	Synthesis of 1-deazapurine 1-(4-nitrophenyl)-3-(2-tolyl)urea (1:1), DP:U14	108
6.2.5.5.	Synthesis of 1-deazapurine thiourea (1:1), DP:U15 .....	108

6.2.6.	Structure descriptions.....	108
6.2.6.1.	Crystal structure of 1-deazapurine diphenylurea (1:1), DP:U1 .....	108
6.2.6.2.	Crystal structure of 1-deazapurine 1-(2-cyanophenyl)-3-phenylurea (1:1), DP:U3	109
6.2.6.3.	Crystal structure of 1-deazapurine 1-(4-bromophenyl)-3-phenylurea (1:1), DP:U4	110
6.2.6.4.	Crystal structure of 1-deazapurine 1-(4-nitrophenyl)-3-(2-tolyl)urea (1:1), DP:U13	110
6.2.6.5.	Crystal structure of 1-deazapurine thiourea (1:1), DP:U15 .....	111
6.3.	Discussion .....	112
6.4.	Conclusion .....	116
Appendix A - NMR Spectra .....		118
Appendix B - Index of abbreviations.....		138

## List of Figures

Figure 1.1 Covalent synthesis vs. Supramolecular synthesis .....	1
Figure 1.2 Self-assembly of a supramolecular tetramer .....	2
Figure 1.3 The highly specific enzyme-substrate interaction (lock and key mechanism).....	3
Figure 1.4 Primary hydrogen bonding interactions between isonicotinamide with (a) 3-nitrobenzoic acid and (b) 4-chlorobenzoic acid.....	4
Figure 1.5 A schematic representation of a typical hydrogen bond .....	5
Figure 1.6 Hydrogen bonded base pairing of DNA.....	5
Figure 1.7 Graph set notation.....	7
Figure 1.8 Recrystallization vs co-crystallization.....	8
Figure 1.9 Reasons why active pharmaceutical compounds do not make it to the market .....	9
Figure 1.10 A 1:1:1 ternary cocrystal of 3,5-dinitrobenzoic acid : iso-nicotinamide : 3-methylbenzoic acid designed based on pKa .....	10
Figure 1.11 Molecular electrostatic potential surfaces calculated from SPARTAN .....	11
Figure 2.1 (a) Reactivation of acetylcholine esterase inhibited by a nerve agent with pralidoxime. (b) Platinum(II)oximes – potential anti-cancer drug (c) Perillartine, an artificial sweetener.....	15
Figure 2.2 Hydrogen bonding sites on the oxime moiety.....	16
Figure 2.3 Different binding modes of oximes (a) self-complementary two point homomeric dimer (b) Single-point homomeric interactions resulting in chains or catemers. (c) Most common heteromeric interactions. ....	16
Figure 2.4 Alternate binding interactions observed in (a) amideoximes (b) cyanooximes .....	17
Figure 2.5 Molecular electrostatic potential calculations .....	18
Figure 2.6 Substitution of the R group with electron donating and electron withdrawing groups to tune the hydrogen bond donor ability of the donor site .....	19
Figure 2.7 Library of symmetric ditopic oximes .....	19
Figure 2.8 Library of hydrogen bond acceptors used in this study.....	20
Figure 2.9 The supramolecular trimer in the 1:1 binary co-crystal of di(H)ox:4po .....	29
Figure 2.10 The infinite chain in the 1:1 binary co-crystal of di(CN)ox:4po.....	29
Figure 2.11 The supramolecular trimer in the 1:2 binary co-crystal of di(CN)ox:4bp.....	30

Figure 2.12 The supramolecular trimer in the 1:2 binary co-crystal of di(CN)ox:3bp.....	31
Figure 2.13 The supramolecular tetramer in the 1:2 binary solvate of di(NH <sub>2</sub> )ox:DMSO .....	31
Figure 2.14 The IR spectrum of the 1:1 grind of di(CN)ox:dbim clearly showing both O-H···N stretches at 1862 cm <sup>-1</sup> and 2467 cm <sup>-1</sup> .....	32
Figure 2.15 The IR spectra of di(H)ox and the 1:1 grind of di(H)ox and dbim .....	33
Figure 2.16 Expected supramolecular architectures (a) 1D chains (b) 0D trimers.....	34
Figure 2.17 oximes arranged according to increasing donor ability with matching trends in MEP and pK <sub>A</sub> values. ....	35
Figure 2.18 Tuning the melting point of a pharmaceutical via co-crystallization .....	36
Figure 3.1 The four possible outcomes with a pair of symmetric ditopic donors and acceptors (an expansion of Etter's rules). ....	39
Figure 3.2 A 1:1:1 ternary cocrystal of 3,5-dinitrobenzoic acid : iso-nicotinamide : 3- methylbenzoic acid designed based on pK <sub>a</sub> differences.....	39
Figure 3.3 The pK <sub>a</sub> slide scale .....	40
Figure 3.4 Plots of logK (acids against reference base) vs <b>logKAHi</b> .....	41
Figure 3.5 asymmetric ditopic donors containing –COOH groups .....	43
Figure 3.6 The library of asymmetric ditopic acceptors .....	44
Figure 3.7 The IR spectrum of the crystal 4HBA:4PMB .....	48
Figure 3.8 The primary hydrogen-bond interactions in the crystal structure of 4HBA:3PB.....	49
Figure 3.9 The primary hydrogen-bond interactions in the crystal structure of 3HBA:3PB.....	50
Figure 3.10 The primary hydrogen-bond interactions in the crystal structure of 4HBA:4PMB ..	50
Figure 3.11 The primary hydrogen-bond interactions in the crystal structure of 3HBA:3PMB:CH <sub>3</sub> CN.H <sub>2</sub> O.....	51
Figure 3.12 The primary hydrogen-bond interactions in the crystal structure of 4ABA:4PMB ..	51
Figure 3.13 The primary hydrogen-bond interactions in the crystal structure of 4ABA:1PB.....	52
Figure 3.14 4-Hydroxybenzoic acid with an asymmetric ditopic acceptor .....	53
Figure 3.15 The primary hydrogen-bond interactions in the crystal structure of 4HBA:PzO.....	53
Figure 3.16 The primary hydrogen-bond interactions in the crystal structure of 4HBA:BPO.....	54
Figure 3.17 The –OH group (the weaker donor according to pK <sub>a</sub> ) forms a hydrogen bond with the pyridine instead of the acid. ....	54

Figure 3.18 All nine co-crystals formed according to Etter's rules as predicted based on MEP values. ....	55
Figure 4.1 (a) Typical oxime-oxime dimer (b) Chain motif formed by cyanooximes .....	57
Figure 4.2 Oximes arranged according to increasing donor based on observed supramolecular yields ability with matching trends in MEP and pKA values. ....	58
Figure 4.3 Hypothesis on selectivity based on Etter's rules' (Figure 4.3).....	60
Figure 4.4 Three asymmetric ditopic donors with a cyanooxime functionality. ....	60
Figure 4.5 The nine acceptors used in this study .....	61
Figure 4.6 Synthetic scheme for 4BaOx .....	64
Figure 4.7 Synthetic scheme for 3BaOx .....	65
Figure 4.8 The primary hydrogen-bond interactions in the crystal structure of PhOx:MPzO .....	68
Figure 4.9 The primary hydrogen-bond interactions in the crystal structure of PhOx:BPO .....	69
Figure 4.10 The primary hydrogen-bond interactions in the crystal structure of PhOx:3PI .....	69
Figure 4.11 The primary hydrogen-bond interactions in the crystal structure of PhOx:3PMB ...	70
Figure 4.12 The primary hydrogen-bond interactions in the crystal structure of PhOx:4PMB. ..	70
Figure 4.13 The primary hydrogen-bond interactions in the crystal structure of 3BAOx:4PB....	71
Figure 4.14 The primary hydrogen-bond interactions in the crystal structure of 3BAOx:4MPB	72
Figure 4.15 The primary hydrogen-bond interactions in the crystal structure of 4BaOx:PzO.....	72
Figure 4.16 The primary hydrogen-bond interactions in the crystal structure of 4BaOx:MPzO .	73
Figure 4.17 The published structure of the 1:1 co-crystal of 4BaOx and 4PMB .....	77
Figure 5.1 A pair of tautomers where the group X acts as either an electrofuge or a nucleofuge during isomerization .....	80
Figure 5.2 The five most stable tautomeric forms of cytosine. ....	80
Figure 5.3 Each tautomer of 1-deazapurine leads to a different isomeric product. ....	81
Figure 5.4 Different hydrogen bonding environments of adenine (left) and 1-deazapurine (right) .....	81
Figure 5.5 The primary hydrogen-bonding interactions in the crystal structure of 1-deazapurine .....	82
Figure 5.6 Possible synthons for stabilizing the possible supramolecular outcome for the 3H tautomer .....	83
Figure 5.7 Synthetic scheme for 1-deazapurine.....	85

Figure 5.8 The primary hydrogen-bond interactions in the crystal structure of DP:I1.....	91
Figure 5.9 The primary hydrogen-bond interactions in the crystal structure of DP:I2.....	92
Figure 5.10 The primary hydrogen-bond interactions in the crystal structure of DP:DA1.....	92
Figure 5.11 The primary hydrogen-bond interactions in the crystal structure of DP:DA4.....	93
Figure 5.12 The primary hydrogen-bond interactions in the crystal structure of DP:A4.....	93
Figure 5.13 The two supramolecular motifs observed with the 3H tautomer.....	94
Figure 5.14 The 3H tautomer of the deazapurine and the acid are geometrically compatible.....	95
Figure 5.15 IR spectra of 1-deazapurine (red) and the 1:1 co-crystal of 1-deazapurine:adipic acid (blue).....	95
Figure 5.16 Both hydrogen and halogen bond donors can be used to isolate the 3H tautomer of 1-deazapurine.....	97
Figure 6.1 The 1H tautomer of 1-deazapurine is compatible with urea.....	99
Figure 6.2 (a) homomeric interaction of triurea (b) urea based carboxylate sensor.....	100
Figure 6.3 Donors, acceptors and the $\alpha$ tape motif of N,N-disubstituted urea.....	101
Figure 6.4 (a) N,N-bistritylurea forms solvates due to steric crowding (b) 1-(4-chlorophenyl)-3-pyridyl urea forms a N-H...N interaction instead of the $\alpha$ tape synthon.....	101
Figure 6.5 Suggested motif for the co-crystal of the 1H tautomer of 1-deazapurine and urea...	101
Figure 6.6 Co-crystals were identified by the shifting carbonyl peak on the urea(1644 – 1678 cm <sup>-1</sup> for diphenylurea).....	107
Figure 6.7 The primary hydrogen-bond interactions in the crystal structure of DP:U1.....	109
Figure 6.8 The primary hydrogen-bond interactions in the crystal structure of DP:U3.....	109
Figure 6.9 The primary hydrogen-bond interactions in the crystal structure of DP:U4.....	110
Figure 6.10 The primary hydrogen-bond interactions in the crystal structure of DP:U13.....	111
Figure 6.11 The primary hydrogen-bond interactions in the crystal structure of DP:U15.....	111
Figure 6.12 Comparing IR spectra of the two tautomers of 1-deazapurine.....	112
Figure 6.13 Geometrically compatible urea was successfully used to isolate the 1H tautomer of 1-deazapurine.....	116
Figure A.1 <sup>1</sup> HNMR spectrum of di(H)ox.....	118
Figure A.2 <sup>1</sup> HNMR spectrum of di(CH <sub>3</sub> )ox.....	119
Figure A.3 <sup>1</sup> HNMR spectrum of di(Cl)ox.....	120
Figure A.4 <sup>1</sup> HNMR spectrum of 1,4-dicyanomethylbenzene.....	121



Figure A.5 $^1\text{HNMR}$ spectrum of di(CN)ox.....	122
Figure A.6 $^1\text{HNMR}$ spectrum of di(NH <sub>2</sub> )ox.....	123
Figure A.7 $^1\text{HNMR}$ spectrum of ABA.....	124
Figure A.8 $^1\text{HNMR}$ spectrum of PhOx.....	125
Figure A.9 $^1\text{HNMR}$ spectrum of 4-bromomethylbenzoic acid.....	126
Figure A.10 $^1\text{HNMR}$ spectrum of 4-cyanomethylbenzoic acid.....	127
Figure A.11 $^1\text{HNMR}$ spectrum of 4BaOx.....	128
Figure A.12 $^1\text{HNMR}$ spectrum of 3-bromomethylbenzoic acid.....	129
Figure A.13 $^1\text{HNMR}$ spectrum of 3-cyanomethylbenzoic acid.....	130
Figure A.14 $^1\text{HNMR}$ spectrum of 3BaOx.....	131
Figure A.15 $^1\text{HNMR}$ spectrum of 4PB.....	132
Figure A.16 $^1\text{HNMR}$ spectrum of 2-amino-5-bromopyridine.....	133
Figure A.17 $^1\text{HNMR}$ spectrum of 2-amino-3-nitro-5-bromopyridine.....	134
Figure A.18 $^1\text{HNMR}$ spectrum of 2,3-diaminopyridine.....	135
Figure A.19 $^1\text{HNMR}$ spectrum of 1-deazapurine.....	136
Figure A.20 $^1\text{HNMR}$ spectrum of diphenylurea(U1).....	137

## List of Tables

Table 1.1 comparison of energies for different molecular interactions .....	6
Table 2.1 A CSD survey of multicomponent structures for each donor moiety.....	17
Table 2.2 Calculated molecular electrostatic potential values for the five donors .....	26
Table 2.3 Calculated molecular electrostatic potential values for the 20 acceptors .....	26
Table 2.4 Supramolecular yields based on IR spectroscopy.....	28
Table 2.5 The effect of the MEP values and pKa on supramolecular yield .....	33
Table 2.6 Calculated pKa values of the donors .....	36
Table 3.1 MEP calculations on the donors show the carboxylic acid to be the weaker donor .....	47
Table 3.2 MEP calculations for the acceptors .....	47
Table 3.3 Relevant IR results from solvent drop grinding experiments .....	48
Table 4.1 AM1 and DFT molecular electrostatic potential surface on the three donors. ....	62
Table 4.2 Calculated AM1 and DFT molecular electrostatic potential values of the acceptors...	62
Table 4.3 pairing energy calculations for 4-Phenolcyanooxime .....	74
Table 4.4 pairing energy calculations for 4-acidcyanooxime.....	74
Table 4.5 pairing energy calculations for 3-Acidcyanooxime.....	75
Table 4.6 Outcomes for the nine co-crystals obtained.....	76
Table 5.1 Selection of hydrogen and halogen bond donors.....	84
Table 6.1 Family of ureas with varying donor and acceptor strengths. ....	102
Table 6.2 AM1 and DFT values for the 1H tautomer of 1-deazapurine.....	103
Table 6.3 AM1 and DFT values for the library of ureas .....	104
Table 6.4 Correlating MEP values with synthesized outcomes.....	113
Table 6.5 Only the diarylureas with electron-withdrawing substituents form co-crystals .....	114

## Acknowledgements

First and foremost, I would like to thank my major professor, Prof. Christer Aakeröy, for giving me the opportunity to work in your group, and your continuous patience and guidance in my research without which, this work would not have been possible.

The members of the Aakeröy, Group grad, undergrad, past and present. It's been wonderful working with all of you.

I would like to thank the members of my committee Dr. Stefan Bossman, Dr. Kenneth Klabunde, Dr. Jennifer Anthony and Dr. Stephen Chapes for their valuable time and input.

Thanks to Dr John Desper, who is responsible for collecting data and solving all of the crystal structures.

I would like to thank Earline Dikeman, Leila Maurmann, Tobe Eggers, Ron Jackson, Jim Hodgson, Mary Dooley, Donna Wright, Connie Cusimano, Lisa Percival and Kim Ross for helping me in various ways and creating a very friendly and pleasant environment in the department.

I'm grateful to NSF (CHE-0957607) and the Johnson Center for Basic Cancer Research for financial support

To my family thank you so much for all your support throughout these years. Without you, I would not have been able to come this far.

# Chapter 1. Introduction

## 1.1. Supramolecular chemistry

Supramolecular chemistry is the chemistry of the intermolecular bond. It can be defined as the chemistry beyond the molecule<sup>1</sup>. It goes beyond the scope of molecular or covalent chemistry that deals with combining atoms with covalent bonds to form molecules, their properties and reactions. In supramolecular chemistry, weaker reversible interactions bring molecules together to form large aggregates or “supermolecules”

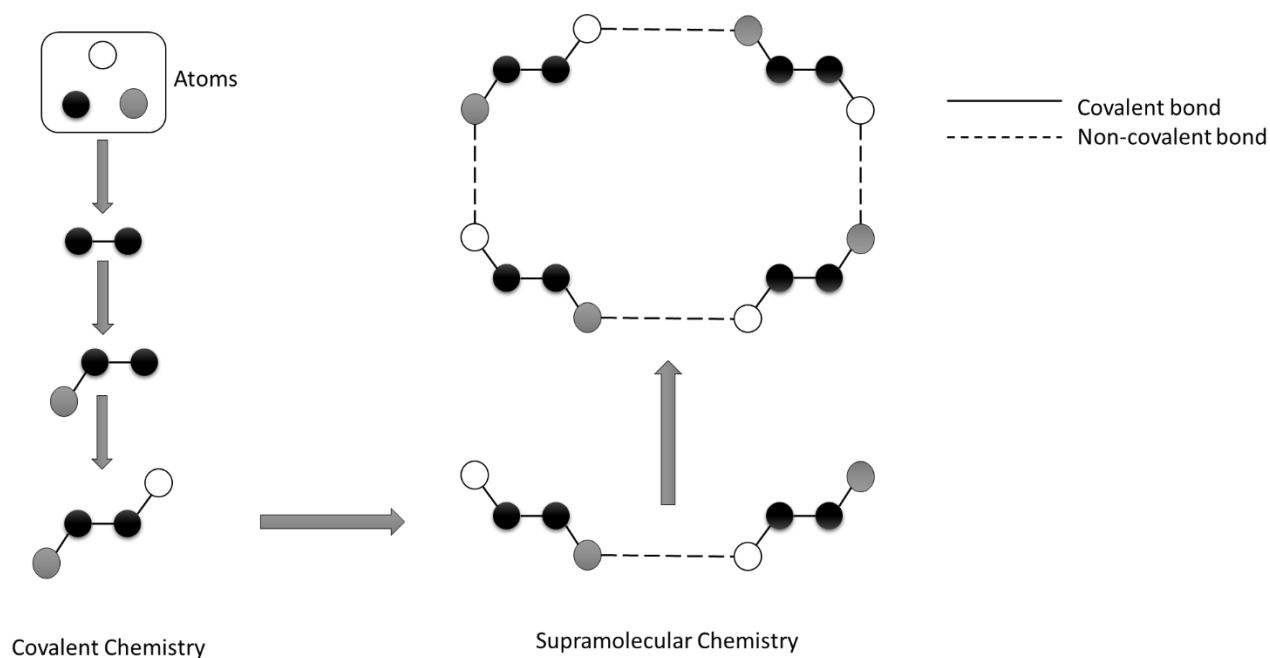


**Figure 1.1 Covalent synthesis vs. Supramolecular synthesis**

In the field of crystal engineering, the crystal engineer harnesses non-covalent interactions in order to rationally design and construct supramolecular aggregates. Unlike covalent chemistry, where many steps can be followed to get from reactant to product allowing the chemist a fair degree of control on how the atoms are brought together (Figure 1.1), most supramolecular reactions are single step processes and therefore a proper understanding is required of the underlying interactions in order to attain the desired aggregate.

### 1.1.1. Self-assembly

Self-assembly is the spontaneous non-covalent association of two or more molecules under equilibrium conditions into stable well-defined aggregates<sup>2</sup>. As shown in Figure 1.2 the two molecules have come together in a specific manner in aqueous solution to form a large ordered structure.

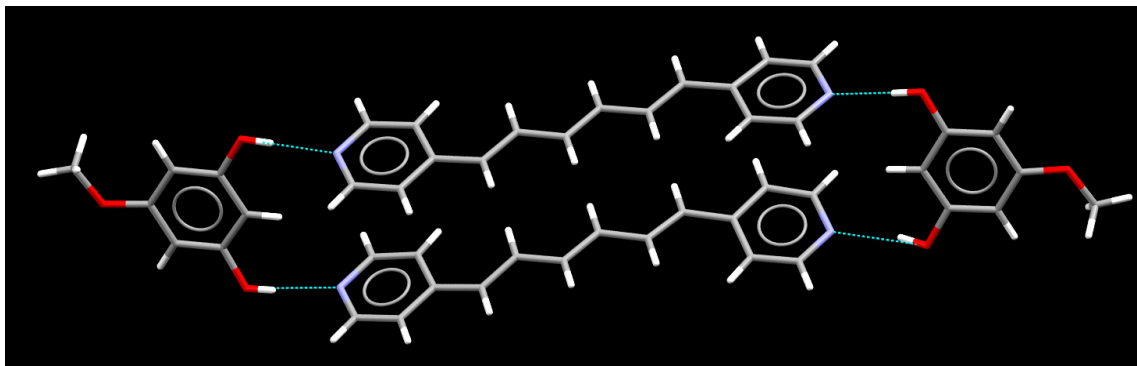


**Figure 1.2 Self-assembly of a supramolecular tetramer<sup>3</sup>**

This type of self-assembly is due to preferences in forming supramolecular interactions or due to certain pairs of groups always forming non-covalent interactions to each other. This phenomenon is known as molecular recognition.

### 1.1.2. Molecular recognition

One interesting feature of non-covalent interactions is the high degree of selectivity involved. This is seen in biological systems where reversible non-covalent interactions facilitate aggregation whilst maintaining the dynamic nature required of biological function. For example the binding of an enzyme to its substrate (Figure 1.3)<sup>4</sup> and the binding molecule to its specific receptor site and base pairing of nucleic acids all involve a great deal of specificity and all result from non-covalent interactions.

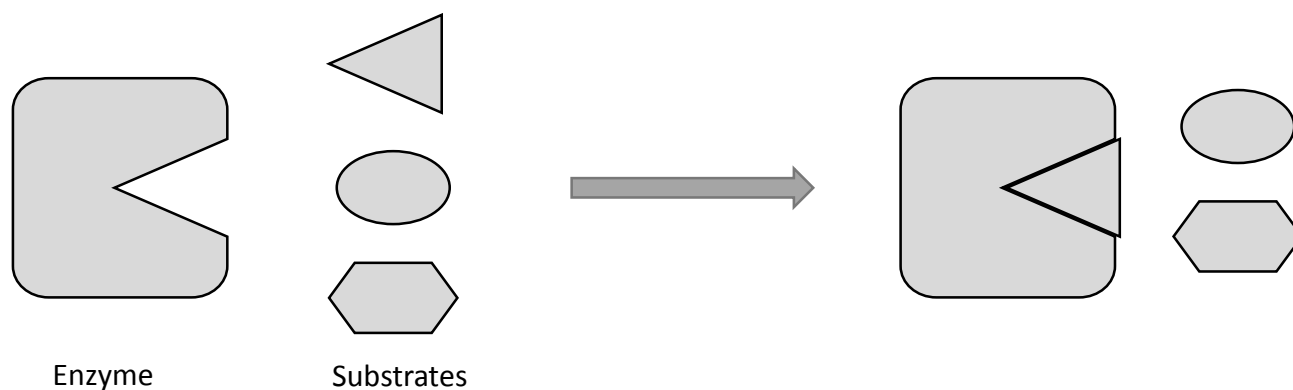


**Figure 1.3 The highly specific enzyme-substrate interaction (lock and key mechanism).**

Molecular recognition was first observed by Emil Fisher in the selective binding of an enzyme to its substrate<sup>5</sup>. He suggested a lock and key mechanism where, as shown in Figure 1.3, the enzyme has a choice of three substrates but selectively binds to the substrate that is the correct geometric fit for its active site. In the words of J. M. Lehn, molecular recognition is “binding with a purpose”<sup>6</sup> therefore these events need to be geometrically compatible and energetically favored in order to take place. In a competitive system consisting of multiple functional groups capable of non-covalent interactions, molecular recognition will result in some groups selectively binding to others. For example, in the multi-component crystal of iso-nicotinamide and carboxylic acids<sup>7</sup> there are three groups capable of hydrogen bonding, a carboxylic acid group, an amide group and a pyridyl site. As shown in Figure 1.4, the acid selectively binds to the pyridyl nitrogen atom and the amide to itself in both cases with different acids.

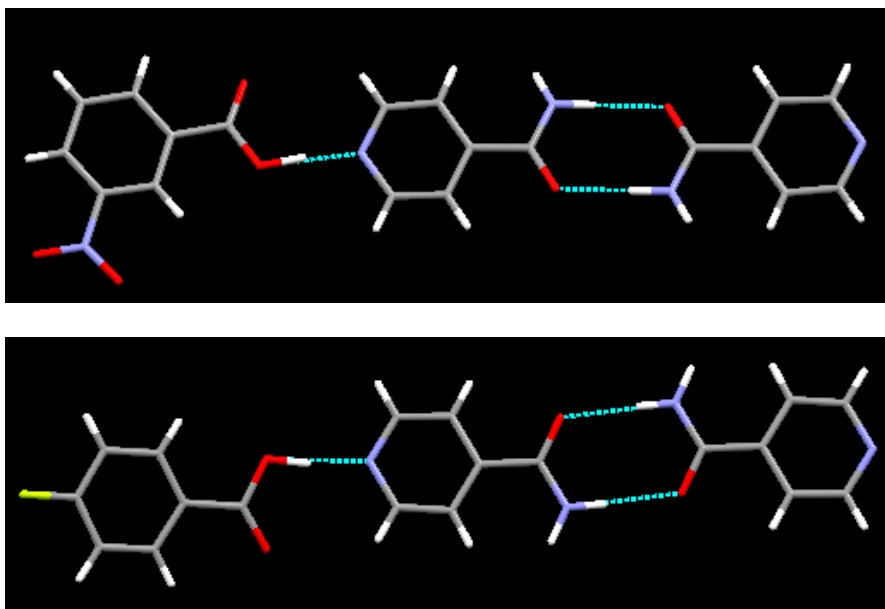


**Figure 1.4 Primary hydrogen bonding interactions between isonicotinamide with (a) 3-nitrobenzoic acid and (b) 4-chlorobenzoic acid<sup>7</sup>**

## 1.2. The Hydrogen bond

Of all the non-covalent interactions, the hydrogen bond has received most attention. The idea was first introduced by Latimer and Rodebush<sup>8</sup> in 1920 and later brought to attention by Pauling in 1939<sup>9</sup>. The simplest definition for a hydrogen bond is “a weak electrostatic chemical bond which forms between covalently bonded hydrogen atoms and a strongly electronegative atom with a lone pair of electrons<sup>10</sup>” The current IUPAC definition for a hydrogen bond is as follows “*The hydrogen bond is an attractive interaction between a hydrogen atom from a molecule or a molecular fragment X–H in which X is more electronegative than H, and an atom or a group of atoms in the same or a different molecule, in which there is evidence of bond formation.*”<sup>11</sup> The X–H group is known as the hydrogen bond donor and the group it binds to is known as a hydrogen bond acceptor (Figure 1.5).

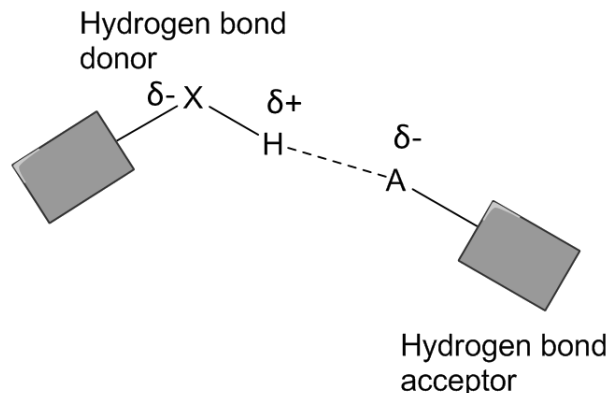


**Figure 1.5 A schematic representation of a typical hydrogen bond**

The actual attractive forces behind hydrogen bonding has been subjected to a lot of debate. Some consider the hydrogen bond to be strong and directional dipole-dipole interaction<sup>12</sup>. Others considered hydrogen bond to comprise of an electrostatic component and a covalent component<sup>13</sup>.

Examples of co-operativity<sup>14</sup> and resonance stabilized hydrogen bonds<sup>15,16</sup> indicate that there may be some covalent nature involved in hydrogen bonding. Experimental evidence for covalent behavior in hydrogen bonding was provided in a Compton scattering experiment on ice which show a periodic shift in hydrogen bond length corresponding to distances of 1.72 and 2.85 Å, which are similar to the hydrogen bond length and O-O distance, respectively<sup>17</sup>. Energy decomposition studies however, show the electrostatic contribution to be the dominant factor in hydrogen bonding<sup>18</sup>.

Hydrogen bonds are of utmost importance in biological systems. It is the main driving force behind many substrate-receptor interactions. In addition it plays a vital role in the three dimensional structure of proteins and in the structure of nucleic acids<sup>19</sup>(Figure 1.6).

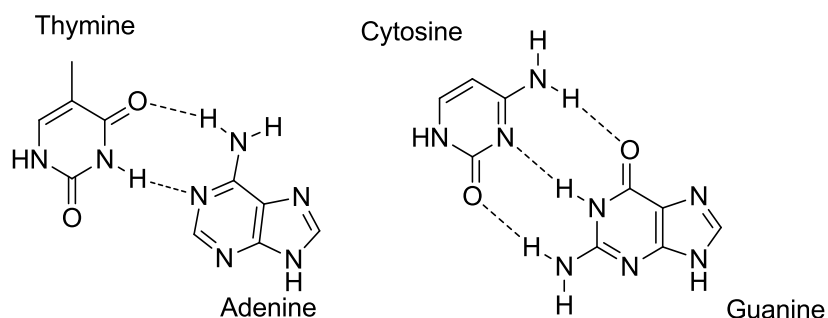


**Figure 1.6 Hydrogen bonded base pairing of DNA**



Table 1.1 gives a comparison of energies of hydrogen bonds compared to other intermolecular interactions. Apart from ionic and ion dipole interactions, hydrogen bonds can be classified as one of the stronger non-covalent interactions. Unlike ionic or ion-dipole interactions, hydrogen bonds are directional<sup>20</sup>, which makes them ideal candidates in the design of supramolecular architectures. Hydrogen bonds are classified as strong, medium and weak hydrogen bonds<sup>21</sup>. This property arises from the two species (hydrogen bond donor and hydrogen bond acceptor) between which the bond is formed.

**Table 1.1 comparison of energies for different molecular interactions<sup>21</sup>**

Interaction	Strength/kJmol <sup>-1</sup>	Example
Ion-ion	200 - 300	Tetrabutylammonium chloride
Ion-dipole	50 – 200	Sodium [15]crown-5
Dipole-dipole	5 - 50	Acetone
Strong hydrogen bond	60 - 120	HF
Medium hydrogen bond	16 – 60	Carboxylic Acids, DNA/RNA
Weak Hydrogen bond	< 12	C-H...O
Halogen bond <sup>22</sup>	5 - 180	I...I <sub>2</sub>
Cation- $\pi$	5 - 80	K <sup>+</sup> in benzene
$\pi - \pi$	0 - 50	Benzene
Van der Waals	< 5 kJmol <sup>-1</sup> variable depending on surface area	Argon

### ***1.2.1. Selectivity in hydrogen bonding and Etter's rules***

As mentioned above, hydrogen bonds are highly selective intermolecular interactions and the driving force behind molecular recognition, therefore, to better understand molecular recognition a better understanding of the selectivity involving hydrogen bonding is required.

The first comprehensive study on hydrogen bond selectivity was carried out by Etter et. al. Analysis of the Cambridge Structural Database for groups of neutral molecules with sterically accessible hydrogen bonding groups allowed Etter and co-workers to determine the possible

preferences for individual functional groups in terms of selectivity and patterns of aggregation in solids. They also developed a method to depict these aggregation patterns called “graph set notations” (Figure 1.7).

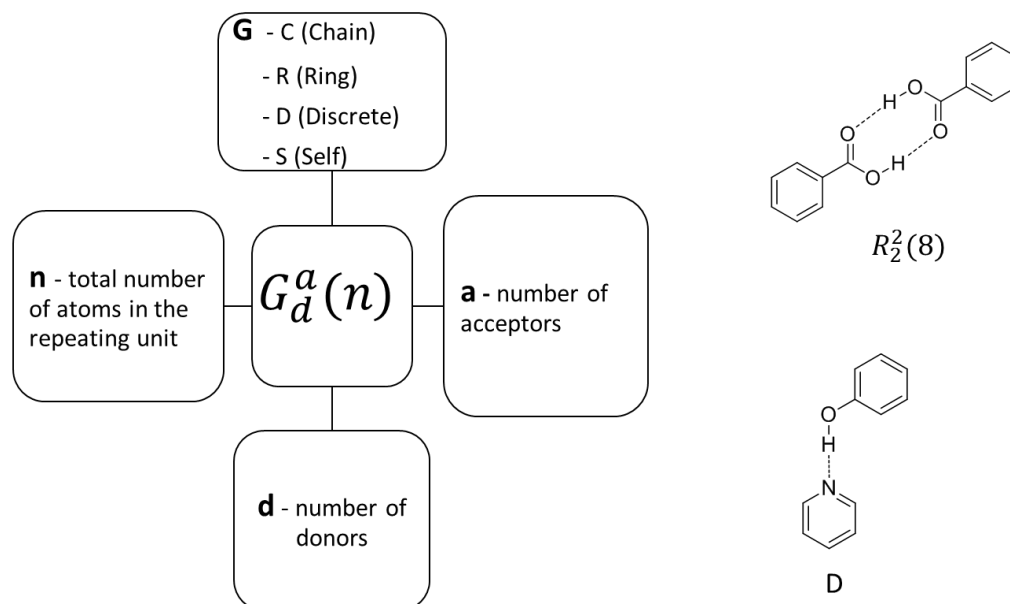


**Figure 1.7 Graph set notation**

Based on their observations, Etter and co-workers proposed a set of guidelines<sup>23,24</sup> on the selectivity of hydrogen bonding. These guidelines are currently known as Etter’s rules the first three of which are shown below.

1. All **good** proton donors and acceptors are **used** in hydrogen bonding
2. If a six-membered intramolecular hydrogen bond can form, it will usually do **so** in preference to forming intermolecular hydrogen bonds
3. The best proton donors and acceptors remaining after intramolecular hydrogen-bond formation, form intermolecular hydrogen bonds to one another

### 1.3.Co-crystals

The definition of the term co-crystal has been subjected to some debate<sup>25,26</sup>. The purpose of co-crystallization is to combine two or more different species in the solid state. A co-crystal can be defined as a structurally homogeneous crystalline material that contains two or more neutral building blocks that are present in definite stoichiometric amounts where all the building blocks

are solids at ambient conditions.<sup>27</sup> Multicomponent systems such as solvates and clathrates are not considered to be co-crystals under this definition.

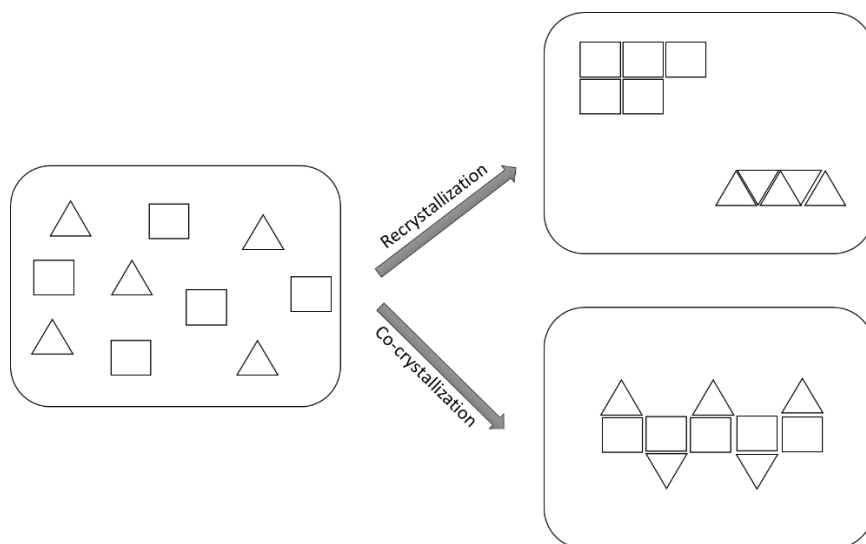


**Figure 1.8 Recrystallization vs co-crystallization**

Co-crystallization is not to be confused with recrystallization which results in like molecules binding to each other (Figure 1.8). This type of aggregation is more common due to the “selfish” nature of molecules and is commonly used as a method of purification. In order to synthesize multicomponent solids or co-crystals, the natural propensity for recrystallization needs to be overcome. A proper understanding of the underlying interactions enables the supramolecular chemist to overcome this barrier to design and construct multi-component architectures.

### ***1.3.1. Importance in industry***

Bringing different molecules together in the solid state using inter-molecular interactions does not affect the chemical properties of any of the constituents as no covalent modification takes place. Using the tools of crystal engineering it is possible to tune the physical properties such as melting point<sup>28</sup>, solubility<sup>28</sup> hygroscopicity<sup>29</sup> of a given compound without affecting its intrinsic chemical properties or activity.

In the pharmaceutical industry for example a significant number (41%) of pharmaceutical ingredients fail to make it to the market due to poor physical properties (Figure 1.9). As co-crystallization does not affect the chemical nature of the drug, it is conceivable that a co-crystal of the said compound can be synthesized that does not contain any of the undesired physical properties.

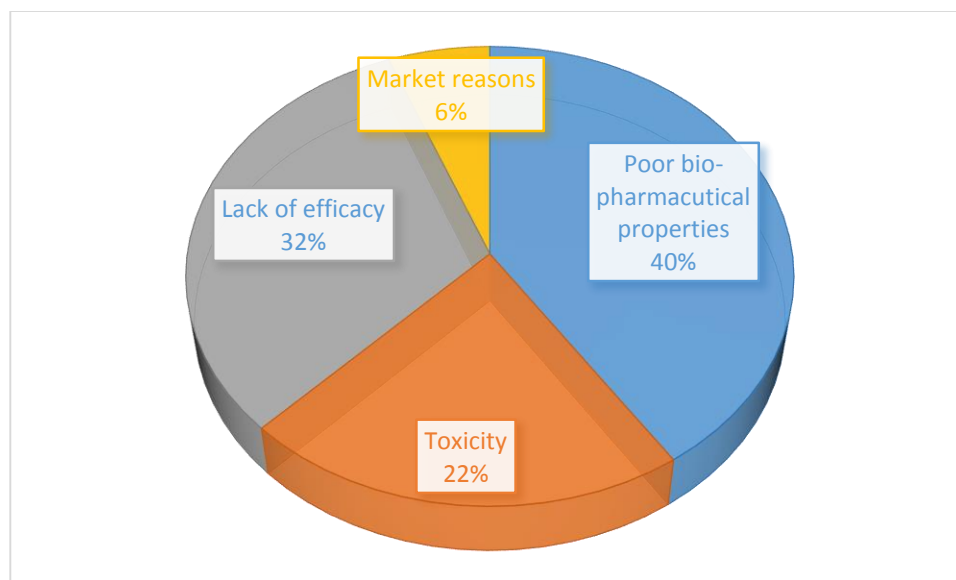


**Figure 1.9 Reasons why active pharmaceutical compounds do not make it to the market<sup>30</sup>**

This has in recent times made certain areas such as pharmaceuticals<sup>28,31</sup>, agrochemicals<sup>32</sup>, non-linear optics<sup>33</sup>, explosives<sup>34</sup>, and organic semiconductors<sup>35</sup> look to supramolecular chemistry for answers.

The current methods for identifying possible co-crystal formers involves screening the molecule of interest against a series of potential co-crystal formers and analyzing them for the formation of co-crystals. This type of blind large-scale screening is time-consuming and costly. A proper understanding of the underlying supramolecular interactions makes it possible to pick the best cofomers based on the functionalities present on the molecule of interest. It also makes it possible to custom design the supramolecular architecture in order to attain desired physical properties.

### ***1.3.2. Visualizing molecular interactions***

Many different methods such as IR spectroscopy, powder X-ray diffraction and NMR based methods can be used to detect the formation of co-crystals. Even though these methods provide evidence for co-crystal formation, they provide little information as to the actual interactions responsible for the formation of the co-crystal. The exact molecular interactions taking place in solution are not easily observed due to the dynamic nature of these weak reversible interactions. The actual intermolecular interactions or the molecular recognition events responsible for the formation of co-crystals can be visualized through single crystal X-ray diffraction of the

said co-crystal. This however, requires a crystal of sufficient quality for X-ray diffraction to be grown which may prove difficult at times.

Experimental methods such as NMR binding studies or isothermal titration calorimetry are used to experimentally determine the binding constants for hydrogen bonding<sup>36</sup>. The ability to perform such analyses is system specific. In addition experimentally determining the binding constants for hundreds of potential co-crystal formers is time consuming and expensive and therefore unfeasible in an industrial environment<sup>37</sup>.

#### 1.4. Predicting molecular recognition

The direct use of pKa based methods have proven effective in some studies as predictors for hydrogen bond donor ability, donors with lower pKa values (more acidic) are considered to be better hydrogen bond donors. There are many examples in literature where the supramolecular outcome has been successfully predicted based on pKa values<sup>38</sup>. As shown in Figure 1.10, a ternary co crystal was designed with the asymmetric ditopic acceptor iso-nicotinamide and two aromatic acids, where 3,5-dinitrobenzoic acid with the lower pKa of 2.8 selectively binds to the pyridyl nitrogen, which is the stronger acceptor of iso-nicotinamide and 3-methylbenzoic acid (pKa = 4.3) binds to the weaker amide group.

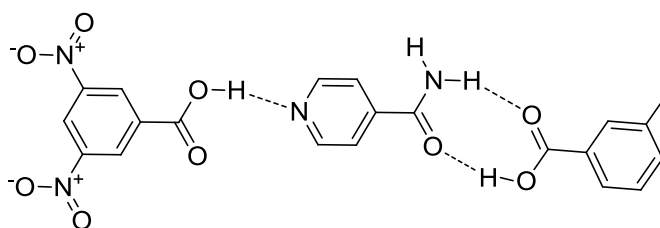


**Figure 1.10 A 1:1:1 ternary cocrystal of 3,5-dinitrobenzoic acid : iso-nicotinamide : 3-methylbenzoic acid designed based on pKa<sup>39</sup>**

This method is effective if limited to a single class of compound upon comparing in the case of phenols and thiophenols, thiophenol has a pKa of 6.61 which is considerably lower than that of phenol (pKa=9.86), which indicates that thiourea should be a better hydrogen bond donor. Experimentally however, phenols have significant hydrogen bond donor ability<sup>40</sup> and are commonly used as hydrogen bond donors whereas thioureas hardly exhibit any hydrogen bond donor ability<sup>41</sup>.

## 1.5. Predicting hydrogen bonding through calculated molecular electrostatic potential surfaces.

Assuming that hydrogen bonds are mostly electrostatic a computational method was developed by Hunter et. al.. where, they attempt to explain hydrogen bonding based on electrostatics. Where the association constant (K) of two simple molecules can be treated as shown in Equation 1.1 where,  $\alpha^{H_2}$  and  $\beta^{H_2}$  are functional group constants that relate to the hydrogen bond donor and hydrogen-bond acceptor properties. This is equivalent to the expression of the electrostatics of the hydrogen bonding interaction, where the free energy of interaction changes with the product of the positive charge on the hydrogen-bond donor ( $\alpha^{H_2}$ ) and the negative charge on the hydrogen bond acceptor ( $\beta^{H_2}$ )

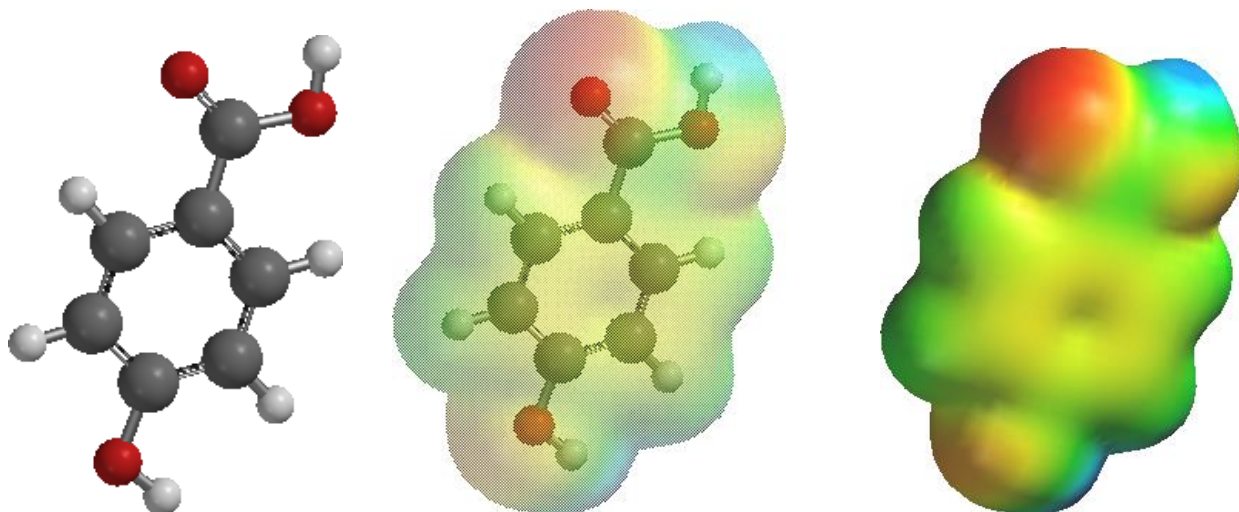


**Figure 1.11 Molecular electrostatic potential surfaces calculated from SPARTAN**

$$\log K = c_1 \alpha^{H_2} \beta^{H_2} + c_2 \quad 1.1$$

The charge parameter can be determined by a molecular electrostatic potential surface constructed around the molecule through a semiempirical AM1 calculation (Figure 1.11) where the maxima (shown in blue) correspond to the charges on the donors and the minima (shown in red) correspond to the charge on the acceptors (equation 1.2 and 1.3)<sup>42</sup>.

$$\alpha = E_{\max}/52 \text{ kJmol}^{-1} = 4.1 (\alpha^{H_2} + 0.33) \quad 1.2$$

$$\beta = -E_{\text{min}}/52 \text{ kJmol}^{-1} = 10.3 (\beta^{\text{H}_2} + 0.06) \quad 1.3$$

Even though these equations were designed to explain hydrogen bonding with solvents. These  $\alpha$  and  $\beta$  values can be used for the comparison and ranking of hydrogen bond donor and acceptor groups respectively.

The values obtained have no relation to actual charge or any other thermodynamic parameters on the molecule. Predictions based on calculated values have been shown to be consistent with experimental observations<sup>42</sup> and therefore can be used as a scale of comparing different molecules and functional groups. This type of prediction provides a cheap and reliable means to postulate the hydrogen bonding abilities and preferences of different molecules in order to select the best candidates for experimental screening.

## 1.6.Goals

In order to construct multi-component non-covalently bound architectures, a proper understanding of the underlying interactions is required. Computational tools provides a convenient means to rank and compare different donor and acceptor groups. Little parallel experimental exploration exists to validate predictions based on calculated values.

The goal of this thesis is to

- Study the effects of covalent modification on the supramolecular behavior of oximes
- Synthesize asymmetric ditopic donors comprising the strong hydrogen bond donor groups phenol, carboxylic acid, cyanooxime and aldoximes in order to rank these hydrogen bond donor functionalities by the synthesis and analysis of co-crystals.
- Compare predictions based on computational results with experimental results to explore their validity.
- Use the tools of crystal engineering to design supramolecular agents that can isolate two tautomeric forms of 1-deazapurine in the solid state.

## References

---

- <sup>1</sup> J. M. Lehn *Angew. Chem. Int. Ed. Engl.* **1988**, *27*, 89-112
- <sup>2</sup> G. M. Whitesides. B. Grzybowski. *Science*, **2002**, *295*, **5564**, 2418-2421.
- <sup>3</sup> X. Gao, T. Friščić, and L. R. MacGillivray, *Angew. Chem. Int. Ed.*, **2004**, *43*, 232–236
- <sup>4</sup> Y. Shen, A. Joachimiak, M. R. Rosner and W. Tang, *Nature*, **2006**, *443*, 870-874
- <sup>5</sup> E. Fischer, *Ber. Deutsch. Chem. Ges.*, **1894**, *27*, 2985.
- <sup>6</sup> J. M. Lehn. *Pure Appl. Chem*, **1978**, *50*, 871
- <sup>7</sup> C. B. Aakeroy, J. Desper and B. A. Helfrich *CrystEngComm*, **2004**, *6*, **5**, 19–24
- <sup>8</sup> W. M. Latimer and W. H. Rodebush, *J. Am. Chem. Soc.*, **1920**, *42*, 1419-1433.
- <sup>9</sup> L. Pauling, *The Nature of the Chemical Bond*, Cornell University Press, Ithaca, NY. 1960
- <sup>10</sup> *The Penguin Dictionary of Science*, Penguin, London (1971).
- <sup>11</sup> E. Arunan, G. R. Desiraju, R. A. Klein, J. Sadlej, S. Scheiner, I. Alkorta, D. C. Clary, R. H. Crabtree, J. J. Dannenberg, P. Hobza, H. G. Kjaergaard, A. C. Legon, B. Mennucci, and D. J. Nesbitt, *Pure Appl. Chem.*, **2011**, *83*, **8**, 1637–1641.
- <sup>12</sup> J. Israelachvili. *Intermolecular and Surface Forces*, 2nd ed., Academic Press, New York 1991.
- <sup>13</sup> F. Weinhold, C. R. Landis. *Valency and Bonding*, Cambridge University Press, Cambridge. 2005.
- <sup>14</sup> J. J. Dannenberg. *J. Mol. Struct.* **2002**, *615*, 219.
- <sup>15</sup> P. Gilli, V. Bertolasi, V. Ferrati, G. Gilli. *J. Am. Chem. Soc.* **1994**, *116*, 909
- <sup>16</sup> P. Gilli, V. Bertolasi, V. Ferretti, and G. Gilli, *J. Am. Chem. Soc.* **2000**, *122*, 10405-10417
- <sup>17</sup> E. D. Isaacs, A. Shukla, P. M. Platzman, D. R. Harman, B. Barbiellini, C. A. Tulk. *Phys. Rev. Lett.*, **1999**, *82*, 600.
- <sup>18</sup> H. Umeyama, K. Morokuma. *J. Am. Chem. Soc.* **1977**, *99*, 1316
- <sup>19</sup> G. A. Jeffrey, W. Saenger, *Hydrogen Bonding in Biological Structures*, Springer-Verlag, 1991.
- <sup>20</sup> A. C. Legon and D. J. Millen, *Accounts of Chemical Research* **1987**, *20*, **1**, 39-46
- <sup>21</sup> Jonathan W. Steed, David R. Turner, Karl J. Wallace, *Core Concepts in Supramolecular Chemistry and Nanochemistry*, John Wiley & Sons, Ltd, 2007
- <sup>22</sup> P. Metrangolo, H. Neukirch, T. Pilati, and G. Resnati, *Accounts of Chemical Research*, **2005**, *38*, **5**, 386-395
- <sup>23</sup> M.C. Etter, *J. Phys. Chem.* **1991**, *95*, 4601
- <sup>24</sup> M. C., Etter, G. M. Frankenbach, *Chem. Mater.* **1989**, *1*, 10.
- <sup>25</sup> G. R. Desiraju, *CrystEngComm*, **2003**, *5*, 466
- <sup>26</sup> J. D. Dunitz, *CrystEngComm*, **2003**, *5*, 506
- <sup>27</sup> C. B. Aakeröy and D. J. Salmon, *CrystEngComm*, **2005**, *7*, 439
- <sup>28</sup> M. K. Stanton and A. Bak, *Cryst. Growth Des.*, **2008**, *8*, **10**, 3856–3862
- <sup>29</sup> M. Viertelhaus, R. Hilfiker, F. Blatter M. and Neuburger, *Cryst. Growth Des.*, **2009**, *9*, **5**, 2220–2228
- <sup>30</sup> E. H. Kerns, L. Di, *Drug-Like Properties: Concepts, Structure Design and Methods: from ADME to Toxicity Optimization*; Elsevier, Amsterdam, **2008**, 7-9;



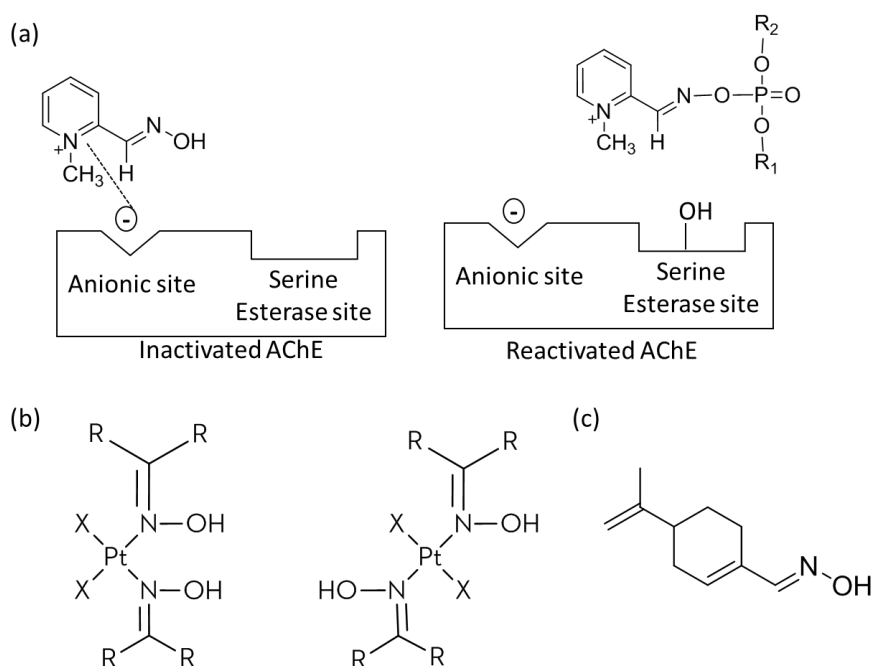
- 
- <sup>31</sup> M. L. Cheney, D. R. Weyna, N. Shan, M. Hanna, L. Wojtas, M. J. Zaworotko, *Crystal Growth & Design*, **2010**, *10*, 4401-4413
- <sup>32</sup> E. Nauha, E. Kolehmainen and M. Nissinen, *CrystEngComm*, **2011**, *13*, 6531-6537
- <sup>33</sup> C. B. Aakeröy, G. S. Bahra, P.B. Hitchcock, Y. Patell, and K. R. Seddon, *J. Chem. Soc., Chem. Commun.*, **1993**, 152-156.
- <sup>34</sup> D. I. A. Millar, H. E. Maynard-Casely, D. R. Allan, A. S. Cumming, A. R. Lennie, A. J. Mackay, I. D. H. Oswald C. C. Tang and C. R. Pulham, *CrystEngComm*, **2012**, *14*, 3742-374
- <sup>35</sup> G. Wang and Y. Huang, *Journal of Physics and Chemistry of Solids*, **2007**, *68*, 2003-2007.
- <sup>36</sup> C. Dethlefs, J. Eckelmann, H. Kobarg, T. Weyrich, S. Brammer, C. Näther and U. Lüning, *European Journal of Organic Chemistry*, **2011**, *11*, 2066-2074
- <sup>37</sup> S. L. Morisette, O. Almarsson, M. L. Peterson, J. F. Remenar, M. J. Read, A. V. Lemmo, S. Ellis, M. J. Cima and C. R. Gardner, *Adv. Drug Delivery Rev.*, 2004, *56*, 275-300
- <sup>38</sup> D. E. Lynch, P. Sandhu and S. Parsons, *Aust. J. Chem.*, **2000**, *53*, 383-387.
- <sup>39</sup> C. B. Aakeröy, A. M. Beatty, B. A. Helfrich, *Angew. Chem. Int. Ed.* **2001**, *17*, 3240-3242.
- <sup>40</sup> K. Huang, D. Britton, M. C. Etter and S. R. Byrn *J. Mater. Chem.*, **1997**, *7*, 713-720
- <sup>41</sup> G. R. Desiraju, "Crystal Engineering. The Design of Organic Solids", Elsevier, **1989**.
- <sup>42</sup> C.A. Hunter, *Angew. Chem. Int. Ed.* **2004**, *43*, 5310-5324.

## Chapter 2. Fine-tuning the hydrogen bond donor ability of oximes

### 2.1. Introduction

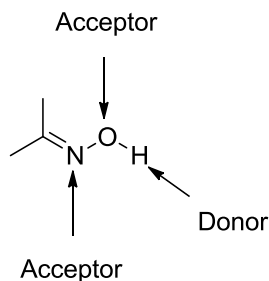
#### 2.1.1. Oximes

Molecules containing an oxime functionality have found importance in pharmaceutical<sup>1,2</sup> (Figure 2.1 a), agrochemical<sup>3</sup>, organometallic<sup>4,5</sup> (Figure 2.1 b) and biological materials<sup>6</sup> (Figure 2.1 c). In most of these areas, function is related to the reactivity and structure of the oxime moiety.



**Figure 2.1 (a) Reactivation of acetylcholine esterase inhibited by a nerve agent with pralidoxime.<sup>7</sup> (b) Platinum(II)oximes – potential anti-cancer drug<sup>4</sup> (c) Perillartine, an artificial sweetener<sup>6</sup>.**

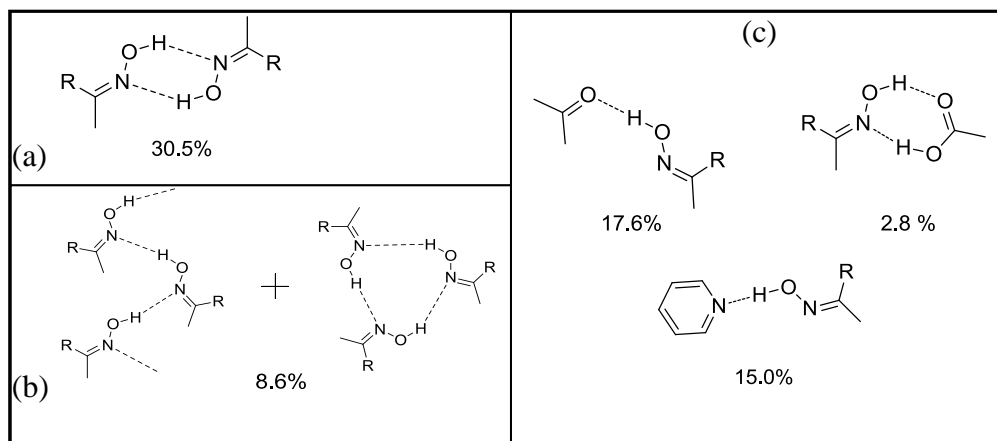
The oxime group contains a hydrogen bond donor site and two acceptor sites (Figure 2.2) that can have potential applications in supramolecular chemistry.



**Figure 2.2 Hydrogen bonding sites on the oxime moiety**

As explained in Chapter 1 the supramolecular chemist can modify the physical properties of a certain species without altering its chemical properties by synthesizing multi component solids or co-crystals with neutral organic molecules. Hydrogen-bond donors like carboxylic acids<sup>8</sup>, hydroxyl groups<sup>9</sup>, and amides form robust reliable supramolecular synthons that can be used to engineer such multicomponent solids or co-crystals with various acceptors<sup>10</sup>.

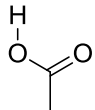
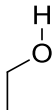
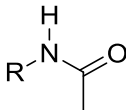
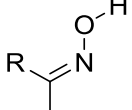
A CSD survey of the oxime moiety yields 573 structures that exhibit a diverse spread of connectivities and synthons. Oxime-oxime homomeric interactions result in dimeric, catemeric or chain type structures<sup>11</sup> as shown in Figure 2.3 (a) and (b). They also form heteromeric interactions, complementary two point dimers with acids and amides, single point interactions with the carbonyl groups and aromatic N atoms of heterocyclic molecules as shown in Figure 2.3 (c).



**Figure 2.3 Different binding modes of oximes (a) self-complementary two point homomeric dimer (b) Single-point homomeric interactions resulting in chains or catemers. (c) Most common heteromeric interactions.**

As shown in Figure 2.3, the oxime moiety is capable of a diverse array of supramolecular connectivities. Its ability to form reliable robust supramolecular synthons requires further exploration. As shown in Table 2.1, a CSD survey of neutral multi-component solids of different donor groups shows that compared to other hydrogen bond donor functionalities, very little has been published on the oxime moiety.

**Table 2.1 A CSD survey of multicomponent structures for each donor moiety**

				
Multi component solids	1793	2184	2576	87

The oxime group possesses a unique tunability that is not present in other hydrogen bond donors. By changing the group R, it is possible not only to change the donor ability of the –OH but also to alter the type of binding interaction. Most oximes form an O-H...N homomeric interaction to itself resulting in either dimers (Figure 2.3(a)), chains or catemers (Figure 2.3(b)) but changing the R group can alter this behavior.

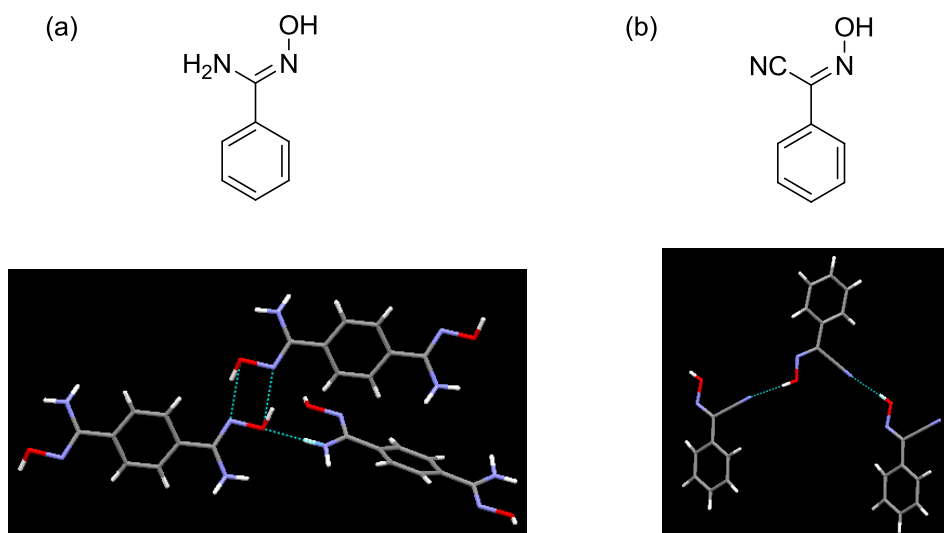


**Figure 2.4 Alternate binding interactions observed in (a) amideoximes (b) cyanooximes<sup>12</sup>**

As shown in Figure 2.4, the amide oxime shows a secondary interaction (Figure 2.4 (a)) where the amide N-H group binds to the oxygen atom on the oxime moiety. Similarly the cyanooxime group does not show the typical oxime-oxime O-H...N interaction instead the O-H group binds to the CN on the cyanooxime (Figure 2.4 (b)) resulting in catemers.

### 2.1.2. Predicting the supramolecular outcome

To predict the supramolecular outcome it is necessary to establish a hierarchy of hydrogen bond donors and acceptors. A range of methods can be utilized for this purpose as the comparison here involves the same functionality such as pKa<sup>13</sup>, hydrogen bond acidity<sup>14</sup> or molecular electrostatic potential calculations<sup>15,16</sup>.

Since hydrogen bonding is mostly electrostatic in nature, we have chosen molecular electrostatic potential calculations to rank our hydrogen bond donors. Here we plot molecular electrostatic potential surfaces using AM1 calculations. Donors are ranked by values of the maxima of the MEP surfaces plotted.

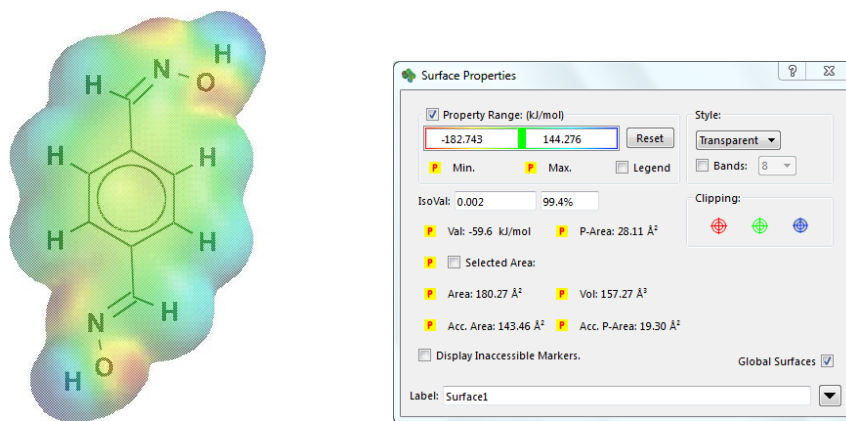
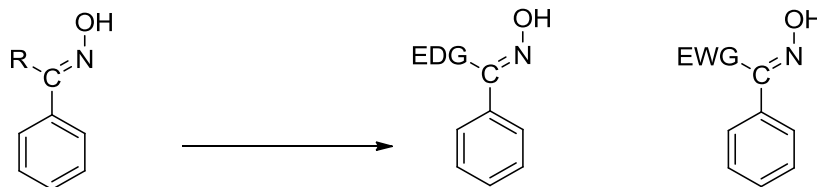


Figure 2.5 Molecular electrostatic potential calculations

### 2.1.3. Hypothesis

We hypothesize that the hydrogen bond donor ability of oxime groups can be tuned by changing the R substituent. (Figure 2.6) The hydrogen bond donating ability of the ligands can be compared by the comparing the supramolecular yields<sup>17</sup>, or the frequency of co-crystal formation under similar reaction conditions. The supramolecular yield can be determined by screening donors against a selection of acceptors of different acceptor strengths. Stronger donors will exhibit

a higher frequency of co-crystal formation or supramolecular yield, compared to weaker donor groups.



**Figure 2.6 Substitution of the R group with electron donating and electron withdrawing groups to tune the hydrogen bond donor ability of the donor site**

The goals of this chapter are to,

- Synthesize five symmetric aromatic dioximes. (Figure 2.7)
- Perform molecular electrostatic potential calculations on the five synthesized donors and the 20 acceptors

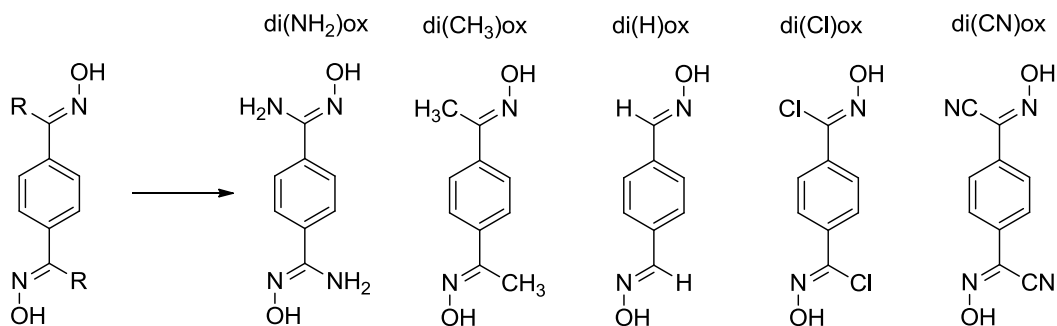


**Figure 2.7 Library of symmetric ditopic oximes**

- Screen the dioximes against a library of 20 monotopic, symmetric ditopic and symmetric tritopic acceptors.(Figure 2.8)

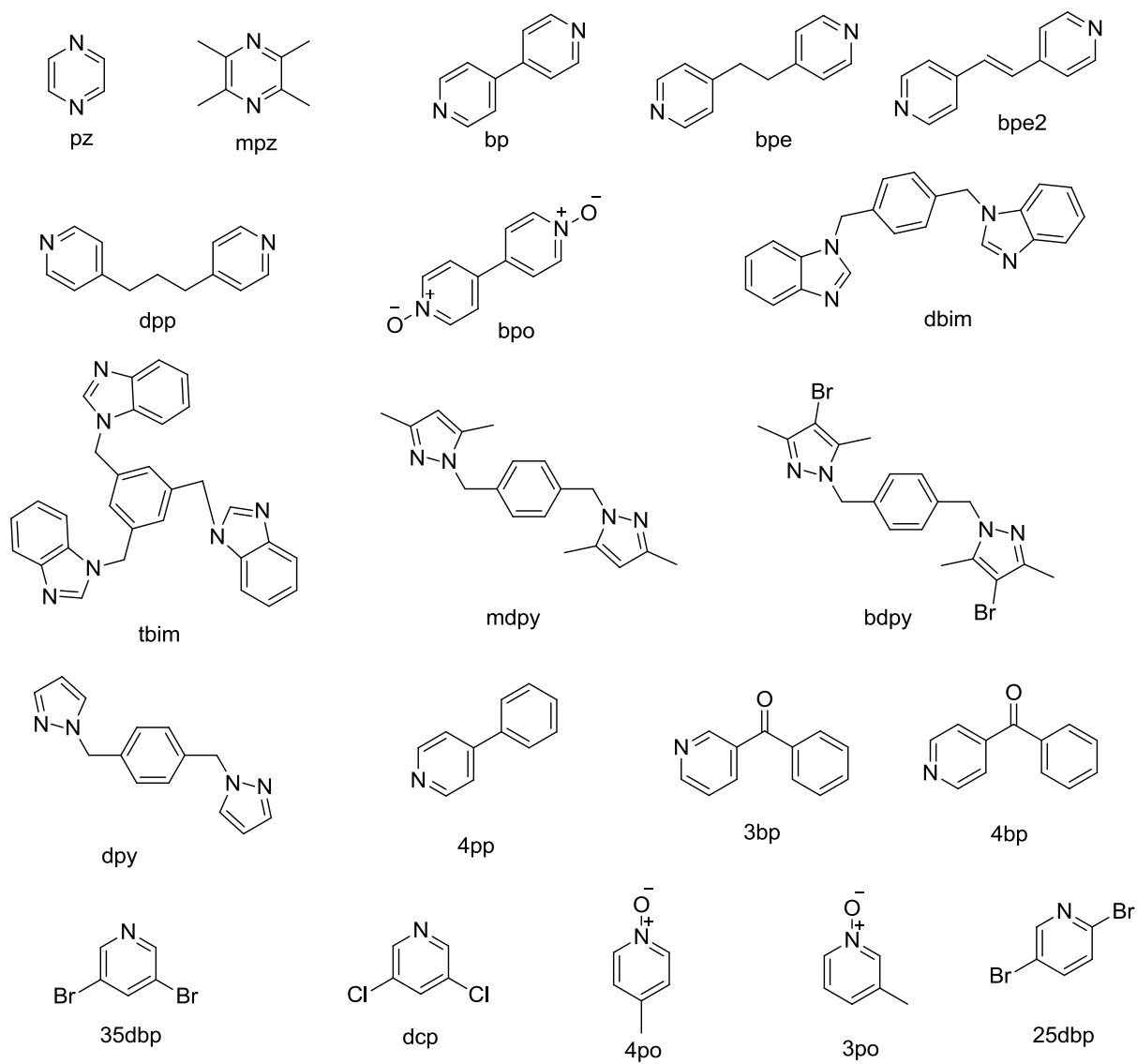


**Figure 2.8 Library of hydrogen bond acceptors used in this study**

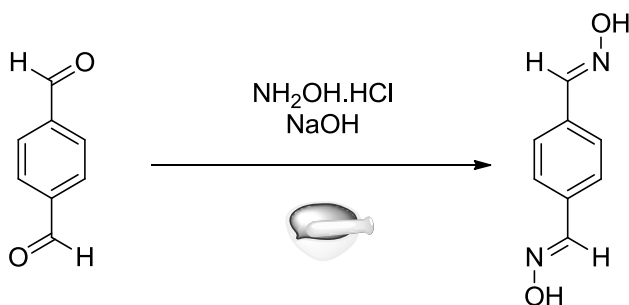
- Establish if it is possible to correlate the MEP values of each oxime with its ability to form co-crystals.

## 2.2. Experimental

### 2.2.1. Synthesis of dioximes

All chemicals were purchased from Aldrich, Fisher Scientific and used without further purification, Melting points were determined on a Gallenkamp melting point apparatus and are reported uncorrected.  $^1\text{H}$  and  $^{13}\text{C}$  NMR spectra were recorded on a Varian Unity plus 400 MHz spectrometer in  $\text{DMSO-}d_6$ . Compounds were prepared for infrared spectroscopic (IR) analysis on a ZnSe ATR crystal.

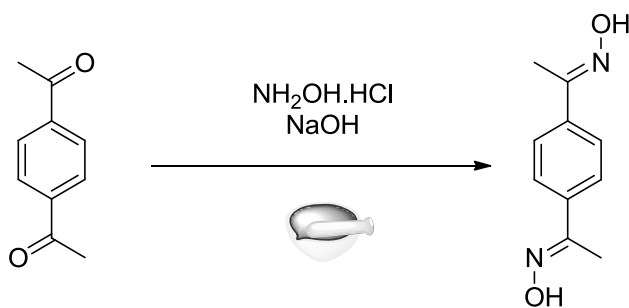
#### 2.2.1.1. Synthesis of 1,4-benzenedicarboxaldehyde dioxime, di(H)ox



Terephthalaldehyde (2.00 g, 14.9 mmol) and  $\text{NH}_2\text{OH}\cdot\text{HCl}$  (1.24 g 17.9 mmol) were ground together to a fine powder with a mortar and pestle.  $\text{NaOH}$  pellets (0.72 g, 17.9 mmol) were crushed and ground into the mixture. Two drops of methanol were added and grinding was continued for two more minutes. The mixture was allowed to stand for ten minutes, then ground again for two minutes. The absence of starting material was confirmed via TLC. The solid was dissolved in 200 ml of a 1:1 mixture of water and ethanol. The ethanol was removed under reduced pressure to isolate an off white solid. (2.2 g, 89.9%) m.p.  $218 - 220^\circ\text{C}$  (lit.  $219 - 220^\circ\text{C}$ )<sup>11</sup>  $^1\text{H}$  NMR (400 MHz,  $\text{DMSO-}d_6$ )  $\delta$  ppm 7.61 (4 H, s), 8.14 (2 H, s), 11.36 (2 H, s) IR:  $\nu$  1623  $\text{cm}^{-1}$  (C=N),  $\nu$  3143  $\text{cm}^{-1}$  (O-H),  $\nu$  962  $\text{cm}^{-1}$  (O-N)

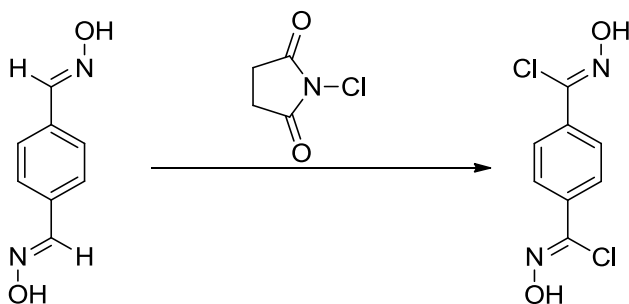


### 2.2.1.2. *Synthesis of 1,4-diacetylbenzene dioxime, di(CH<sub>3</sub>)ox*



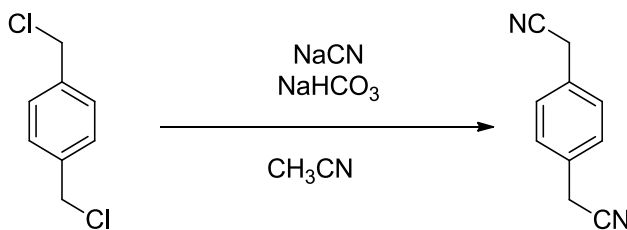
1,4-diacetylbenzene (2.00 g, 12.3 mmol) and  $\text{NH}_2\text{OH}\cdot\text{HCl}$  (1.03 g 14.8 mmol) were ground together to a fine powder with a mortar and pestle.  $\text{NaOH}$  pellets (0.59 g, 14.8 mmol) were crushed and ground into the mixture. Two drops of methanol were added and grinding was continued for two more minutes. The mixture was allowed to stand for ten minutes, and ground again for two minutes. The absence of starting material was confirmed via TLC. The solid was dissolved in 200 ml of a 1:1 mixture of water and ethanol. The ethanol was removed under reduced pressure to isolate a white solid. m.p. 165 - 170 °C (lit. 170 °C)<sup>11</sup>  $^1\text{H}$  NMR (400 MHz,  $\text{DMSO}-d_6$ )  $\delta$  ppm 2.15 (6 H, s), 7.66 (4 H, s), 11.28 (2 H, s) IR:  $\nu$  1660  $\text{cm}^{-1}$  (C=N),  $\nu$  3244  $\text{cm}^{-1}$  (O-H),  $\nu$  921  $\text{cm}^{-1}$  (O-N)

### 2.2.1.3. *Synthesis of N'1,N'4-dihydroxyterephthalimidoyl dichloride, di(Cl)ox*



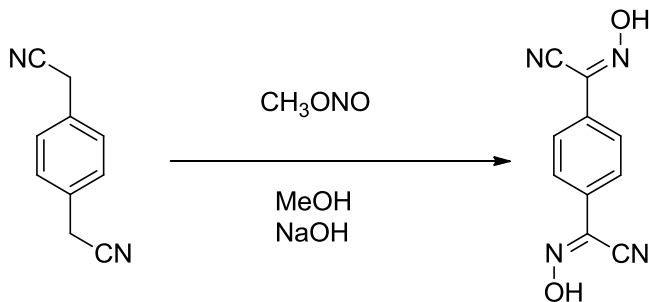
**di(H)ox** (0.75 g 0.0045 mol) was dissolved in 250 ml  $\text{CHCl}_3$ . N-chlorosuccinimide (2.7 g 0.020 mol) was added to the stirring suspension with a few drops of pyridine. The mixture was allowed to stir at room temperature for 24 hours. Once no starting material was observed by TLC the reaction mixture was washed with 10%  $\text{NaHCO}_3$ , water and brine. The organic layer was dried over  $\text{MgSO}_4$ , the solvent was removed under reduced pressure to yield a brown solid. (0.68 g 65.0%) m.p. 145 - 150 °C (lit. 177.5 -179 °C)<sup>18</sup>  $^1\text{H}$  NMR (400 MHz,  $\text{DMSO}-d_6$ )  $\delta$  ppm 7.89 (4 H, s), 12.63 (2 H, s) IR:  $\nu$  1686  $\text{cm}^{-1}$  (C=N),  $\nu$  3403  $\text{cm}^{-1}$  (O-H),  $\nu$  991  $\text{cm}^{-1}$  (O-N)

#### 2.2.1.4. *Synthesis of 2,2'-(1,4-phenylene)diacetonitrile*



$\alpha,\alpha'$ -Dichloro-*p*-xylene (2.00 g 11.4 mmol) was dissolved in 150 ml of acetonitrile. NaCN (2.23 g 45.6 mmol) was added to the stirring solution and stirred overnight at 50 °C, until no starting material was observed by TLC, the acetonitrile was removed under reduced pressure. The residue was dissolved in 200 ml ethyl acetate and washed repeatedly with water and brine. The organic layer was then dried over MgSO<sub>4</sub> and ethyl acetate removed under reduced pressure to yield pure product. (1.42 g 80.0%) m.p. 94 -98 °C (lit 96 - 98 °C)<sup>19</sup> <sup>1</sup>H NMR (400 MHz, DMSO-*d*<sub>6</sub>)  $\delta$  ppm 7.89 (4 H, s), 12.63 (2 H, s)

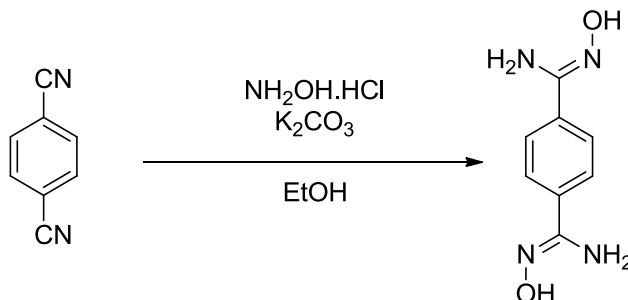
#### 2.2.1.5. *Synthesis of N'1,N'4-dihydroxyterephthalimidoyl cyanide, di(CN)ox*



2,2'-(1,4-Phenylene)diacetonitrile (1.2 g .0077 mol) was dissolved in 50 ml of methanol and poured into a solution of NaOH (10 g) in 300 ml of methanol. This was allowed to stir for 2 hours. MeONO gas was generated by pouring a solution of 16 ml conc. H<sub>2</sub>SO<sub>4</sub> in 32 ml of water dropwise into a solution of NaNO<sub>2</sub> (10 g, 0.145 mol) in 100 ml water and 50 ml methanol. The gas generated was bubbled through the solution of 2,2'-(1,4-phenylene)diacetonitrile over a period of 30 min. Once the bubbling was complete, the solution was stirred at room temperature for 48 hours. Methanol was removed under reduced pressure. The resulting solid was dissolved in 60 ml of water and slowly acidified with 6 M HCl in an ice bath. The resulting yellow solid was filtered off. (1.12 g, 68%) m.p. 170 °C dec. (lit 192-194 °C)<sup>20</sup> <sup>1</sup>H NMR (400 MHz, DMSO-*d*<sub>6</sub>)  $\delta$  ppm 7.86

(4 H, s), 14.07 (2 H, br. s.) IR:  $\nu$  2244  $\text{cm}^{-1}$  ( $\text{C}\equiv\text{N}$ ), 1427  $\text{cm}^{-1}$  ( $\text{C}=\text{N}$ ),  $\nu$  3274  $\text{cm}^{-1}$  ( $\text{O}-\text{H}$ ),  $\nu$  973  $\text{cm}^{-1}$  ( $\text{O}-\text{N}$ )

### 2.2.1.6. Synthesis of *N'*1,*N'*4-dihydroxyterephthalimidamide, *di*( $\text{NH}_2$ )*ox*



1,4-Dicyanobenzene (0.50 g, 0.039 mol) was dissolved in 100 ml ethanol with  $\text{NH}_2\text{OH}\cdot\text{HCl}$  (1.380 g, 0.097 mol). 30 ml of a solution of  $\text{K}_2\text{CO}_3$  (1.35 g, 0.097 mol) in water was then added. The solution was refluxed overnight and monitored by TLC until no starting material remained. The solvent was removed and the white solid was washed with water. (0.45 g, 60%) m.p. 215  $^\circ\text{C}$  dec. (lit. 210  $^\circ\text{C}$  dec.)<sup>11</sup>  $^1\text{H}$  NMR (400 MHz,  $\text{DMSO}-d_6$ )  $\delta$  ppm 5.84 (5 H, br. s.), 7.66 (4 H, s), 9.69 (2 H, s) IR:  $\nu$  1646  $\text{cm}^{-1}$  ( $\text{C}=\text{N}$ ),  $\nu$  3443  $\text{cm}^{-1}$  ( $\text{O}-\text{H}$ ),  $\nu$  923  $\text{cm}^{-1}$  ( $\text{O}-\text{N}$ )

### 2.2.2. Conditions used in the co-crystallization.

#### 2.2.2.1. Synthesis of 1,4-benzenedicarboxaldehyde, 1,4-dioxime 4-picolyyl-*N*-oxide(1:2), *di*( $\text{H}$ )*ox*:4*po*

**di**( $\text{H}$ )**ox** (0.010g, 0.061 mmol) was ground together with **4po** (0.007 g, 0.061 mmol) with a few drops of methanol until a homogenous mixture was obtained. The solid obtained was dissolved in 3 ml of methanol with heat and allowed to stand at room temperature for slow evaporation. Colorless prisms were obtained in two weeks. (m.p. 116 - 120  $^\circ\text{C}$ )

#### 2.2.2.2. Synthesis of *N'*1,*N'*4-dihydroxyterephthalimidoyl cyanide 4-picolyyl-*N*-oxide(1:1), *di*( $\text{CN}$ )*ox*:4*po*

**di**( $\text{CN}$ )**ox** (0.010g, 0.047 mmol) was ground together with **4po** (0.005 g, 0.047 mmol) with a few drops of methanol until a homogenous mixture was obtained. The solid obtained was dissolved in 4 ml of methanol with heat and allowed to stand at room temperature for slow evaporation. Yellow plates were obtained in 10 days. (m.p. 230  $^\circ\text{C}$  dec)

**2.2.2.3. Synthesis of N'1,N'4-dihydroxyterephthalimidoyl cyanide 4-benzoylpyridine (1:2), di(CN)ox:4bp**

**di(CN)ox** (0.010g, 0.047 mmol) was ground together with **3bp** (0.009 g, 0.047 mmol) with a few drops of methanol until a homogenous mixture was obtained. The solid obtained was dissolved in 4 ml of methanol with heat and allowed to stand at room temperature for slow evaporation. Colorless plates were obtained in 10 days. (m.p. 98 - 102 °C)

**2.2.2.4. Synthesis of N'1,N'4-dihydroxyterephthalimidoyl cyanide 4-benzoylpyridine (1:2), di(CN)ox:3bp**

**di(CN)ox** (0.010g, 0.047 mmol) was ground together with **3bp** (0.009 g, 0.047 mmol) with a few drops of methanol until a homogenous mixture was obtained. The solid obtained was dissolved in 4 ml of methanol with heat and allowed to stand at room temperature for slow evaporation. Yellow plates were obtained in 14 days. (m.p. 95 - 100 °C)

**2.2.2.5. Synthesis of N'1,N'4-dihydroxyterephthalimidamide DMSO (1:2), di(NH<sub>2</sub>)ox:DMSO**

**di(NH<sub>2</sub>)ox** (0.010g, 0.051 mmol) was ground together with **bpe** (0.009 g, 0.051 mmol) with a two drop of methanol until a homogenous mixture was obtained. The solid obtained was dissolved in 1 ml of DMSO with heat and allowed to stand at room temperature for slow evaporation. Colorless plates were obtained in 30 days. (m.p. 210 °C dec.)

**2.2.3. Semi empirical AM1 calculations**

The molecular structures of the five donors and the 20 acceptors were constructed using Spartan '06 (Wavefunction, Inc. Irvine, CA). All molecules were optimized using Semi-empirical AM1 with the maxima and minima in the electrostatic potential surface (0.002 e/au isosurface) determined using a positive point charge in the vacuum as a probe.

**2.2.4. Solvent drop grinding experiments**

0.01 g of the donor was ground together with the acceptor in a 1:1 molar ratio on a well plate with a drop of methanol. After two minutes of grinding the solid was analyzed via infra-red spectroscopy.

## 2.3.Results

### 2.3.1. Molecular electrostatic potential calculations

AM1 Calculations were carried out on the five donors (Table 2.2) and the 20 acceptors (Table 2.3) with Spartan 06.

**Table 2.2 Calculated molecular electrostatic potential values for the five donors**

	<b>di(NH<sub>2</sub>)ox</b>	<b>di(CH<sub>3</sub>)ox</b>	<b>di(H)ox</b>	<b>di(Cl)ox</b>	<b>di(CN)ox</b>
Donor					
MEP/kJmol <sup>-1</sup>	124	140	144	163	185

The calculated molecular electrostatic potential values for the oxime proton changes significantly with different substituents. Electron donating groups decrease the MEP value and electron withdrawing groups increase the MEP value.

**Table 2.3 Calculated molecular electrostatic potential values for the 20 acceptors**

		Name	MEP(AM1)/kJmol <sup>-1</sup>
N-Oxides	3po	3-Picolyl-N-oxide	-313
	4po	4-Picolyl-N-oxide	-312
	bpo	4,4'-Bipyridine-bis-N-oxide	-287
Benzimidazoles	dbim	1,4-Bis((1H-benzo[d]imidazol-1-yl)methyl)benzene	-295
	tbim	1,3,5-Tris((1H-benzo[d]imidazol-1-yl)methyl)benzene	-289
Bipyridyls	bpe	1,2-Bis(4-pyridyl)ethane	-285
	bpe2	(E)-1,2-Di(pyridin-4-yl)ethene	-285
	dpp	4,4'-Trimethylenedipyridine	-281

	bp	4,4'-Bipyridine	-269
Pyridine	3bp	3-Benzoylpyridine	-271
	4bp	4-Benzoylpyridine	-268
	4pp	4-Phenylpyridine	-267
	25dbp	2,5-Dibromopyridine	-257
	dcp	3,5-Dichloropyridine	-232
	35dbp	3,5-Dibromopyridine	-230
Pyrazoles	dmpy	1,4-Bis((3,5-dimethyl-1H-pyrazol-1-yl)methyl)benzene	-254
	dpy	1,4-Bis((1H-pyrazol-1-yl)methyl)benzene	-248
	bdpy	1,4-Bis((4-br-3,5-dime-1H-pyrazol-1-yl)methyl)benzene	-237
Pyrazines	mpz	2,3,5,6-Tetramethylpyrazine	-273
	pz	Pyrazine	-224

Calculated MEP values for the acceptors show a wide spread of AM1 values which can be roughly grouped according to the class of compound as N-oxides > benzimidazoles > bipyridyls > pyridines > pyrazoles > pyrazine.

### 2.3.2. Solvent drop grinding experiments

Table 2.4 contains the summarized results obtained through solvent drop grinding. The donors are arranged according to increasing MEP charge from left to right, and the acceptors are arranged according to decreasing negative MEP value from top to bottom.

It can be observed in table 2.4, that there is a higher incidence of positive hits at higher positive MEP value of the donors and higher negative MEP values of the acceptors.

**Table 2.4 Supramolecular yields based on IR spectroscopy**

	Name	di(NH <sub>2</sub> )ox	di(CH <sub>3</sub> )ox	di(H)ox	di(Cl)ox	di(CN)ox
MEP(AM1)		124	140	144	163	185
-313	3po	√	√	√	√	√
-312	4po	√	√	√	√	√
-295	Dbim	-	√	√	√	√
-289	Tbim	-	√	√	√	√
-287	Bpo	√	√	√	√	√
-285	Bpe	√	√	√	√	√
-285	bpe2	-	√	√	√	√
-281	dpp	√	√	√	√	√
-273	mpz	-	-	√	√	√
-271	3bp	-	-	√	√	√
-269	bp	√	√	√	√	√
-268	4bp	-	-	√	√	√
-267	4pp	-	√	√	√	√
-257	25dbp	-	-	-	-	√
-254	dmpy	-	√	√	√	√
-248	dpy	-	-	-	√	√
-237	bdpy	-	-	-	√	√
-232	dcp	-	-	-	-	√
-230	35dbp	-	-	-	-	√
-224	pz	-	-	-	-	√
Number of positive hits		6/20	11/20	14/20	16/20	20/20
Supramolecular yield		30%	55%	70%	80%	100%

2.3.2.1. *Crystal structure of 1,4-Benzenedicarboxaldehyde dioxime 4-picolyl-N-oxide(1:2), di(H)ox:4po*

The crystal structure of **di(H)ox:4po** contains one molecule of **di(H)ox** and two molecules of **4-picoline-N-oxide**. The supermolecule is constructed through O-H...O hydrogen bonds between the O-H of the oxime and the 4-picoly-N-oxide oxygen atom O17...O21, 2.644(2) Å, forming a zero dimensional trimer. (Figure 2.9) The two acceptor sites on the oxime moiety, showed no hydrogen-bonding activity.

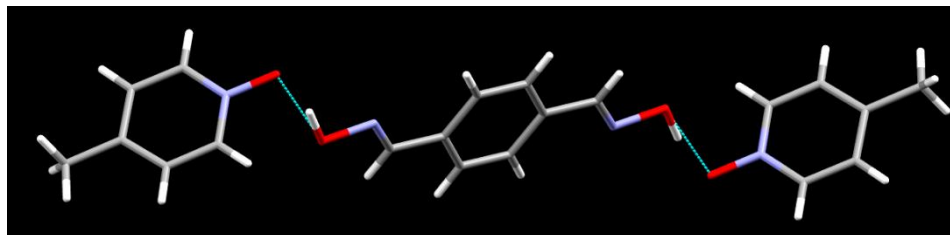


Figure 2.9 The supramolecular trimer in the 1:1 binary co-crystal of di(H)ox:4po

2.3.2.2. *Crystal structure of N'1,N'4-dihydroxyterephthalimidoyl cyanide, 1,4-dioxime 4-picolyl-N-oxide(1:1), di(CN)ox:4po*

The crystal structure of **di(CN)ox:4po** contains one molecule **di(CN)ox** and one molecule of **4-picoline-N-oxide**. The supermolecule is constructed through O-H...O hydrogen bonds between the O-H of the oxime and the 4-picoly-N-oxide oxygen atom O31...O21, 2.591(3) Å, the N-oxide oxygen binds to two oxime O-H groups forming a one dimensional chain.(Figure 2.10) The two acceptor sites on the oxime moiety, showed no hydrogen-bonding activity in this co-crystal.

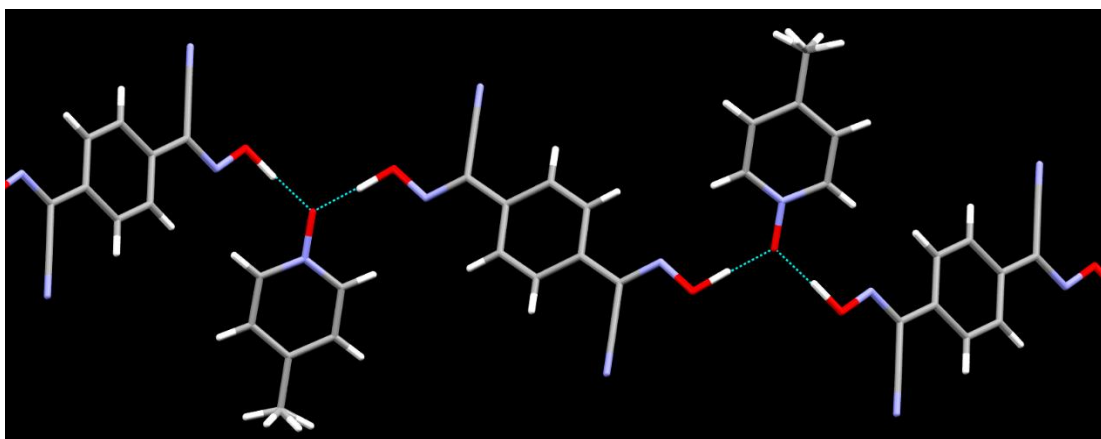


Figure 2.10 The infinite chain in the 1:1 binary co-crystal of di(CN)ox:4po



2.3.2.3. *Crystal structure of N'1,N'4-dihydroxyterephthalimidoyl cyanide, 1,4-dioxime 4-benzoylpyridine (1:2), di(CN)ox:4bp*

The crystal structure of **di(CN)ox:4bp** contains one molecule **di(CN)ox** and two molecules of **4-benzoylpyridine**. The supermolecule is constructed through O-H...N hydrogen bonds between the O-H of the oxime and the 4-picolyl-N-oxide oxygen atom O17...N21, 2.714(2) Å, forming a zero dimensional trimer.(Figure 2.11) The two acceptor sites on the oxime and the carbonyl oxygen on the acceptor, showed no hydrogen-bonding activity.

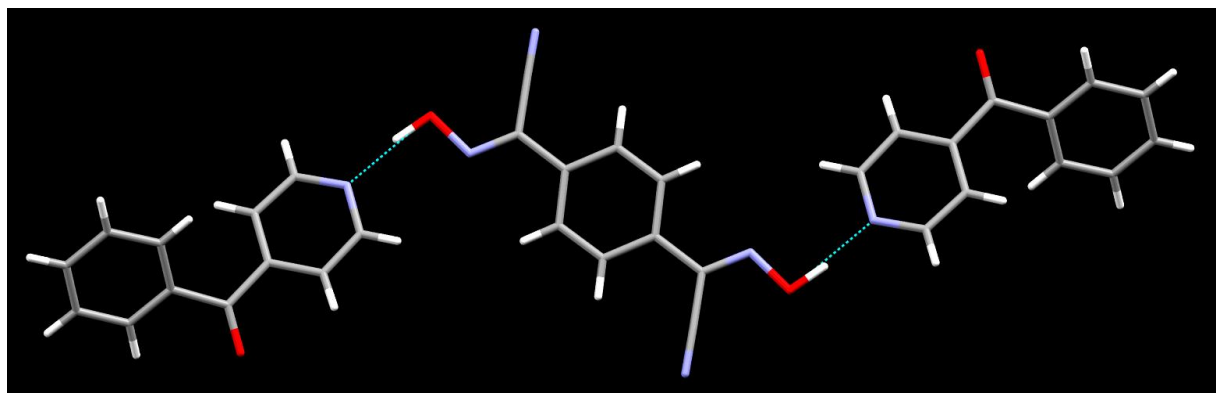
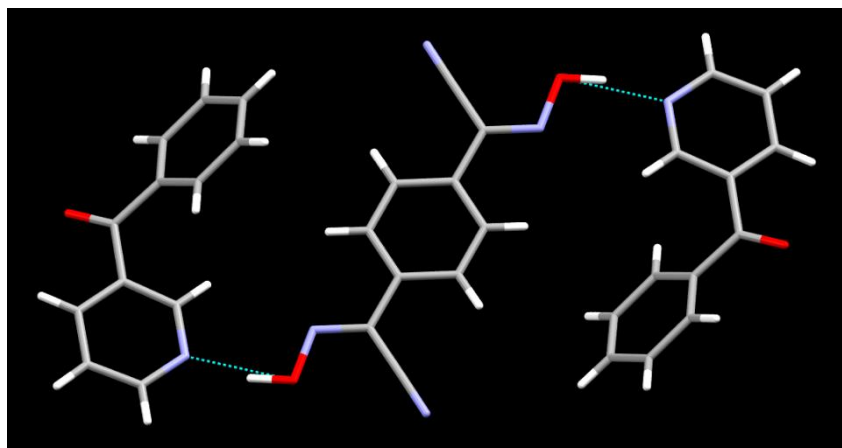


Figure 2.11 The supramolecular trimer in the 1:2 binary co-crystal of di(CN)ox:4bp

2.3.2.4. *Crystal structure of N'1,N'4-dihydroxyterephthalimidoyl cyanide, 1,4-dioxime 3-benzoylpyridine (1:2), di(CN)ox:3bp*

The crystal structure of **di(CN)ox:3bp** contains one molecule **di(CN)ox** and two molecules of **3-benzoylpyridine**. The supermolecule is constructed through O-H...N hydrogen bonds between the O-H of the oxime and the 4-picolyl-N-oxide oxygen atom O17...N21, 2.673(4) Å, forming a zero dimensional trimer.(Figure 2.12) The two acceptor sites on the oxime and the carbonyl oxygen on the acceptor, showed no hydrogen bonding activity in this structure.



**Figure 2.12** The supramolecular trimer in the 1:2 binary co-crystal of di(CN)ox:3bp

**2.3.2.5. Crystal structure of *N*'1,*N*'4-dihydroxyterephthalimidamide, DMSO (1:2), *di*(NH<sub>2</sub>)ox:DMSO**

The crystal structure of **di(NH<sub>2</sub>)ox:DMSO** contains one molecule of **di(NH<sub>2</sub>)ox** and two molecules of **DMSO**. The supermolecule is constructed through an oxime-oxime dimer with O-H···N hydrogen bonds between the O-H and the nitrogen atom on the oxime O17···N17, 2.743(3) Å, and the NH<sub>2</sub> group picks up two DMSO molecules O1S···N18, 3.004 (3) Å, O1S···N18, 3.007(3) Å resulting in a solvate.(Figure 2.13)

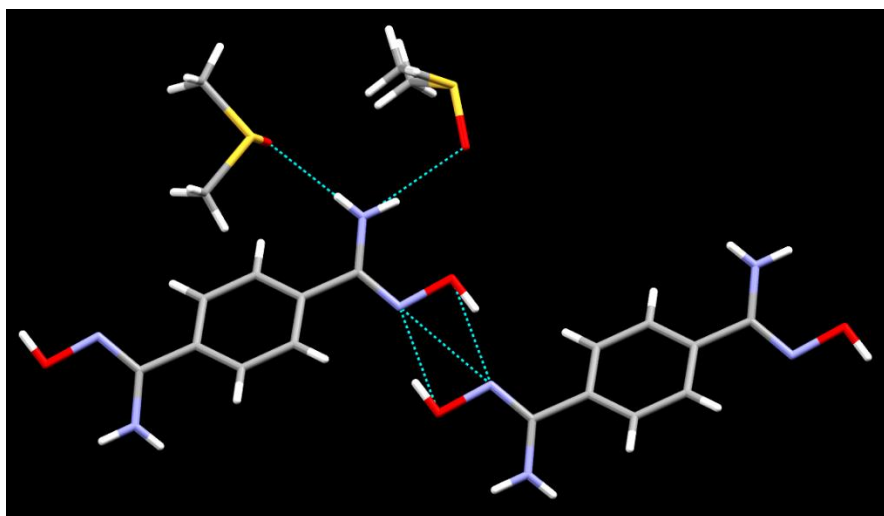


**Figure 2.13** The supramolecular tetramer in the 1:2 binary solvate of di(NH<sub>2</sub>)ox:DMSO

## 2.4. Discussion

### 2.4.1. Synthesis

The five dioximes were synthesized with little difficulty. **Di(H)ox** and **di(CH<sub>3</sub>)ox** were synthesized through a solid state approach<sup>21</sup> where pure product was obtained in a matter of minutes. The same approach was not successful in the synthesis of **di(NH<sub>2</sub>)ox** where only partial reactivity was observed. No column chromatography was used to purify any of these products.

### 2.4.2. Infra-red spectroscopy

Infra-red spectroscopy was the tool of choice in detecting the formation or absence of a new supramolecular species. Typically, hydrogen bonding in this type of screen can be easily detected by the O-H...N interaction which provides the unmistakable broad stretches in the 1,900 cm<sup>-1</sup> and 2,500cm<sup>-1</sup><sup>13</sup>(Figure 2.14).

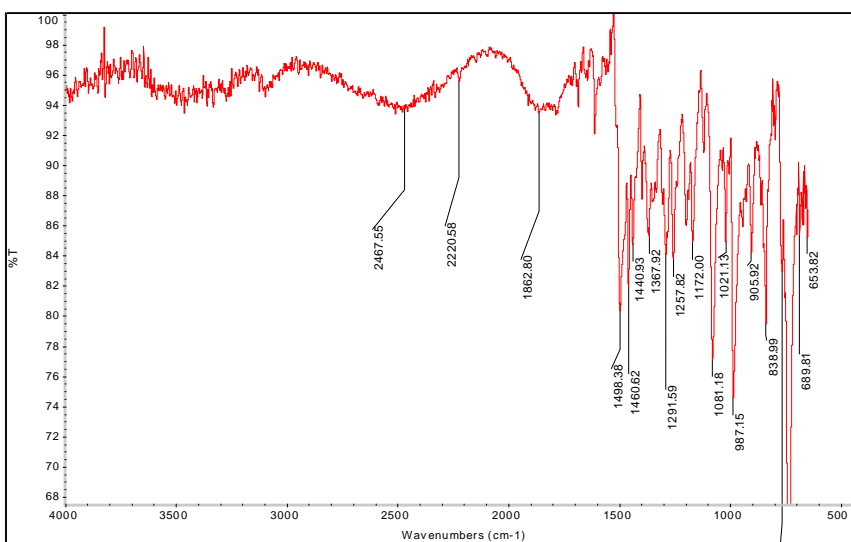


**Figure 2.14 The IR spectrum of the 1:1 grind of di(CN)ox:dbim clearly showing both O-H...N stretches at 1862 cm<sup>-1</sup> and 2467 cm<sup>-1</sup>.**

In this study it was observed that with both donors and acceptors with lower MEP values that this stretch was not observed. Evidence of supramolecular interaction was still observed by the shift of the C=N stretch around 1660 cm<sup>-1</sup> and the C≡N stretch around 2240 cm<sup>-1</sup> in the case of cyanooximes. For example the C=N stretch of **di(H)ox** (1,4-Benzenedicarboxaldehyde, 1,4-dioxime) at 1623 cm<sup>-1</sup> shifts to 1603 cm<sup>-1</sup> after it was ground with **dbim** (1,4-bis((1H-benzo[d]imidazol-1-yl)methyl)benzene), Figure 2.15. Similarly, the C=N stretch is observed at

1615  $\text{cm}^{-1}$  in the co-crystal **di(H)ox:dbim** which proves that this shift is indicative of the formation of a co-crystal.

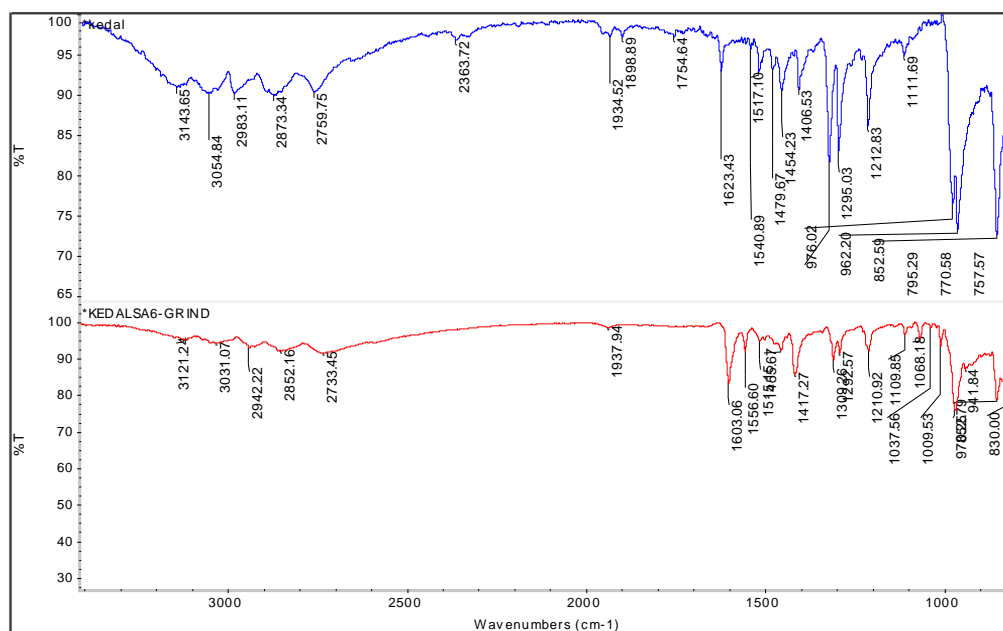


**Figure 2.15** The IR spectra of **di(H)ox** and the 1:1 grind of **di(H)ox** and **dbim**

### 2.4.3. The effect of the MEP values and pKa on supramolecular yield

pKa has commonly been used to rank hydrogen bond donor ability<sup>13,22</sup>. The hierarchy of donors established based on pKa values matches that established via calculated MEP values. The combined results of the grinding experiments clearly show a trend between the calculated MEP values of the oximes and the supramolecular yield as shown in Table 2.5. The donor with the lowest MEP value (**di(NH<sub>2</sub>)ox**) exhibits the lowest supramolecular yield and **di(CN)ox** with the highest MEP value exhibit a 100% supramolecular yield. These observations present the possibility of increasing the supramolecular yields by increasing the MEP potential value of the donor sites via covalent modification.

**Table 2.5** The effect of the MEP values and pKa on supramolecular yield

Donor	<b>di(NH<sub>2</sub>)ox</b>	<b>di(CH<sub>3</sub>)ox</b>	<b>di(H)ox</b>	<b>di(Cl)ox</b>	<b>di(CN)ox</b>
MEP/kJmol <sup>-1</sup>	124	140	144	163	185
pKa <sup>23</sup>	14.43	10.97	10.27	9.70	7.47
Supramolecular yield	30%	55%	70%	80%	100%

The two supramolecular architectures to be expected in this study are zero dimensional trimers with the monotopic acceptors and one dimensional chains with the symmetric ditopic acceptors. (Figure 2.16)

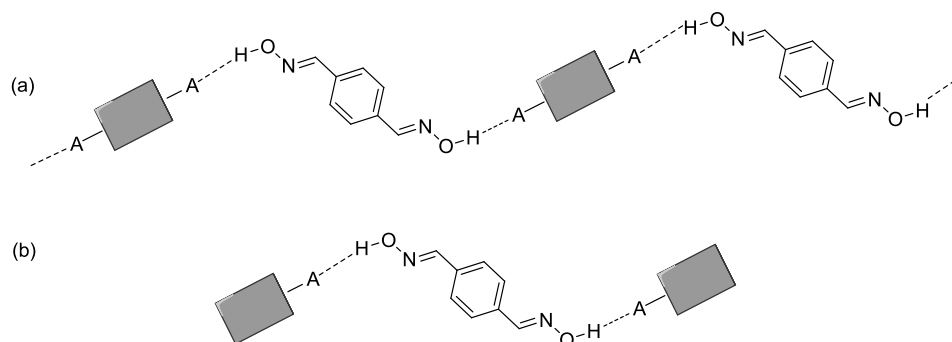


**Figure 2.16 Expected supramolecular architectures (a) 1D chains (b) 0D trimers**

The structures obtained so far, exhibit the expected architectures. In the case of 4-picoline-N-oxide (**4po**) the N-oxide group contains two lone pairs and therefore can accommodate two hydrogen bonds. In the cases of **di(H)ox:4po** and **di(CN)ox:4po**, with 1,4-benzenedicarboxaldehyde dioxime (**di(H)ox**), the N-oxide (**4po**) acts as a single point acceptor as the oxime (**1**) picks up a single lone pair in **di(H)ox:4po**. In the case of N'1,N'4-dihydroxyterephthalimidoyl cyanide, 1,4-dioxime (**di(CN)ox**) both lone pairs on **4po** are picked up by cyanooxime molecules forming an infinite chain.

Another observation was that the two acceptor sites on the oxime moiety (Figure 2.2) showed no hydrogen bond activity in any of the co-crystals obtained. A CSD survey also confirms this trend where no oxime-oxime homomeric interactions were observed in the presence of sterically unhindered acceptor groups. Calculated AM1 values show the charge on the nitrogen atom on the cyanooxime moiety to be between 180-238 kJ/mol which is in the same range as the weaker acceptors in our screen that had a very low supramolecular yield. Therefore it seems that the donor selectively picks up the stronger acceptor.

No co-crystals suitable for X-ray diffraction were obtained from N'1,N'4-dihydroxyterephthalimidamide (**di(NH<sub>2</sub>)ox**) in solution experiments due to its low solubility which resulted in the oxime crashing out in all 20 cases. Using DMSO to improve solubility resulted in the formation of a single 1:2 solvate with DMSO where the oxime group formed an oxime-oxime dimer and the -NH<sub>2</sub> group formed hydrogen bonds with the oxygen atom on DMSO instead of the oxygen atom on the oxime group (Figure 2.4 (a)). No crystals suitable for X-ray

diffraction were obtained with N'1,N'4-dihydroxyterephthalimidoyl dichloride (**di(Cl)ox**) as the ligand decomposed over time resulting in an opaque solution/solid.

## 2.5. Conclusions

The molecular electrostatic potential value of the oxime moiety can be tuned by altering the R substituent (Figure 2.4) where, the donor ability increases with the electron withdrawing substituents and is reduced by electron donating substituents. Similar trends for donor ability were predicted through pKa values and calculated MEP values which matched perfectly with supramolecular yields showing the following trend for increasing donor ability,  $\text{NH}_2 < \text{CH}_3 < \text{H} < \text{Cl} < \text{CN}$ . (Figure 2.17)

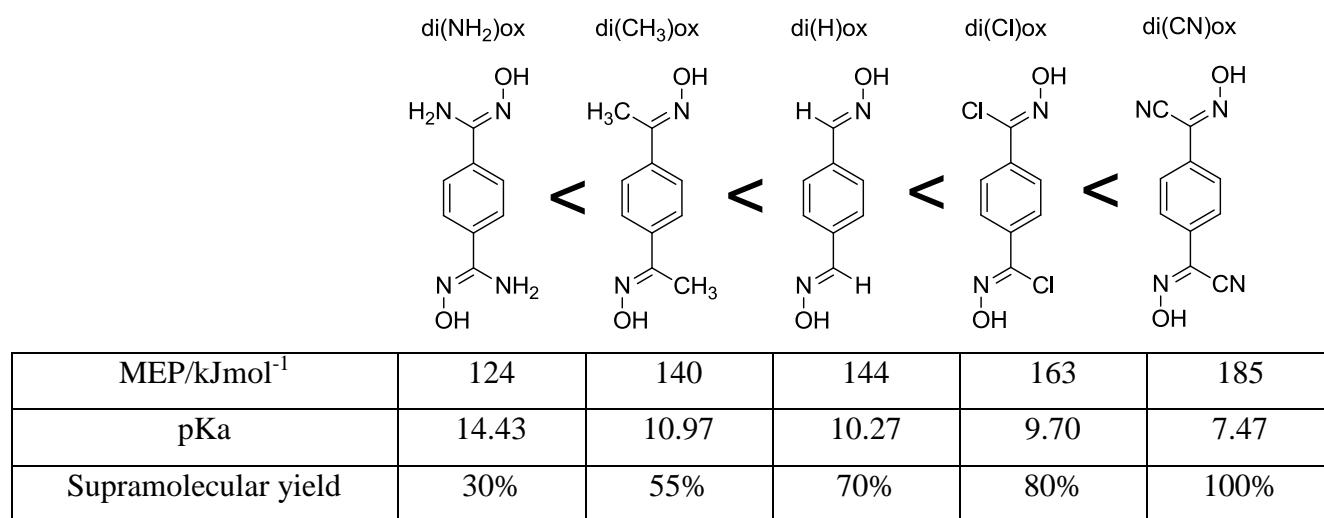
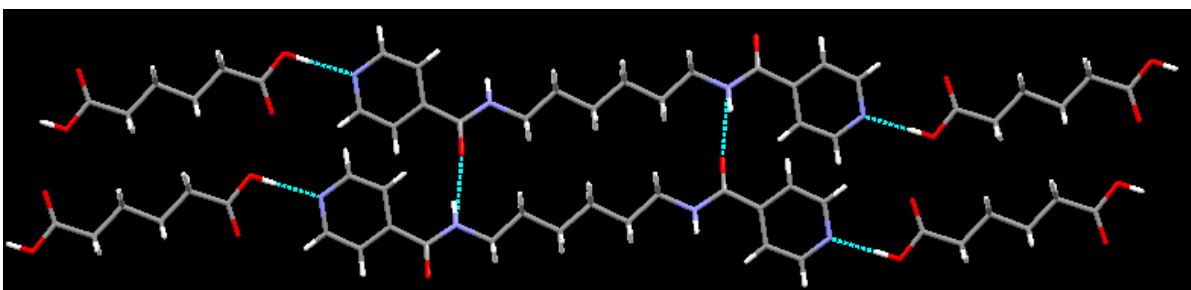


**Figure 2.17 oximes arranged according to increasing donor ability with matching trends in MEP and pKa values.**

Based on the results obtained from solvent drop grinding experiments, the supramolecular yield can be tuned by changing the MEP value on the oxime moiety through covalent modification. The hydrogen bond donating ability of the oxime can be decreased by using electron donating groups as substituents and increased by using electron withdrawing substituents.

Symmetric ditopic donors such as aliphatic di-carboxylic acids have been used to improve the physical properties of pharmaceuticals and agrochemicals by forming one dimensional chain type co-crystals<sup>24</sup> (Figure 2.18).



8

**Figure 2.18 Tuning the melting point of a pharmaceutical via co-crystallization<sup>24</sup>**

Exploring the same possibility with aromatic symmetric ditopic acids like terephthalic acid has been limited due to its lower solubility. The lower pKa of carboxylic acids (benzoic acid, pKa= 4.2) results in the formation of salts with stronger bases<sup>25</sup> which makes targeted supramolecular synthesis increasingly difficult<sup>26</sup>. Tuning the hydrogen bonding ability of acids is limited to functionalizing the aromatic rings in aromatic acids<sup>27</sup>. Symmetric ditopic oximes have better solubility compared to similar acids. They have pKa values that are much higher than that of carboxylic acids (Table 2.6) and therefore have a reduced tendency to form salts.

**Table 2.6 Calculated pKa values of the donors**

Donor	di(NH <sub>2</sub> )ox	di(CH <sub>3</sub> )ox	di(H)ox	di(Cl)ox	di(CN)ox	Terephthalic acid
pKa <sup>23</sup>	14.43	10.97	10.27	9.70	7.47	3.51
MEP/kJmol <sup>-1</sup>	124	140	144	163	185	154

## References

---

- <sup>1</sup> M. Kato, S. Nishino, M. Ohno, S. Fukuyama, Y. Kita, Y. Hirasawa, and Y. Nakanishi, H. Takasugi, K. Sakane, *Bioorg. Med. Chem. Lett.*, **1996**, *6*, 33–38
- <sup>2</sup> H. J. de Silva, R. Wijewickrema, N. Senanayake, *Lancet* **1992**, *339*, 1136-38
- <sup>3</sup> A. Nakayama, H. Iwamura, A. Niwa, Nakagawa, and Y. Fujita, *J. Agric. Food Chem.* **1985**, *33*, 1034–1041
- <sup>4</sup> Y. Yu. Scaffidi-Domianello, K. Meelich, M. A. Jakupec, V. B. Arion, V. Yu. Kukushkin, M. Galanski and B. K. Keppler, *Inorg. Chem.*, **2010**, *49*, **12**, 5669–5678
- <sup>5</sup> C. B. Aakeröy, A. M. Beatty and D. S. Leinen, *CrystEngComm*, **2002**, *4*, 310-314
- <sup>6</sup> H. Iwamura *J. Med. Chem.*, **1980**, *23*, 308–312
- <sup>7</sup> S. W. Wiener, and R. S. Hoffman, *Journal of Intensive Care Medicine* **2004**, *19*, **1**, 22-37
- <sup>8</sup> G. S. Papaefstathiou, A. J. Kipp and L. R. MacGillivray, *Chem. Commun.*, **2001**, 2462-2463
- <sup>9</sup> T. Friščić, D. M. Drab, and L. R. MacGillivray *Org. Lett.* **2004**, *6*, **25**, 4647–4650
- <sup>10</sup> C. B. Aakeröy, J. Desper and B. A. Helfrich, *CrystEngComm*, **2004**, *6*, 19-24
- <sup>11</sup> E. A. Bruton, L. Brammer, F. C. Pigge, C. B. Aakeröy and D. S. Leinen, *New J. Chem.*, **2003**, *27*, 1084–1094
- <sup>12</sup> A. A. Espenbetov, Yu. T. Struchkov, L. V. Rybakova, *J. Struct. Chem.* **1986**, *27*, 180-181
- <sup>13</sup> C. B. Aakeröy, D. J. Salmon, M. M. Smith, and J. Desper *Crystal Growth & Design*, **2006**, *6*, **4**, 1033-1042
- <sup>14</sup> M. H. Abraham, J. Gil-Lostes, J. E. Cometto-Muñiz, W. S. Cain, C. F. Poole, S. N. Atapattu, R. J. Abraham and P. Leonard, *New J. Chem.*, **2009**, *33*, 76-81
- <sup>15</sup> C.A. Hunter, *Angew. Chem. Int. Ed.* **2004**, *43*, 5310-5324.
- <sup>16</sup> D. Musumeci, C.A. Hunter, R. Prohens, S. Scuderi and J. F. McCabe, *Chem. Sci.*, **2011**, *2*, 883-890.
- <sup>17</sup> C. B. Aakeröy, A. M. Beatty, and B. A. Helfrich, *J. Am. Chem. Soc.*, **2002**, *124*, **48**, 14425–14432
- <sup>18</sup> I. Özyaytekin and I. Karatas, *J. Heterocyclic Chem.*, **2005**, *42*, 1283.
- <sup>19</sup> C. R. Harrison, P. Hodge, *Synthesis*, **1980**, *4*, 299-301
- <sup>20</sup> I. V. Ovchinnikov, A. O. Finogenov, M. A. Epishina, Y. A. Strelenko and N. N. Makhova, *Mendeleev Communications*, **2009**, *19*, 217-219
- <sup>21</sup> C. B. Aakeröy, A. S. Sinha, K. N. Epa and J. Desper, *Chem. Commun.*, **2012**, *48*, 11289-11291
- <sup>22</sup> C. B. Aakeröy, J. Desper and J. F. Urbina *Chem. Commun.*, **2005**, 2820-2822
- <sup>23</sup> Calculated using Advanced Chemistry Development (ACD/Labs) Software V11.02 (© 1994-2012 ACD/Labs)
- <sup>24</sup> C. B. Aakeröy, S. Forbes, J. Desper, *J. Am. Chem. Soc.*, **2009**, *131*, **47**, 17048–17049
- <sup>25</sup> J. A. Bis and M. J. Zaworotko *Crystal Growth & Design*, **2005**, *5*, **3**, 1169–1179
- <sup>26</sup> C. B. Aakeröy, M. E. Fasulo, and J. Desper, *Mol. Pharmaceutics*, **2007**, *4*, **3**, 317–322
- <sup>27</sup> C. B. Aakeröy, P. D. Chopade, C. Ganser, A. Rajbanshi and J. Desper *CrystEngComm*, **2012**, *14*, 5845-5853



## Chapter 3. $pK_a$ vs calculated molecular electrostatic potential values: which is better at predicting molecular recognition?

### 3.1. Introduction

The synthesis of solid forms that consist of more than a single component (co-crystals) offer the possibility for a molecule of interest to exist in a variety of physical forms. Co-crystals provide means for modulating and fine-tuning physical properties such as melting point<sup>1</sup>, solubility,<sup>28</sup> and hygroscopicity<sup>2</sup> of a given compound without affecting its intrinsic chemical properties or activity. This function of multi-component solid-state architectures have drawn interest from areas such as pharmaceuticals<sup>28,3</sup>, agrochemicals<sup>4</sup>, non-linear optics<sup>5</sup>, explosives<sup>6</sup>, and organic semiconductors<sup>7</sup>. A clear understanding of the underlying non-covalent interactions and selectivity is required for the rational design of co-crystals. A comprehensive analysis of the Cambridge Structural Database for groups of neutral molecules with sterically accessible hydrogen-bonding groups was carried out by Etter and co-workers to determine the possible preferences for individual functional groups in terms of selectivity and patterns of aggregation in solids. Based on their results, a set of guidelines was proposed<sup>8</sup>.

- All **good** proton donors and acceptors are **used** in hydrogen bonding
- If a six-membered intramolecular hydrogen bond can form, it will usually do **so** in preference to forming intermolecular hydrogen bonds
- The best proton donors and acceptors remaining after intramolecular hydrogen-bond formation, form intermolecular hydrogen bonds to one another

To expand on rule number three we propose that in a competitive situation with multiple donors and acceptors, the best donor will selectively bind to the best acceptor and the second best donor will bind to the second best acceptor (Figure 3.1).

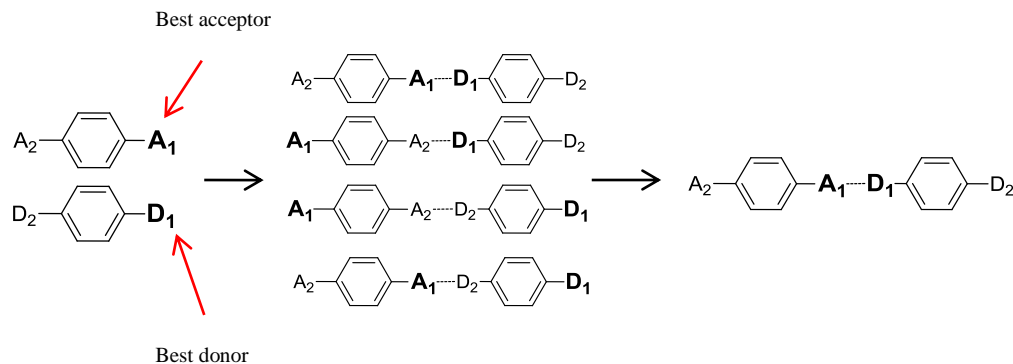


**Figure 3.1** The four possible outcomes with a pair of symmetric ditopic donors and acceptors (an expansion of Etter's rules).

The classification of best donors and acceptors requires a way to rank hydrogen-bond donors and acceptors within some form of hierarchy.

The direct use of pKa or pKa based methods have proven effective in some studies as predictors for hydrogen-bond donor ability. As shown in Figure 3.2, a ternary co-crystal was designed with the asymmetric ditopic acceptor iso-nicotinamide and two aromatic acids, where 3,5-dinitrobenzoic acid (pKa 2.8) selectively binds to the pyridyl nitrogen, which is the stronger acceptor of iso-nicotinamide and 3-methylbenzoic acid (pKa = 4.3) binds to the weaker amide group.

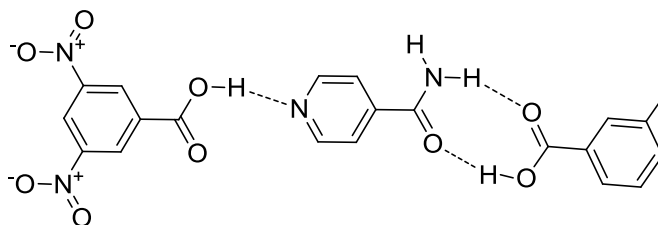


**Figure 3.2** A 1:1:1 ternary cocrystal of 3,5-dinitrobenzoic acid : iso-nicotinamide : 3-methylbenzoic acid designed based on pKa<sup>9</sup> differences.

A pKa based “slide rule”<sup>10</sup> was proposed by Gilli et. al. using the concept of resonance assisted hydrogen bonding<sup>11</sup>. According to this approach, weaker hydrogen bonds are considered to be electrostatic and stronger hydrogen bonds have a covalent component that increases as the difference in pKa between the donor and the protonated acceptor approaches zero. The scale (Figure 3.3) consists of two columns of donors and protonated acceptors arranged according to pKa values and strongest donor acceptor pairs are matched along horizontal lines. The hierarchy of donors however, is still decided by the pKa values.

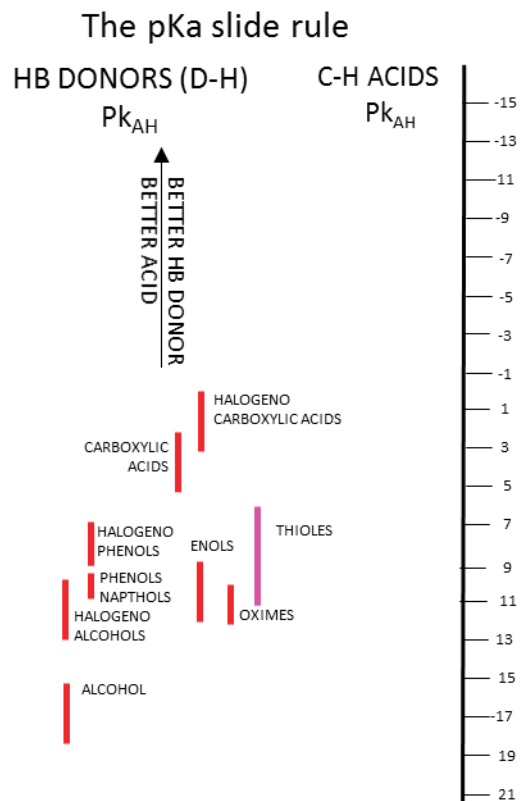


**Figure 3.3 The pKa slide scale<sup>10</sup>**

The pKa based method appears to work well in systems limited to one type of donor functionality but does not hold well when comparing different donor groups. For example if we consider phenols and thiophenols, thiophenols ( $pK_a = 6.61$ ) have a higher pKa compared to phenols ( $pK_a = 9.86$ ) and are better donors according to the slide scale. Upon looking at experimental data, however phenols have proven to be strong hydrogen bond donors while thiophenols show little hydrogen bond donor ability compared to the<sup>12,13,14</sup>.

A linear relationship was observed by Abraham et. al. when association constants ( $\log K$ ) for various acids were recorded for a given base (Figure 3.4). Data analyzed similarly for 45 different bases resulted in 45 linear relationships all in the form of Equation 3.1<sup>15</sup>.

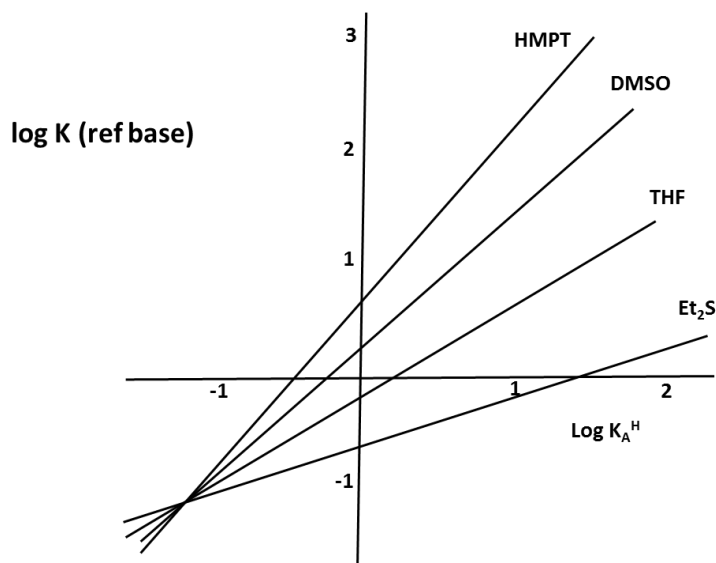


**Figure 3.4 Plots of  $\log K$  (acids against reference base) vs  $\log K_A^{Hi}$  <sup>15</sup>**

The  $\log K_A^{Hi}$  value characterizes the acid and the  $L_B$  and  $D_B$  values characterize the base. The  $\log K_A^{Hi}$  values can be used as a quantitative scale of hydrogen-bond acidity which can be calculated from experimentally obtained association constants<sup>16</sup> using equation 3.1

$$\log K^i = L_B \log K_A^{Hi} + D_B \quad 3.1$$

The Abraham model for determining solute properties (SP) incorporates parameters to indicate hydrogen bonding ability as shown in equation 3.2

$$\log SP = c + eE + sS + aA + bB + vV \quad 3.2$$

E is the excess molar refraction, V is the McGowan volume, S is the dipolarity/polarizability, A is hydrogen bond acidity and B is hydrogen bond basicity. These values can be calculated from GLC or HPLC data<sup>17</sup> by calibrating the stationary phase with solutes where the other values are known using Equation 3.2. Computational methods have also been used to predict Abraham parameters<sup>18,19</sup>.

An alternative computational method was suggested by Hunter et. al.. who attempt to explain hydrogen bonding based on electrostatics. Where the association constant (K) of two simple molecules can be treated as shown in Equation 3.3 where,  $\alpha^H_2$  and  $\beta^H_2$  are functional group constants that relate to the hydrogen bond donor and hydrogen-bond acceptor properties. This is

equivalent to the expression of the electrostatics of the hydrogen bonding interaction, where the free energy of interaction changes with the product of the positive charge on the hydrogen-bond donor ( $\alpha^H_2$ ) and the negative charge on the hydrogen bond acceptor ( $\beta^H_2$ )

$$\log K = c_1 \alpha^H_2 \beta^H_2 + c_2 \quad 3.3$$

The charge parameter can be determined by a molecular electrostatic potential surface constructed around the molecule where the maxima correspond to the charges on the donors and the minima correspond to the charge on the acceptors (equation 3.4 and 3.5)<sup>20</sup>.

$$\alpha = E_{\max}/52 \text{ kJmol}^{-1} = 4.1 (\alpha^H_2 + 0.33) \quad 3.4$$

$$\beta = -E_{\min}/52 \text{ kJmol}^{-1} = 10.3 (\beta^H_2 + 0.06) \quad 3.5$$

These  $\alpha$  and  $\beta$  values can be used for the comparison and ranking of hydrogen bond donor and acceptor groups respectively

An extension of the above approach was used to predict co-crystallization in systems with multiple donor and acceptor sites<sup>21</sup>.

$$E = -\sum_{ij} \alpha_i \beta_j \quad 3.6$$

Here  $\alpha$  and  $\beta$  were calculated based on MEP values obtained using a higher level of theory where energy was minimized using DFT B3LYP/6-31+G\* *ab initio* calculations.  $\alpha$  and  $\beta$  values were calculated using equations 3.7 and 3.8. Calculated in this method were closer to experimental values compared to that by AM1.

$$\alpha = 0.0000162 \text{ MEP}_{\max}^2 + 0.00962 \text{ MEP}_{\max} \quad 3.7$$

$$\beta = 0.000146 \text{ MEP}_{\min}^2 - 0.00930 \text{ MEP}_{\min} \quad 3.8$$

In this chapter we will explore the possibility of using calculated molecular electrostatic potential values to qualitatively rank different hydrogen bond donor groups by screening asymmetric ditopic donors with geometrically unbiased acceptors.

For this study we have selected carboxylic acids, which according to its pKa is one of the strongest donor functionalities available (benzoic acid - pKa = 4.20), to compare with phenols and aldoximes. Phenols are widely used as donor functionalities in the synthesis of co-crystals<sup>22</sup>, but are considered weaker donors due to their lower pKa values (phenol - pKa= 9.86). Similarly, aldoximes have shown potential as a hydrogen-bond donor functionality that is capable of forming co-crystals<sup>23</sup>, but it too has been considered to be weaker compared to carboxylic acids based on pKa. (benzaldehyde oxime - pKa=10.80) No data has been published to date comparing these two functionalities.

To examine the balance and competition between carboxylic acids phenols and aldoximes, we have selected three asymmetric ditopic donors, which contain the carboxylic acid functionality and with a phenol or an aldoxime group as shown in Figure 3.5. These three donors were screened against nine geometrically unbiased acceptors shown in Figure 3.6. The selectivity of donors and acceptors can be established by studying the crystal structures obtained through single crystal X-ray diffraction.

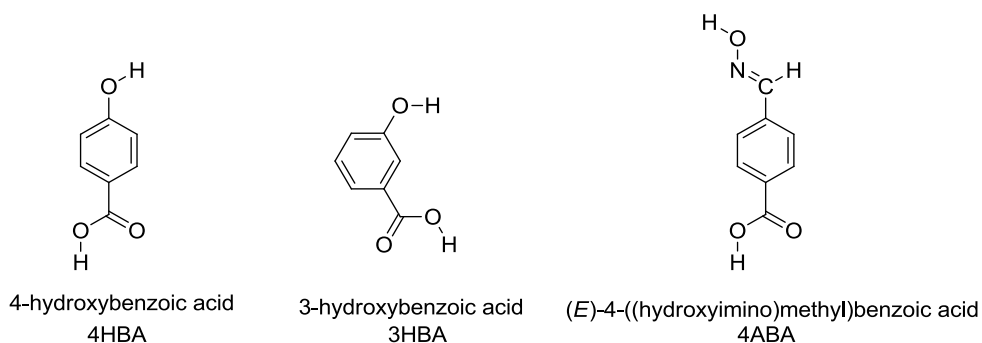


**Figure 3.5 asymmetric ditopic donors containing –COOH groups**

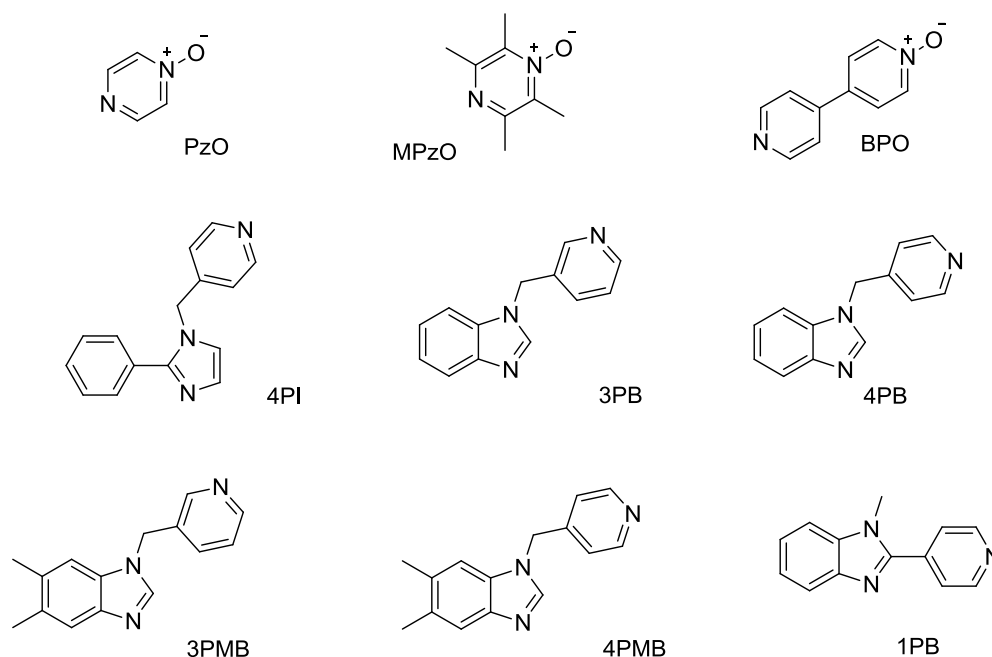


**Figure 3.6 The library of asymmetric ditopic acceptors**

The goals for this chapter are to,

- Synthesize the required donors and acceptors from Figure 3.5 and Figure 3.6.
- Perform DFT and AM1 molecular electrostatic potential calculations on the three donors and the nine acceptors.
- Screen the donors against the acceptors using solvent assisted grinding and slow evaporation.
- Examine structural data and evaluate the initial hypothesis.

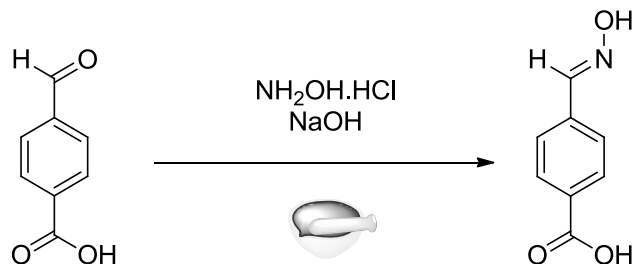
## 3.2.Experimental

### 3.2.1. Synthesis

All chemicals were purchased from Aldrich, Fisher Scientific and used without further purification, Melting points were determined on a Gallenkamp melting point apparatus and are reported uncorrected.  $^1\text{H}$  and  $^{13}\text{C}$  NMR spectra were recorded on a Varian Unity plus 400 MHz spectrometer in DMSO- $d_6$ . Compounds were prepared for infrared spectroscopic (IR) analysis on

a ZnSe ATR crystal. 3-Hydroxybenzoic acid (3HBA) and 4-hydroxybenzoic acid (4HBA) were purchased from Sigma-Aldrich and used without further purification.

#### 1.1.1.1. *Synthesis of 4-((hydroxyimino)methyl)benzoic acid, 4ABA*



4-Formylbenzoic acid (2.00 g, 13.3 mmol) and  $\text{NH}_2\text{OH}\cdot\text{HCl}$  (1.11 g 16.0 mmol) were ground together to a fine powder with a mortar and pestle.  $\text{NaOH}$  pellets (0.64 g, 16.0 mmol) were crushed and ground into the above mixture. Four drops of methanol were added and grinding was continued for two more minutes. The mixture allowed to stand for ten minutes, then ground again for two minutes. The absence of starting material was confirmed via TLC. The solid was dissolved in 200 ml of a 1:1 mixture of water and ethanol. Ethanol was removed under reduced pressure and the product was extracted into ethyl acetate, washed with brine and dried over  $\text{MgSO}_4$ . The ethyl acetate was removed under reduced pressure to isolate an off white solid. (1.76 g 80%) m.p. 212 - 216  $^\circ\text{C}$  (lit. 218  $^\circ\text{C}$ )  $^1\text{H}$  NMR (400 MHz,  $\text{DMSO}-d_6$ )  $\delta$  ppm 7.70 (2 H, d,  $J=8.59$  Hz), 7.95 (8 H, d,  $J=8.20$  Hz), 8.21 (1 H, s), 11.53 (1 H, s), 13.04 (1 H, br. s.)

#### 1.1.1.2. *Synthesis of 1-(pyridin-4-ylmethyl)-1H-benzo[d]imidazole,*

Benzimidazole (0.5 g, 4.23 mmol) was dissolved in 50 ml of acetonitrile. Crushed  $\text{NaOH}$  (0.508 g 12.7 mmol) was added to the solution and was stirred for 3 hours. 4-Picolylchloride hydrogen chloride (0.69 g, 4.23 mmol) was dissolved in 50 ml of acetonitrile and added to the benzimidazole solution and stirred for 6 hours. Once the absence of the picolyl chloride was confirmed via TLC, the acetonitrile was removed under reduced pressure. The resulting oil was dissolved in ethyl acetate and washed with 1 N  $\text{NaOH}$ , distilled water and brine. The solution was dried over  $\text{MgSO}_4$ . Ethyl acetate was removed under reduced pressure to yield a brown solid. (5.40 g, 69.4%) m.p. 105-110  $^\circ\text{C}$  (lit. 130  $^\circ\text{C}$ )<sup>24</sup>  $^1\text{H}$  NMR ( $\text{DMSO}-d_6$ , 400MHz): d = 8.51 (d,  $J=6.2$  Hz, 1 H), 8.42 (s, 1 H), 7.68 (dd,  $J=9.0, 3.5$  Hz, 1 H), 7.46 (dd,  $J=9.4, 3.5$  Hz, 1 H), 7.21 (dd,  $J=9.0, 3.5$  Hz, 1 H), 7.18 (d,  $J=5.5$  Hz, 1 H), 5.58 ppm (s, 1 H)



### 3.2.2. *Synthesis of co-crystals*

#### 3.2.2.1. *Synthesis of 4-hydroxybenzoic acid, 3PB (1:1), 4HBA:3PB*

**4HBA** (0.010g, 0.072 mmol) and **3PB** (0.015 g, 0.072 mmol) were dissolved in 5 ml of ethanol with heat and allowed to stand at room temperature for slow evaporation. Colorless plates were obtained in two weeks. (m.p. 140 -145<sup>0</sup>C)

#### 3.2.2.2. *Synthesis of 3-hydroxybenzoic acid, 3PB (1:1), 3HBA:3PB*

**3HBA** (0.010g, 0.072 mmol) and **3PB** (0.015 g, 0.072 mmol) were dissolved in 5 ml of ethanol with heat and allowed to stand at room temperature for slow evaporation. Colorless prisms were obtained in two weeks.( m.p. 130 – 140<sup>0</sup>C)

#### 3.2.2.3. *Synthesis of 4-hydroxybenzoic acid, 4PMB (1:1), 4HBA:4PMB*

**4HBA** (0.010g, 0.072 mmol) and **4PMB** (0.017 g, 0.072 mmol) were dissolved in 5 ml of ethanol with heat and allowed to stand at room temperature for slow evaporation. Colorless plates were obtained in two weeks. (m.p. 110 – 120 <sup>0</sup>C)

#### 3.2.2.4. *Synthesis of 3-hydroxybenzoic acid, 3PMB (1:1), 3HBA:3PMB*

**3HBA** (0.010g, 0.072 mmol) and **3PMB** (0.017 g, 0.072 mmol) were dissolved in 5 ml of 1:1 acetone:chloroform with a drop of methanol with heat and allowed to stand at room temperature for slow evaporation. Light brown blocks were obtained in five days. (m.p.70 -74 <sup>0</sup>C)

#### 3.2.2.5. *Synthesis of 4-((hydroxyimino)methyl)benzoic acid, 1PB (1:1), 4ABA:1PB*

**4ABA** (0.010g, 0.061 mmol) and **1PB** (0.013 g, 0.061 mmol) were dissolved in 5 ml of methanol with heat and allowed to stand at room temperature for slow evaporation. Yellow prisms were obtained in two weeks. (m.p.88 - 90 <sup>0</sup>C)

#### 3.2.2.6. *Synthesis of 4-((hydroxyimino)methyl)benzoic acid, 4PMB (1:1), 4ABA:4PMB*

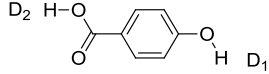
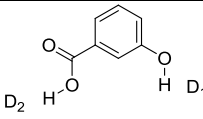
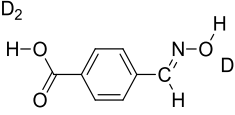
**4ABA** (0.010g, 0.061 mmol) and **4PMB** (0.013 g, 0.061 mmol) were dissolved in 5 ml of methanol with heat and allowed to stand at room temperature for slow evaporation. Colorless prisms were obtained in two weeks. (m.p. 131 - 135 <sup>0</sup>C)

### 3.3.Results

#### 3.3.1. Calculations

##### 3.3.1.1. Molecular electrostatic potential (MEP) calculations

**Table 3.1** MEP calculations on the donors show the carboxylic acid to be the weaker donor

	AM1 MEP /kJmol <sup>-1</sup>		DFT MEP /kJmol <sup>-1</sup>	
	D <sub>1</sub>	D <sub>2</sub>	D <sub>1</sub>	D <sub>2</sub>
	191	138	305	244
	175	144	283	253
	154	139	276	258

Based on the both DFT and AM1 MEP calculations the carboxylic acid is the weaker donor in all three donor molecules. The MEP based ranking of donor groups contradicts the pKa based ranking in all three cases.

**Table 3.2** MEP calculations for the acceptors

Name	AM1 MEP /kJmol <sup>-1</sup>		DFT MEP /kJmol <sup>-1</sup>	
	A <sub>1</sub>	A <sub>2</sub>	A <sub>1</sub>	A <sub>2</sub>
<b>PzO</b>	-266	-232	-161	-144
<b>MPzO</b>	-287	-255	-177	-147
<b>BPO</b>	-294	-249	-182	-168
<b>4PI</b>	-291	-252	-200	-186
<b>1PB</b>	-290	-279	-182	-179
<b>3PB</b>	-292	-262	-201	-175
<b>4PB</b>	-291	-268	-195	-174
<b>3PMB</b>	-296	-261	-210	-180
<b>4PMB</b>	-291	-268	-203	-177

Similar to the donors the hierarchy of functional groups stays the same with the acceptors according to AM1 and DFT calculations.

### 3.3.2. Identification on co-crystals

The formation of co-crystals was confirmed by IR spectroscopy based on the O-H $\cdots$ N stretch (1800-1900 cm<sup>-1</sup>) and changes in the carbonyl peak, Fig 3.7 as an example.

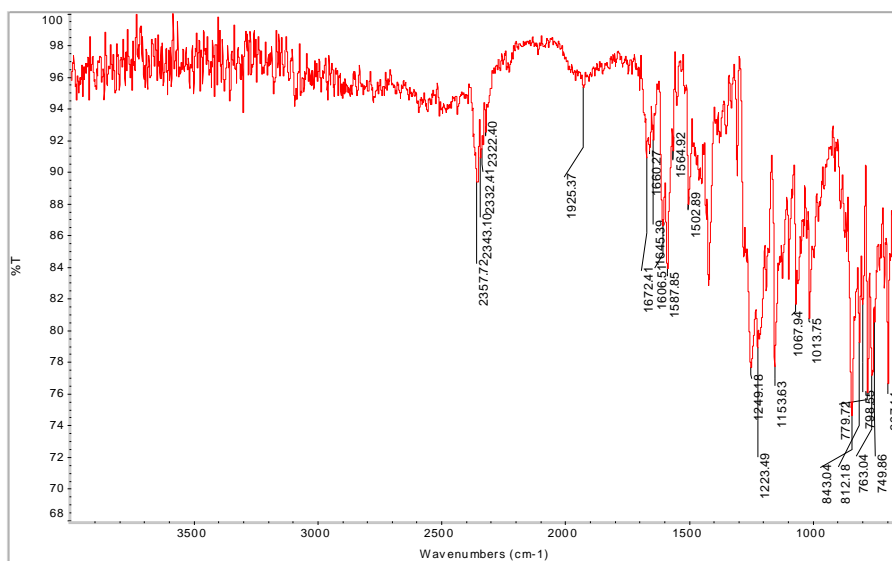


Figure 3.7 The IR spectrum of the crystal 4HBA:4PMB

Table 3.3 Relevant IR results from solvent drop grinding experiments

Acceptor	3-HBA		4-HBA		4-ABA		
	O-H $\cdots$ N	C=O	O-H $\cdots$ N	C=O	C=O	O-H $\cdots$ N	C=N
None	-	1681	-	1669	1662	-	1609
<b>PzO</b>	-	1698	-	1691	1700	1832	1596
<b>MPzO</b>	1932	1692	1904	1681	1683	-	1585
<b>BPO</b>	1935	1687	1940	1666	1681	1884	1606
<b>4PI</b>	1920	1665	1877	1686	1683	1904	1605
<b>1PB</b>	1920	1685	1935	1680	1683	1866	1568
<b>3PB</b>	1928	1693	1864	1666	1683	1925	1605
<b>4PB</b>	1932	1693	1912	1671	1692	1921	1606
<b>3PMB</b>	1935	1692	1912	1667	1688	1934	1582
<b>4PMB</b>	1926	1694	1929	1667	1692	1933	1565

The OH...N stretch and the significant changes in the C=O and C=N stretches indicate the formation of co-crystals in all 27 cases.

### 3.3.3. Description of crystal structures

#### 3.3.3.1. Crystal structure of 4-hydroxybenzoic acid, 3PB (1:1), 4HBA:3PB

The crystal structure of **4HBA:3PB** consists of one molecule of **4-HBA** and one molecule of **3PB**. The best donor, the –OH moiety, forms a hydrogen bond to the benzimidazole site, (O34...N13 2.7238(13) Å) leaving the second-best donor, the –COOH group, to form a hydrogen bond with the second-best acceptor, the pyridyl nitrogen atom, (O31...N21 2.6627(13) Å). (Figure 3.8).

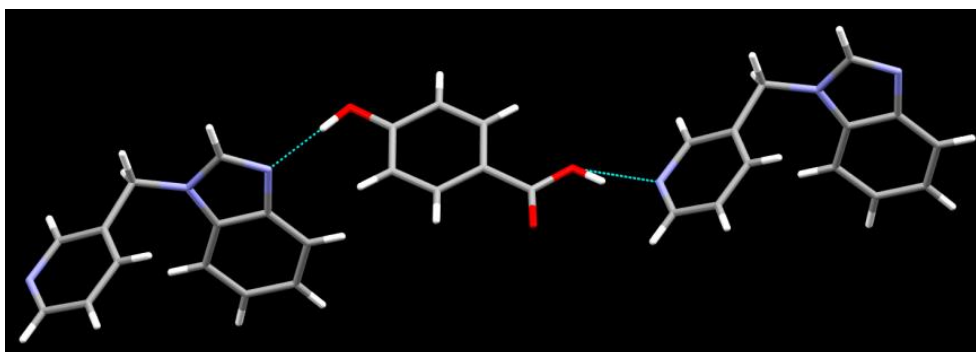
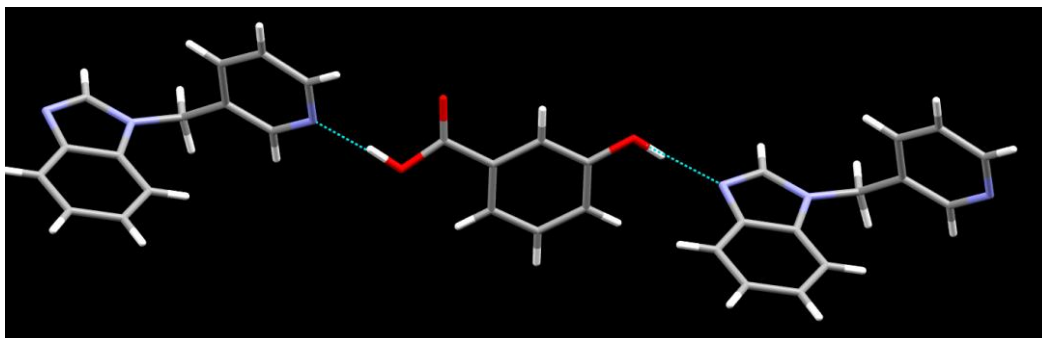


Figure 3.8 The primary hydrogen-bond interactions in the crystal structure of 4HBA:3PB

#### 3.3.3.2. Crystal structure of 3-hydroxybenzoic acid, 3PB (1:1), 3HBA:3PB

The crystal structure of **3HBA:3PB** consists of one molecule of **3-HBA** and one molecule of **3PB** where the –OH moiety, forms a hydrogen bond to the benzimidazole site, (O33...N13 2.6778(16) Å) and the –COOH forms a hydrogen bond with the second-best acceptor, the pyridyl nitrogen atom, (O31...N21 2.6266(17) Å) (Figure 3.9).



**Figure 3.9** The primary hydrogen-bond interactions in the crystal structure of 3HBA:3PB

**3.3.3.3. Crystal structure of 4-hydroxybenzoic acid, 4PMB (1:1), 4HBA:4PMB**

The crystal structure of **4HBA:4PMB** consists of one molecule of **4-HBA** and one molecule of **4PMB** and  $\frac{1}{4}$  of a water molecule. In this hydrated co-crystal, the best donor –OH moiety, forms a hydrogen bond to the benzimidazole site, (O44 $\cdots$ N13 2.683(3) Å), and the second best donor –COOH forms a hydrogen bond with the pyridyl nitrogen atom, second-best acceptor (O41 $\cdots$ N31 2.659(3) Å) (Figure 3.10)

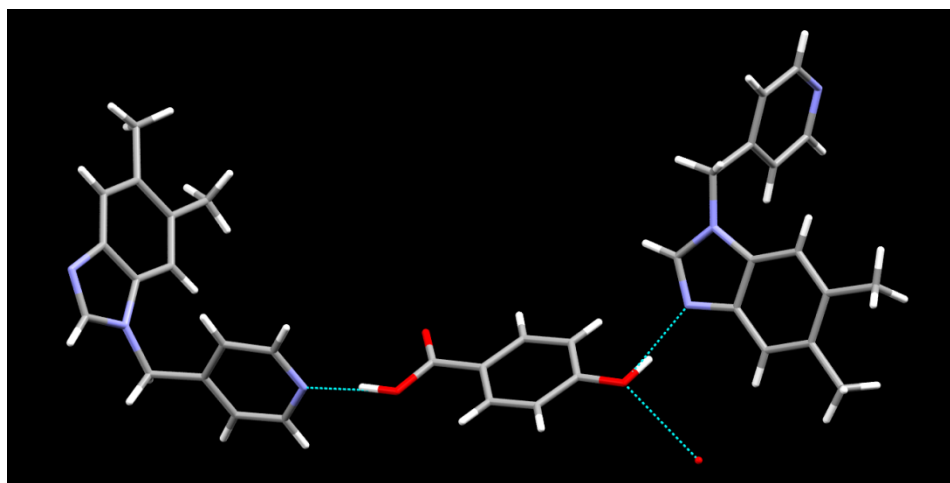


**Figure 3.10** The primary hydrogen-bond interactions in the crystal structure of 4HBA:4PMB

**3.3.3.4. Crystal structure of 3-hydroxybenzoic acid, 3PMB (1:1), 3HBA:3PMB:CH<sub>3</sub>CN.H<sub>2</sub>O**

The crystal structure of **4HBA:4PMB** consists of one molecule of **4-HBA** and one molecule of **4PMB**. In this solvated co-crystal, the best donor –OH moiety, forms a hydrogen bond to the

benzimidazole site, (O43...N13 2.728(3) Å), and the second best donor –COOH forms a hydrogen bond with the pyridyl nitrogen atom, second-best acceptor (O41...N31 2.669(3) Å) (Figure 3.11)

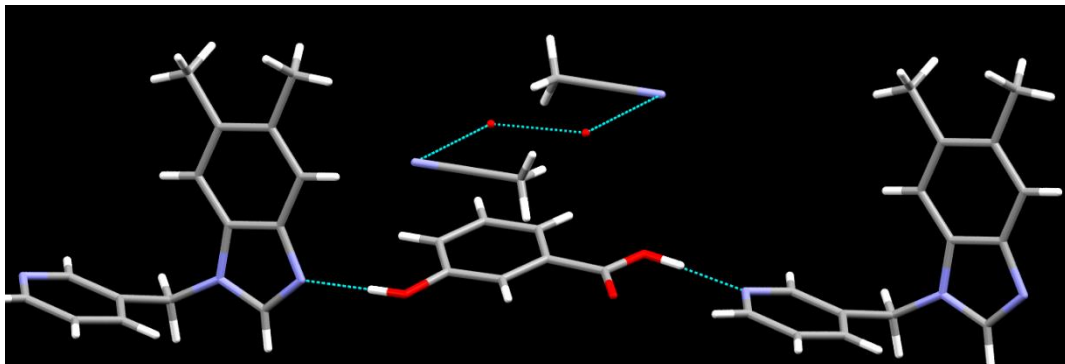


**Figure 3.11** The primary hydrogen-bond interactions in the crystal structure of 3HBA:3PMB:CH<sub>3</sub>CN.H<sub>2</sub>O

**3.3.3.5.** *Crystal structure of 4-((hydroxyimino)methyl)benzoic acid, 4PMB (1:1), 4ABA:4PMB*

The crystal structure of **4ABA:4PMB** consists of one molecule of **4-ABA** and one molecule of **1PB**. In this co-crystal, the best donor, oxime moiety, forms a hydrogen bond to the benzimidazole site, (O48...N13 2.777(15) Å), and the second best donor –COOH forms a hydrogen bond with the pyridyl nitrogen atom, second-best acceptor (O41...N31 2.637(16) Å) (Figure 3.12)

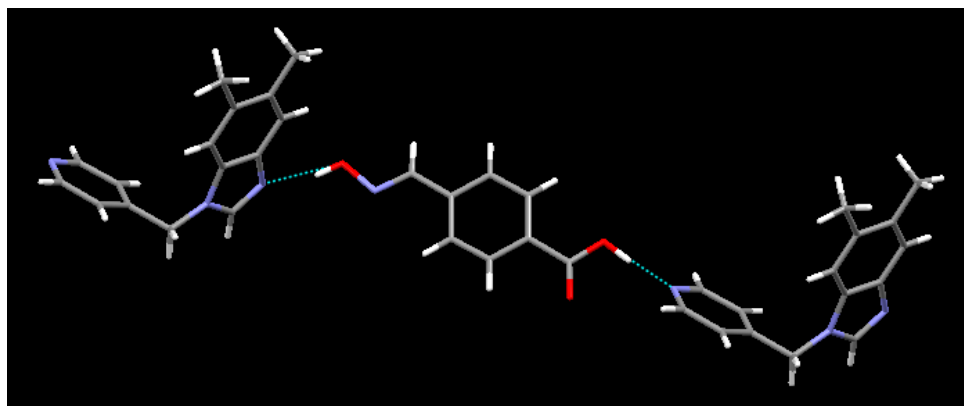


**Figure 3.12** The primary hydrogen-bond interactions in the crystal structure of 4ABA:4PMB

**3.3.3.6.** *Crystal structure of 4-((hydroxyimino)methyl)benzoic acid, 1PB (2:1), 4ABA:1PB*

The crystal structure of **4ABA:1PB** consists of two molecules of **4-ABA** and one molecule of **1PB**. In this co-crystal, the best donor oxime moiety, forms a hydrogen bond to the benzimidazole site, ( $O48 \cdots N13$  2.671(2) Å), and the second best donor –COOH forms a hydrogen bond with the pyridyl nitrogen atom, second-best acceptor ( $O31 \cdots N21$  2.704(2) Å) In addition, it forms an acid-acid dimer ( $O41 \cdots O42$  2.578(2) Å) and an oxime-oxime interaction ( $O38 \cdots O48$  2.797(2) Å) (Figure 3.13)

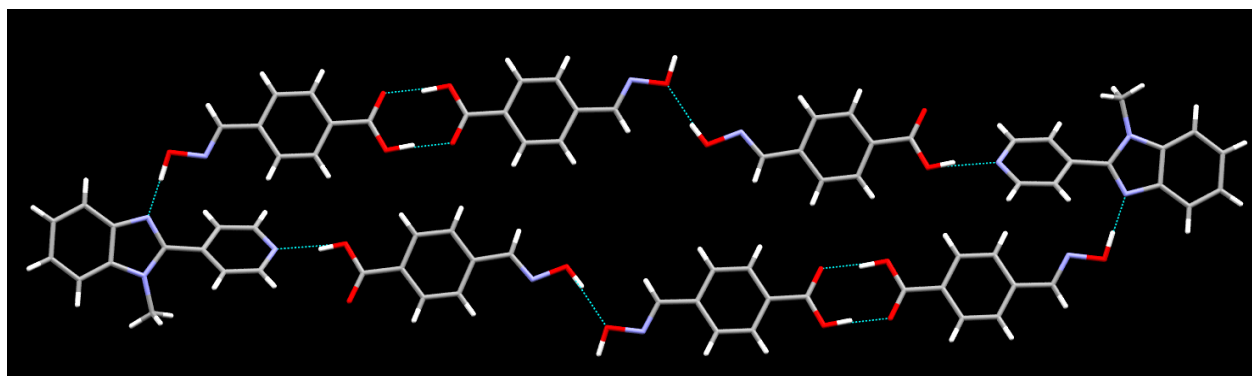


**Figure 3.13** The primary hydrogen-bond interactions in the crystal structure of **4ABA:1PB**

### 3.4. Discussion

#### 3.4.1. Evaluation of co-crystals

Our expansion of Etter's rules propose that in a system comprising multiple hydrogen bond donor and acceptor groups the best donor will selectively bind to the best acceptor and the second best donor will bind to the second best acceptor and so on. In all six structures obtained, the best donor follows the same trend as the example shown in Figure 3.14 where the best donor as determined by MEP calculations selectively forms hydrogen bonds to the best acceptor. The carboxylic acid group, which according to the pKa based approaches, is the best donor by a few orders of magnitude acted as the weaker donor by picking up the weaker acceptor in all six cases. The water molecule in **4HBA:4PB** does not break any of the anticipated O-H $\cdots$ N interactions which are quite unusual in hydrates.<sup>25</sup>

### 3.4.2. Predicting molecular recognition based on pKa and MEP values

The selectivity exhibited by the donors and acceptors in this study is in accordance with the predictions made based on the MEP calculations and completely contradicts predictions made using pKa as a ranking system. This is because hydrogen bonding can be considered mostly electrostatic and pKa values indicate the potential for protonation or deprotonation rather than hydrogen bonding this value is affected by the electrostatic environment but is not a measure of hydrogen bond donor ability.

A published co-crystal 4-hydroxybenzoic acid with **4PI** which consists of pyridine and imidazole acceptor sites also shows that the weaker donor (the hydroxyl group), with the higher pKa group forms a hydrogen bond with the best acceptor site with the higher pKa value (Figure 3.14).

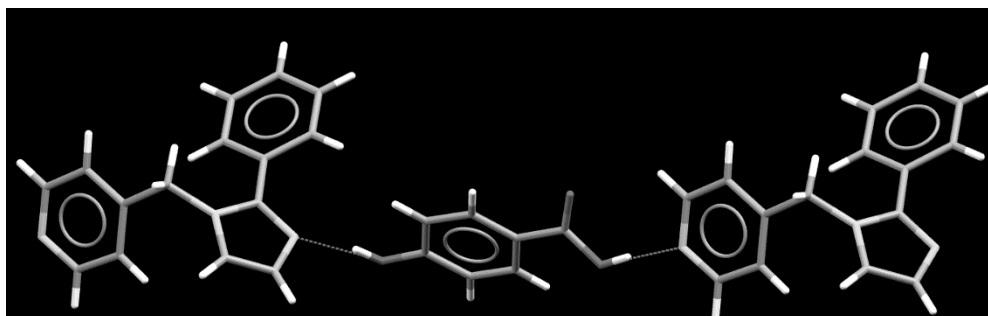


Figure 3.14 4-Hydroxybenzoic acid with an asymmetric ditopic acceptor<sup>26</sup>

In addition unpublished data from our group for co-crystals of **4HBA:PzO** (Figure 3.15) and **4HBA:BPO** (Figure 3.16) also shows the same trend where in both cases the OH group picks up the N-oxide group which is the best acceptor in both cases and the second best donor, carboxylic acid picks up the pyridine and pyrazine nitrogen atoms, respectively.

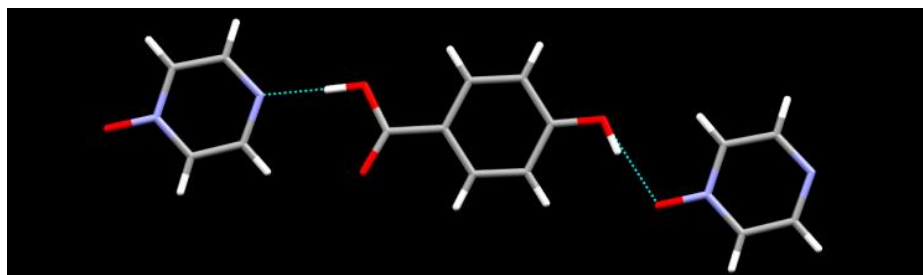
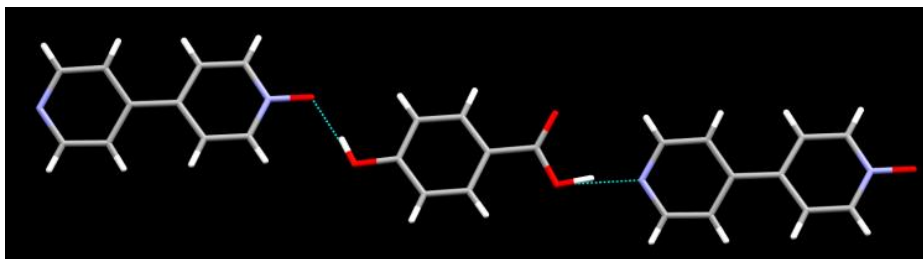


Figure 3.15 The primary hydrogen-bond interactions in the crystal structure of 4HBA:PzO





**Figure 3.16 The primary hydrogen-bond interactions in the crystal structure of 4HBA:BPO**

Including this published structure and the unpublished data we observe that in nine instances where two donors of significantly different pKa value have provided co-crystals with geometrically unbiased acceptors, the outcome differs from that predicted by pKa values or pKa based approaches.

A similar selectivity can be observed in the case of 4-hydroxybenzoic acid and the monotopic acceptor, 4-phenylpyridine where pKa values suggest that the acid group is the best donor with a pKa almost five orders of magnitude higher than the hydroxyl group. But as shown in Figure 3.17, 4-phenylpyridine selectively binds to the hydroxyl group which is considered the weaker donor.

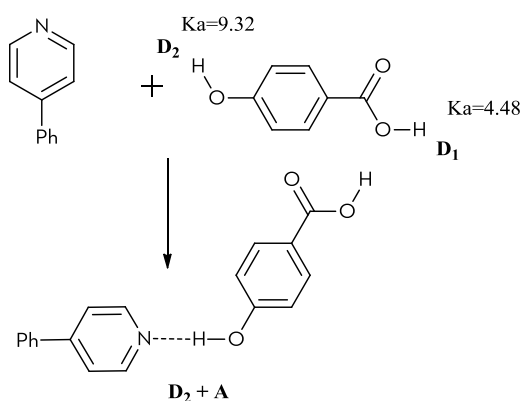


**Figure 3.17 The –OH group (the weaker donor according to pKa) forms a hydrogen bond with the pyridine instead of the acid.**

According to pKa values hydroxyl group is five orders of magnitude weaker than the carboxylic acid group and the aldehyde is almost seven orders of magnitude weaker. Experimentally we have observed that, both the oxime and the phenol pick out the stronger acceptor over the acid and therefore are stronger donors compared to the carboxylic acid.

Therefore, it seems that pKa may not be effective when comparing the hydrogen bond donor ability of different functional groups. The MEP based approaches (both DFT and AM1) on the other hand, have successfully predicted the outcomes of all seven co crystals.

### 3.4.3. Conclusions

Out of the existing method to predict supramolecular outcomes it was observed that pKa based prediction methods cannot be used in situations comparing different families of functional groups. The supramolecular outcomes of the nine co-crystals were correctly predicted by the calculated molecular electrostatic potential values where molecular recognition takes place based on our expansion of Etter's rules.

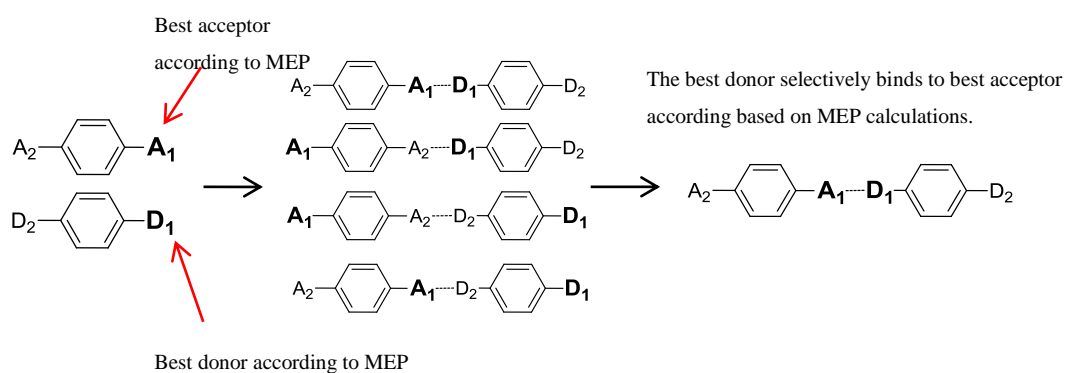


**Figure 3.18 All nine co-crystals formed according to Etter's rules as predicted based on MEP values.**

Based on the experimental observations the phenol group and the aldoximes, both act as stronger hydrogen bond donors than carboxylic acids when the groups are on the same aromatic backbone.

## References

---

- <sup>1</sup> M. K. Stanton and A. Bak, *Cryst. Growth Des.*, **2008**, *8*, **10**, 3856–3862
- <sup>2</sup> M. Viertelhaus, R. Hilfiker, F. Blatter M. and Neuburger, *Cryst. Growth Des.*, **2009**, *9*, **5**, 2220–2228
- <sup>3</sup> M. L. Cheney, D. R. Weyna, N. Shan, M. Hanna, L. Wojtas, M. J. Zaworotko, *Crystal Growth & Design*, **2010**, *10*, 4401-4413
- <sup>4</sup> E. Nauha, E. Kolehmainen and M. Nissinen, *CrystEngComm*, **2011**, *13*, 6531-6537
- <sup>5</sup> C. B. Aakeröy, G. S. Bahra, P.B. Hitchcock, Y. Patell, and K. R. Seddon, *J. Chem. Soc., Chem. Commun.*, **1993**, 152-156.
- <sup>6</sup> D. I. A. Millar, H. E. Maynard-Casely, D. R. Allan, A. S. Cumming, A. R. Lennie, A. J. Mackay, I. D. H. Oswald C. C. Tang and C. R. Pulham, *CrystEngComm*, **2012**, *14*, 3742-374
- <sup>7</sup> G. Wang and Y. Huang, *Journal of Physics and Chemistry of Solids*, **2007**, *68*, 2003-2007.
- <sup>8</sup> M.C. Etter, *J. Phys. Chem.* **1991**, *95*, 4601
- <sup>9</sup> C. B. Aakeröy, A. M. Beatty, B. A. Helfrich, *Angew. Chem. Int. Ed.* **2001**, *17*, 3240-3242.
- <sup>10</sup> P. Gilli, L. Pretto, V. Bertolasi, and G. Gilli, *Accounts of chemical research* **2009**, *42*, **1**, 33-44
- <sup>11</sup> G. Gilli, F. Bellucci, V. Ferretti, and V. Bertolasi, *J. Am. Chem. Soc.* **1989**, *111*, 1023-1028
- <sup>12</sup> G. R. Desiraju, "Crystal Engineering. The Design of Organic Solids", Elsevier, **1989**.
- <sup>13</sup> T. Alison R. Ung, D. C. Bishop, I. Craig, G. Dance, and M. L. Scudder *Chem. Mater.* **1994**, *6*, 1269-1281
- <sup>14</sup> M. Hachiya, M. Ito, T. Matsuo, D. Hashizume, H. Fueno, K. Tanaka, and K. Tamao, *Organic Letters* **2011**, *13* **10**, 2666-2669
- <sup>15</sup> M. H. Abraham, *Chem. Soc. Rev.*, **1993**, *22*, 73-83
- <sup>16</sup> M. H. Abraham, P. L. Grellier, D. V. Prior, P. P. Duce, J. J. Morris and P. J. Taylor *J. Chem. Soc., Perkin Trans.* **1989**, *2*, 699-711
- <sup>17</sup> M. H. Abraham, A. Ibrahim, A. M. Zissimos, *J. Chromatogr. A*, **2004**, *1037*, 29–47
- <sup>18</sup> J. Jover, R. Bosque, and J. Sale, *J. Chem. Inf. Comput. Sci.* **2004**, *44*, 1098-1106
- <sup>19</sup> I. Cacelli, S. Campanile, A. Giolitti, and D. Molin, *J. Chem. Inf. Model.* **2005**, *45*, 327-333.
- <sup>20</sup> C.A. Hunter, *Angew. Chem. Int. Ed.* **2004**, *43*, 5310-5324.
- <sup>21</sup> D. Musumeci, C.A. Hunter, R. Prohens, S. Scuderi and J. F. McCabe, *Chem. Sci.*, **2011**, *2*, 883-890.
- <sup>22</sup> A. N. Sokolov, T. Friščić, S. Blais, J. A. Ripmeester, and L. R. MacGillivray, *Crystal Growth & Design* **2006** *6*, **11**, 2427-2428
- <sup>23</sup> C. B. Aakeröy, M. Fasulo, N. Schultheiss, J. Desper, and C. Moore, *J. Am. Chem. Soc.*, **2007**, *129*, **45**, 13772–13773
- <sup>24</sup> J. Singh, P. Grover, D. Pathak, *Acta Pharmaceutica Scientia*, **2010**, *52*, 511-522.
- <sup>25</sup> S. Karki, T. Friščić, W. Jones and W. Motherwell, *Mol. Pharmaceutics*, **2007**, *4*, 347-354.
- <sup>26</sup> C. B. Aakeröy, J. Desper and M. M. Smith, *Chem. Commun.*, **2007**, 3936-3938

## Chapter 4. Establishing the place of cyanooximes in the hierarchy of hydrogen-bond donors

### 4.1. Introduction

#### 4.1.1. Cyanooximes

The cyanooxime functionality can be found in fungicides<sup>1</sup>, pesticides<sup>2</sup>, organometallics<sup>3</sup> and the treatment of cancer<sup>4</sup>. Another unique attribute observed was that unlike all other oximes cyanooximes do not form an oxime-oxime dimer (Figure 4.1).

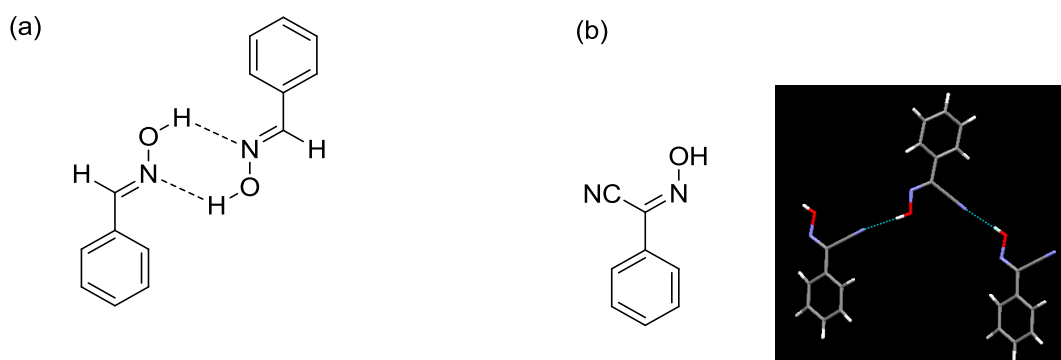
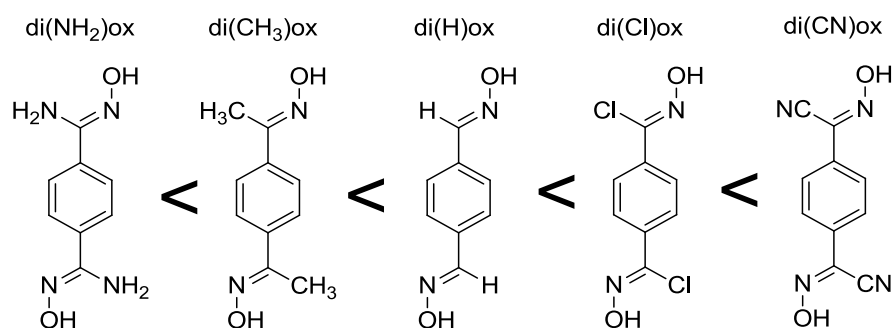


**Figure 4.1 (a) Typical oxime-oxime dimer (b) Chain motif formed by cyanooximes<sup>5</sup>**

Our study of oximes in chapter two showed that based on supramolecular yield, cyanooximes proved to have the strongest donor ability of all the oximes studied (Figure 4.2). This was attributed to the electron withdrawing effect of the  $-CN$  group



MEP/kJmol <sup>-1</sup>	124	140	144	163	185
pKa	14.43	10.97	10.27	9.70	7.47
Supramolecular yield	30%	55%	70%	80%	100%

**Figure 4.2 Oximes arranged according to increasing donor based on observed supramolecular yields ability with matching trends in MEP and pKa values.**

#### 4.1.2. Towards a unified theory for predicting selectivity in hydrogen-bonding

The ability to predict molecular recognition events or supramolecular selectivity enables the rational deliberate design and synthesis of co-crystals. In the case of a molecule containing both donor and acceptor sites, a proper understanding of hydrogen-bond donor and acceptor hierarchy makes it possible to select potential co-crystalizing agents with donor and acceptor sites stronger than those on the molecule itself, thereby increasing the chance of forming co-crystals. This eliminates the need for extensive and expensive co-crystal screens.

In chapter 3 it was shown that calculated molecular electrostatic potential values can be employed to predict hydrogen-bonding preferences between phenols carboxylic acids and aldoximes. These predictions were verified by experimental results. A unified theory to predict molecular recognition should be applicable to any system. In this chapter we attempt to predict the hydrogen-bond donating ability of cyanooximes compared to phenols and carboxylic acids based on molecular electrostatic potential values.

### 4.1.3. Virtual co-crystal screening

A method has been developed by Hunter et. al<sup>6</sup>., to predict the possibility of co-crystal formation by calculating the difference in energy between, the overall pairing energies (eqn. 4.1) of the individual components and the co-crystal.

$$E = -\sum_{ij} \alpha_i \beta_j \quad 4.1$$

$\alpha$  (eqn. 4.2) and  $\beta$  (eqn. 4.3) are based on MEP values obtained using a higher level of theory where the molecular geometry was minimized using DFT B3LYP/6-31+G\* *ab initio* calculations.  $\alpha$  and  $\beta$  values were calculated using equations 4.2 and 4.3. This level of theory provided a better fit compared to AM1.

$$\alpha = 0.0000162 \text{ MEP}_{\max}^2 + 0.00962 \text{ MEP}_{\max} \quad 4.2$$

$$\beta = 0.000146 \text{ MEP}_{\min}^2 - 0.00930 \text{ MEP}_{\min} \quad 4.3$$

By running this analysis on around 846 compounds on the EAFUS list (Everything added to food in the United States) it was observed that 80% of the experimental hits were in the top 11% of the ranking based on analysis. Based on their observations they have set a cut-off value of 11 kJ/mol between the individual constituents and the co-crystal would give a 50% chance of co-crystal formation.

In this study, in addition to ranking based on calculated MEP values, we will attempt to use the same method to calculate the difference in energy between the predicted binding interaction ( $D_1 \dots A_1$  and  $D_2 \dots A_2$ ) and alternative combinations of donors and acceptors ( $D_1 \dots A_2$  and  $D_2 \dots A_1$ ) in order to see if energy calculations for different expected outcomes can be used to predict the actual supramolecular outcome.

#### 4.1.4. Hypothesis

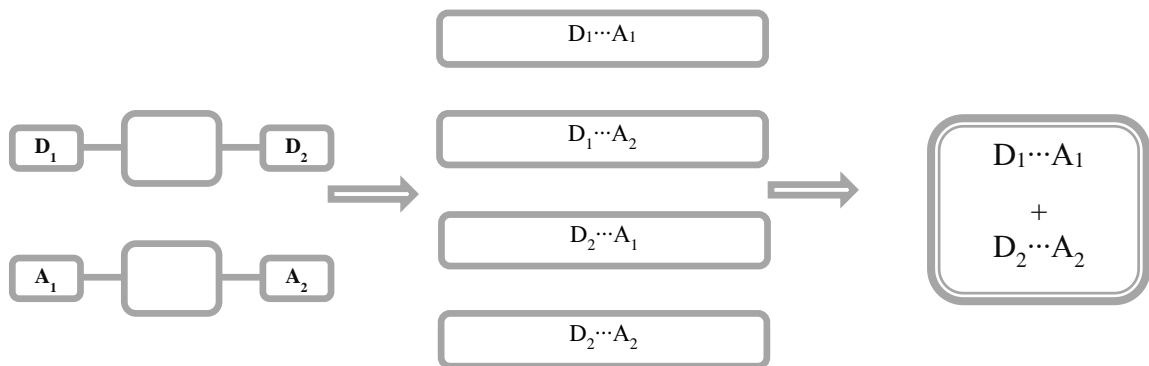


**Figure 4.3 Hypothesis on selectivity based on Etter's rules<sup>7,8</sup> (Figure 4.3)**

Based on our extension of Etter's rules<sup>7,8</sup>, when combining asymmetric ditopic donors and acceptors the best donor should selectively bind to the best acceptor and the second best donor should bind the second best acceptor if our method of ranking donors and acceptors still holds when comparing the cyanooxime group with the phenol and carboxylic acid groups.

The goals of the work described in this chapter are,

- To synthesize three asymmetric ditopic donors containing cyanooxime groups

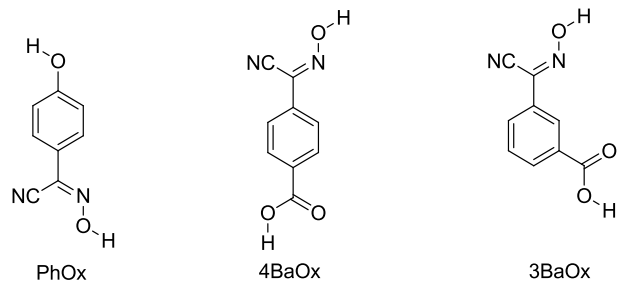


**Figure 4.4 Three asymmetric ditopic donors with a cyanooxime functionality.**

- Perform DFT and AM1 molecular electrostatic potential calculations on the three donors and the nine acceptors.

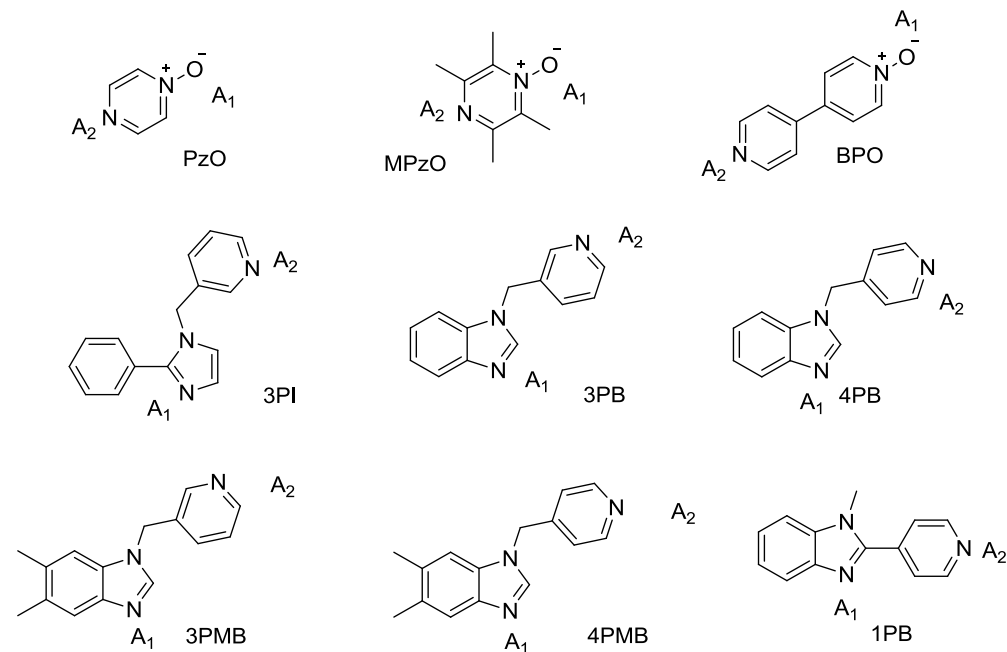


**Figure 4.5** The nine acceptors used in this study

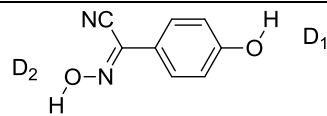
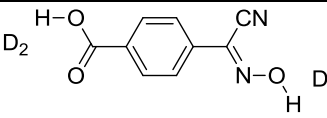
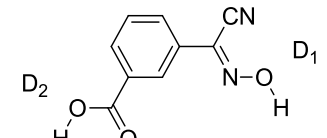
- Calculate relative energies of donor acceptor pairs for possible outcomes.
- Screen the three donors (Figure 4.4) against the nine (Figure 4.5) acceptors using solvent assisted grinding and slow evaporation.
- Examine structural data and evaluate the initial hypothesis.



## 4.2. Experimental

### 4.2.1. Molecular electrostatic potential calculations

**Table 4.1** AM1 and DFT molecular electrostatic potential surface on the three donors.

Donor	AM1		DFT	
	D <sub>1</sub>	D <sub>2</sub>	D <sub>1</sub>	D <sub>2</sub>
	181	171	302	290
	192	147	314	269
	183	147	298	282

As shown in Table 4.1, both DFT and AM1 calculations show the same donor hierarchy in all three ditopic donor molecules. Based on the calculated MEP values of 4-hydroxycyanooxime the phenol is a better donor compared to the cyanooxime. With 3 and 4-acidcyanooximes however, the cyanooxime proves to be the better donor compared to the carboxylic acid based on the calculated MEP values.

**Table 4.2** Calculated AM1 and DFT molecular electrostatic potential values of the acceptors

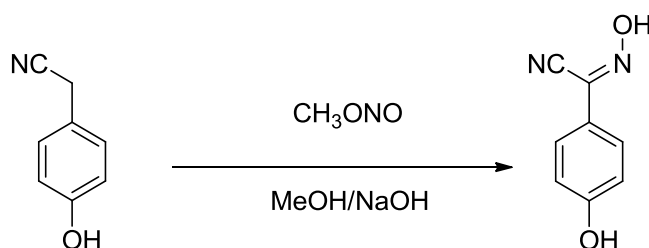
Name	AM1 MEP /kJmol <sup>-1</sup>		DFT MEP /kJmol <sup>-1</sup>	
	A <sub>1</sub>	A <sub>2</sub>	A <sub>1</sub>	A <sub>2</sub>
PzO	-266	-232	-161	-144
MPzO	-287	-255	-177	-147
BPO	-294	-249	-182	-168
3PI	-290	-279	-204	-171
1PB	-290	-279	-182	-179
3PB	-292	-262	-201	-175

4PB	-291	-268	-195	-174
3PMB	-296	-261	-210	-180
4PMB	-291	-268	-203	-177

#### 4.2.2. Synthesis of asymmetric ditopic donors

All chemicals were purchased from Aldrich, Fisher Scientific and used without further purification, Melting points were determined on a Gallenkamp melting point apparatus and are reported uncorrected.  $^1\text{H}$  and  $^{13}\text{C}$  NMR spectra were recorded on a Varian Unity plus 400 MHz spectrometer in DMSO- $d_6$ . Compounds were prepared for infrared spectroscopic (IR) analysis on a ZnSe ATR crystal.

##### 4.2.2.1. Synthesis of (Z)-N,4-dihydroxybenzimidoyl cyanide, PhOx



10 g of NaOH was dissolved in 250 ml of methanol. 2.0 g (15.0 mmol) of 2-(4-hydroxyphenyl)acetonitrile was dissolved in 50 ml of methanol and added to the NaOH solution and allowed to stir for 1 hour. Methyl nitrite was bubbled through the solution over 30 minutes. The resulting solution was allowed to stir at room temperature for 48 hours.

Methanol was removed under reduced pressure. The solid was dissolved in 100 ml of water and cooled in an ice bath. The pH was then slowly lowered to pH=2 with 6 M HCl. The precipitate was filtered and washed with ice water. 1.58 g of pure product was obtained. (Yield 65%) M.p.: 160-165 °C  $^1\text{H}$  NMR (400 MHz, DMSO- $d_6$ )  $\delta$  ppm 6.89 (d,  $J=8.59$  Hz, 2 H) 7.55 (d,  $J=8.98$  Hz, 2 H) 10.13 (br. s., 1 H) 13.29 (br. s., 1 H)

#### 4.2.2.2. (Z)-4-(cyano(hydroxyimino)methyl)benzoic acid, 4BaOx

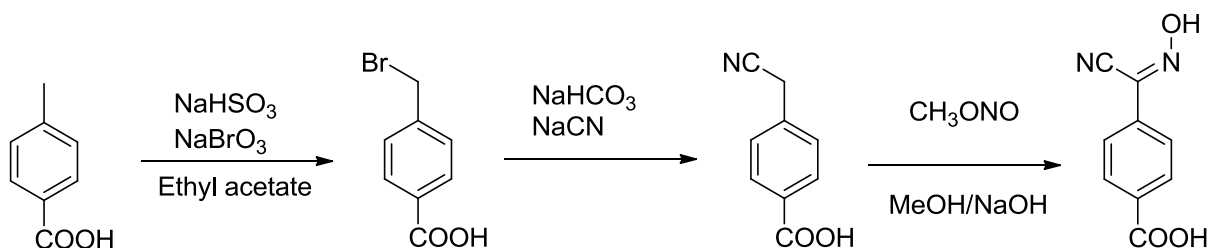


Figure 4.6 Synthetic scheme for 4BaOx

##### 4.2.2.2.1. Synthesis of 4-(bromomethyl)benzoic acid

5 g (36 mmol) of 4-toluic acid was added to 100 ml ethyl acetate. To the resulting slurry a solution of 10 g (66 mmol) sodium bromate in 50 ml of water was added. 7 g (66 mmol) of NaHSO<sub>3</sub> was dissolved in 44 ml of water and added dropwise to the 4-toluic acid solution via a dropping funnel over a time of 20 minutes. The resulting solution was stirred overnight at room temperature. The ethyl acetate was removed under reduced pressure. The resulting white solid was filtered and washed with water. m.p. 200 – 205 °C (lit 228-232 °C)<sup>9</sup> (6.3 g, 82%) <sup>1</sup>H NMR (200 MHz, DMSO-*d*<sub>6</sub>) δ ppm 4.76 (2 H, s), 7.56 (2 H, d, *J*=8.35 Hz), 7.92 (2 H, d, *J*=8.35 Hz), 13.10 (1 H, br. s.)

##### 4.2.2.2.2. Synthesis of 4-(cyanomethyl)benzoic acid

2.6 g (12.2 mmol) of 4-(bromomethyl)benzoic acid was dissolved in 100 ml of ethanol and 50 ml water. 1.02g (12.2 mmol) NaHCO<sub>3</sub> was added to the stirring solution with 1.19 g (24.4 mmol) of sodium cyanide. The solution was stirred at room temperature for 6 hours.

Ethanol was removed under reduced pressure. 50 ml of water was added to the resulting slurry and acidified in an icebath with 2 M HCl. The solid obtained was filtered and washed with water to yield a light brown solid m.p. 193 – 198 °C (lit 195-200 °C)<sup>10</sup> (1.9 g, 96%) <sup>1</sup>H NMR (200 MHz, DMSO-*d*<sub>6</sub>) δ ppm 4.15 (2 H, s), 7.47 (2 H, d, *J*=8.06 Hz), 7.95 (2 H, d, *J*=8.42 Hz)

##### 4.2.2.2.3. (Z)-4-(cyano(hydroxyimino)methyl)benzoic acid, 4BaOx

10 g of NaOH was dissolved in 250 ml of methanol. 1.9 g (11.8 mmol) of 4-(cyanomethyl)benzoic acid was dissolved in 50 ml of methanol and added to the NaOH solution and allowed to stir for 1 hour. Methyl nitrite was generated by pouring a solution of 16 ml H<sub>2</sub>SO<sub>4</sub> in 32 ml of water dropwise into a solution of NaNO<sub>2</sub> in 100 ml water and 50 ml methanol. Methyl

nitrite was bubbled through the solution over 30 minutes. The resulting solution was allowed to stir at room temperature for 48 hours.

The color of the solution changed from yellow to orange. Methanol was removed with reduced pressure. The solid was dissolved in 100 ml of water and cooled in an ice bath. The pH was then slowly lowered to pH=2 with 6 M HCl. The off white solid obtained was filtered and washed with ice water. (1.34 g Yield 60%) M.p. 255-260 °C <sup>1</sup>H NMR (200 MHz, DMSO-*d*<sub>6</sub>) δ ppm 7.83 (2 H, d, *J*=1.00 Hz), 8.05 (2 H, d, *J*=1.00 Hz), 13.25 (1 H, br. s), 14.09 (1 H, br. s.)

#### 4.2.2.3. (Z)-3-(cyano(hydroxyimino)methyl)benzoic acid, 3BaOx

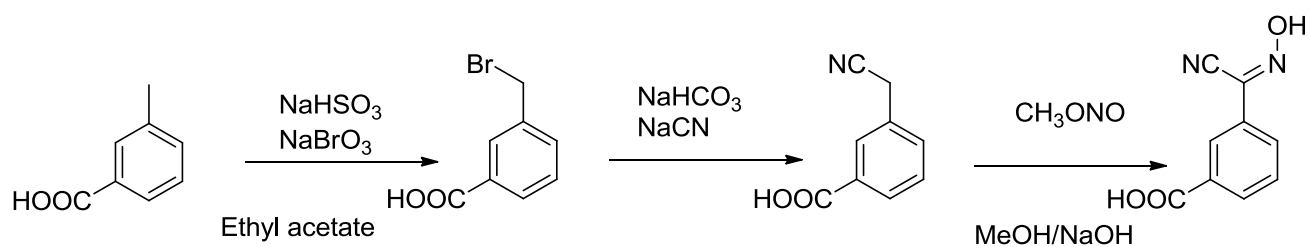


**Figure 4.7 Synthetic scheme for 3BaOx**

##### 4.2.2.3.1. Synthesis of 3-(bromomethyl)benzoic acid,

5 g (36 mmol) of 4-toluic acid was added to 100 ml ethyl acetate. To the resulting slurry a solution of 10 g (66 mmol) sodium bromate in 50 ml of water was added. 7 g (66 mmol) of NaHSO<sub>3</sub> was dissolved in 44 ml of water and added dropwise to the 4-toluic acid solution via a dropping funnel over a time of 20 minutes. The resulting solution was stirred overnight at room temperature. The ethyl acetate was removed under reduced pressure. The resulting white solid was filtered and washed with water. (6.3 g, 75%) m.p. 153 – 157 °C (lit. 155 – 156 °C)<sup>11</sup> <sup>1</sup>H NMR (200 MHz, DMSO-*d*<sub>6</sub>) δ ppm 4.76 (2 H, s), 7.56 (2 H, d, *J*=8.35 Hz), 7.92 (2 H, d, *J*=8.35 Hz), 13.10 (1 H, br. s.)

##### Synthesis of 3-(cyanomethyl)benzoic acid,

2.6 g (12.2 mmol) of 4-(bromomethyl)benzoic acid was dissolved in 100 ml of ethanol and 50 ml water. 1.02g (12.2 mmol) NaHCO<sub>3</sub> was added to the stirring solution with 1.19 g (24.4 mmol) of sodium cyanide. The solution was stirred at room temperature for 6 hours.

Ethanol was removed under reduced pressure. 50 ml of water was added to the resulting slurry and acidified in an icebath with 2 M HCl. The solid obtained was filtered and washed with water. 1.9 g of product was obtained. (Yield 85%) m.p 176 – 180 °C (lit. 175 – 176 °C)<sup>12</sup>

#### ***(Z)-3-(cyano(hydroxyimino)methyl)benzoic acid, 3BaOx***

10 g of NaOH was dissolved in 250 ml of methanol. 1.9 g (11.8 mmol) of 3-(cyanomethyl)benzoic acid was dissolved in 50 ml of methanol and added to the NaOH solution and allowed to stir for 1 hour. Methyl nitrite was generated by pouring a solution of 16 ml H<sub>2</sub>SO<sub>4</sub> in 32 ml of water dropwise into a solution of 10 g NaNO<sub>2</sub> in 100 ml water and 50 ml methanol. Methyl nitrite was bubbled through the solution over 30 minutes. The resulting solution was allowed to stir at room temperature for 48 hours.

The color of the solution changed from yellow to orange. Methanol was removed with reduced pressure. The solid was dissolved in 100 ml of water and cooled in an ice bath. The pH is then slowly lowered to pH=2 with 6 M HCl. The solid obtained was filtered and washed with ice water. 1.34 g of product was obtained. (Yield 60%) M.p.: 230-233 °C dec. <sup>1</sup>H NMR (DMSO-d<sub>6</sub>, 200MHz): δ = 13.99 (br. s., 1 H), 13.39 (br. s., 1 H), 8.07 (d, *J*=7.8 Hz, 1 H), 7.97 (d, *J*=1.0 Hz, 1 H), 7.66 ppm (s, 1 H)

### ***4.2.3. Synthesis of co-crystals***

#### ***4.2.3.1. Synthesis of PhOx:MPzO (1:1)***

**PhOx** (0.010g, 0.062 mmol) and **MPzO** (0.009 g, 0.062 mmol) were dissolved in 5 ml of methanol with heat and allowed to stand at room temperature for slow evaporation. Colorless prisms were obtained in a week. (m.p.160 – 165 °C)

#### ***4.2.3.2. Synthesis of 4-hydroxycyanooxime, BPO (1:1) PhOx:BPO***

**PhOx** (0.010g, 0.062 mmol) and **BPO** (0.011 g, 0.062 mmol) were dissolved in 5 ml of methanol with heat and allowed to stand at room temperature for slow evaporation. Colorless prisms were obtained in three weeks. (m.p.163 – 168 °C).

**4.2.3.3.        *Synthesis of 4-hydroxycyanooxime, 4PI (1:1) PhOx:4PI***

**PhOx** (0.010g, 0.062 mmol) and **4PI** (0.015 g, 0.062 mmol) were dissolved in 5 ml of methanol with heat and allowed to stand at room temperature for slow evaporation. Colorless prisms were obtained in two weeks. (m.p.150 – 154 °C)

**4.2.3.4.        *Synthesis of 4-hydroxycyanooxime, 3PMB (1:1) PhOx: 3PMB***

**PhOx** (0.010g, 0.062 mmol) and **3PMB** (0.015 g, 0.062 mmol) were dissolved in 5 ml of methanol with heat and allowed to stand at room temperature for slow evaporation. Colorless plates were obtained in ten days. (m.p.175 – 178 °C)

**4.2.3.5.        *Synthesis of 4-hydroxycyanooxime, 4PMB (1:1) PhOx: 4PMB***

**PhOx** (0.010g, 0.062 mmol) and **4PMB** (0.015 g, 0.062 mmol) were dissolved in 5 ml of methanol with heat and allowed to stand at room temperature for slow evaporation. Colorless prisms were obtained in two weeks. (m.p.135 – 141 °C)

**4.2.3.6.        *Synthesis of 4-acidcyanooxime, PzO (1:1) 4BAOx:PzO***

**4BAOx** (0.010g, 0.053 mmol) and **PzO** (0.005 g, 0.053 mmol) were dissolved in 5 ml of ethanol with heat and allowed to stand at room temperature for slow evaporation. Colorless plates were obtained in two weeks. (m.p. 170 °C)

**4.2.3.7.        *Synthesis of 4-acidcyanooxime, MPzO (1:1) 4BAOx:MPzO***

**4BAOx** (0.010g, 0.053 mmol) and **MPzO** (0.008 g, 0.053 mmol) were dissolved in 5 ml of ethanol with heat and allowed to stand at room temperature for slow evaporation. Colorless plates were obtained in three weeks. (m.p. 200 - 206°C)

**4.2.3.8.        *Synthesis of 3-acidcyanooxime, 4PMB (1:1) 3BAOx:4PMB***

**3BAOx** (0.010g, 0.053 mmol) and **4PMB** (0.012 g, 0.053 mmol) were dissolved in 5 ml of methanol with heat and allowed to stand at room temperature for slow evaporation. Colorless plates were obtained in ten days. (m.p. 175 – 180 °C)

#### 4.2.3.9. *Synthesis of 3-acidcyanooxime, 4PB (1:1) 3BAOx:4PB*

**3BAOx** (0.010g, 0.053 mmol) and **4PB** (0.012 g, 0.053 mmol) were dissolved in 5 ml of methanol with heat and allowed to stand at room temperature for slow evaporation. Colorless plates were obtained in a week. (m.p. 125 - 130 °C)

### 4.3. Results

#### 4.3.1. *Description of crystal structures*

##### 4.3.1.1. *Crystal structure of PhOx:MPzO*

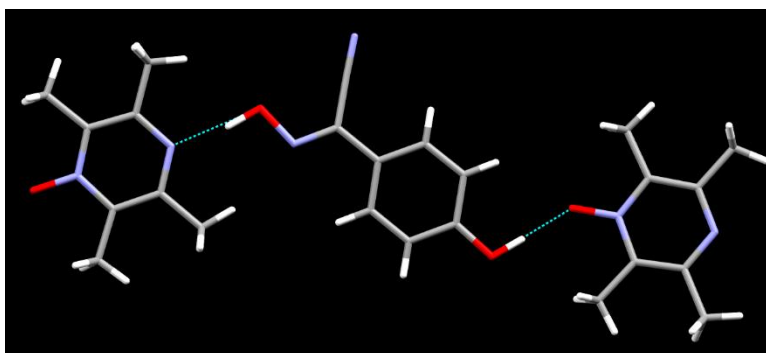


**Figure 4.8** The primary hydrogen-bond interactions in the crystal structure of PhOx:MPzO

The crystal structure determination of **PhOx:MPzO** shows that in the resulting 1:1 co-crystal the best donor, the –OH moiety, forms a hydrogen-bond to the N-oxide oxygen atom, the best acceptor, (O14···O21 2.6631(15) Å, O14-H14···O21 1.70(2) Å), and the second best donor cyanooxime engages in a hydrogen-bond with the pyridyl nitrogen atom, the second-best acceptor, (O17···N24 2.7223(16) Å, O17-H17···N24 1.69(2) Å) (Figure 4.8)

#### 4.3.1.2. Crystal structure of PhOx:BPO

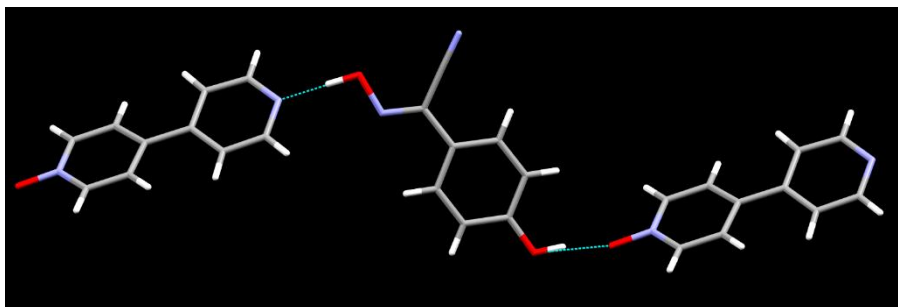


**Figure 4.9** The primary hydrogen-bond interactions in the crystal structure of PhOx:BPO

In the crystal structure of **PhOx:BPO**, a 1:1 co-crystal, the best donor, –OH moiety forms a hydrogen-bond to the N-oxide oxygen atom, the best acceptor, (O14···O21 2.6052(19) Å, O14-H14···O21 1.71(3) Å), and cyanooxime, the second- best donor, forms a hydrogen-bond with the second- best acceptor, the pyridyl nitrogen atom, (O17···N31 2.665(2), O17-H17···N31 1.64 Å) (Figure 4.9)

#### 4.3.1.3. Crystal structure of PhOx:3PI

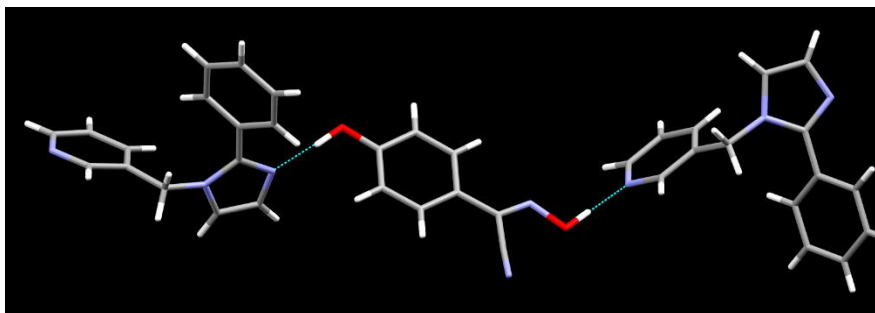


**Figure 4.10** The primary hydrogen-bond interactions in the crystal structure of PhOx:3PI

The 1:1 co-crystal of **PhOx:3PI** shows that the best donor, the –OH moiety, of **PhOx** interacts with the best acceptor, the imidazole site, (O44···N13 2.6695(15) Å, O44-H44···N13 1.685(18) Å), whereas the second- best donor, cyanooxime, forms an O-H···N hydrogen-bond with the pyridyl nitrogen atom (O47···N21 2.6539(14) Å, O47-H47···N21 1.673(18) Å) (Figure 4.10)



#### 4.3.1.4. *Crystal structure of PhOx:3PMB*

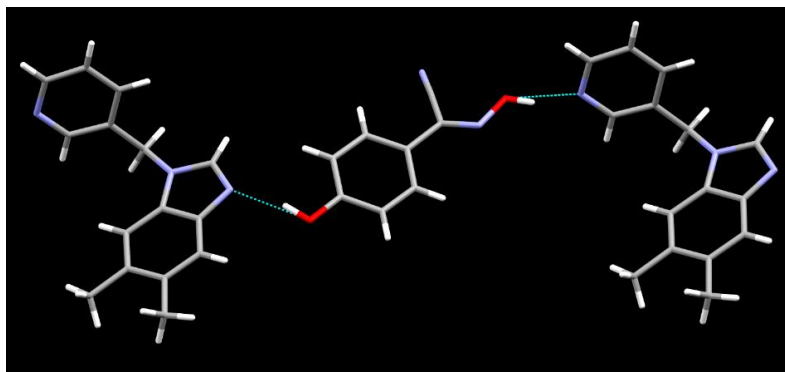


**Figure 4.11** The primary hydrogen-bond interactions in the crystal structure of PhOx:3PMB

The crystal structure determination of **PhOx:3PMB** shows that in the resulting 1:1 co-crystal the phenol, the best donor prefers to bind to the best acceptor, the benzimidazole site, (O44...N13 2.7405(14) Å, O44-H44...N13 1.852(17) Å), while the second-best donor, cyanooxime binds the pyridyl nitrogen which is the second- best acceptor (O47...N31 2.6474(14) Å, O47-H47...N31 1.693(18) Å) (Figure 4.11).

#### 4.3.1.5. *Crystal structure of PhOx:4PMB*

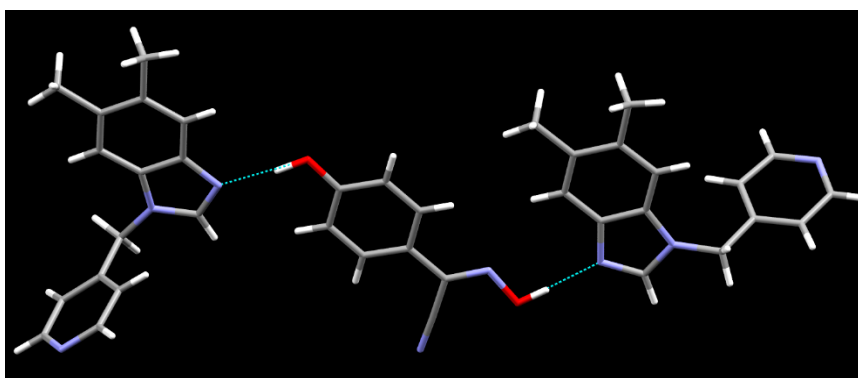


**Figure 4.12** The primary hydrogen-bond interactions in the crystal structure of PhOx:4PMB.

The crystal structure determination of **PhOx:4PMB** produced the an unexpected result. First, the stoichiometry is unexpected with a 1:2 ratio of **PhOx** to **4PMB**. Second, both donor

sites form hydrogen-bonds to the better acceptor, the imidazole moiety, O74...N43 2.6990(12) Å, O74-H74...N43 1.759(17) Å and O77...N13 2.7627(12) Å, O77-H77...N13 2.7627(12) Å with D1 and D2, respectively, Figure 4.12.

#### 4.3.1.6. *Crystal structure of 3BAOx:4PB*

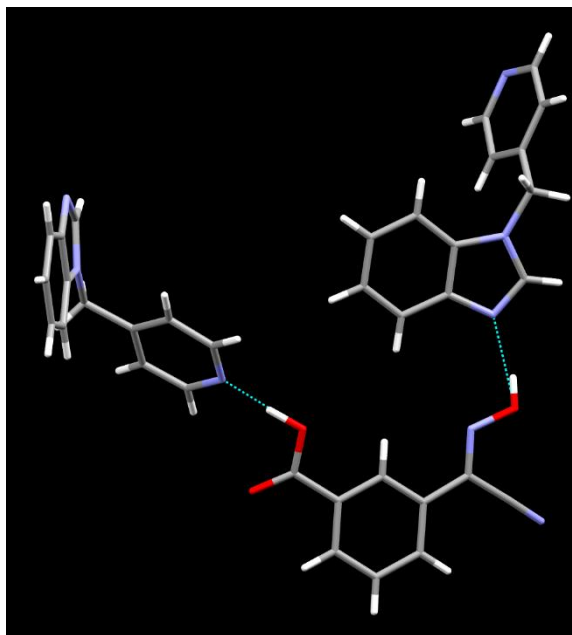


**Figure 4.13** The primary hydrogen-bond interactions in the crystal structure of 3BAOx:4PB.

The crystal structure determination of **3BAOx:4PB** shows that in the resulting 1:1 co-crystal the cyanooxime, the best donor prefers to bind to the best acceptor, the benzimidazole site, (O37A...N13A 2.6514(18) Å) the second best donor, the carboxylic acid picks up the pyridine, the second best acceptor. O39...N21 2.5965(14) Å (Figure 4.13)

4.3.1.7. *Crystal structure of 3BAOx:4PMB*

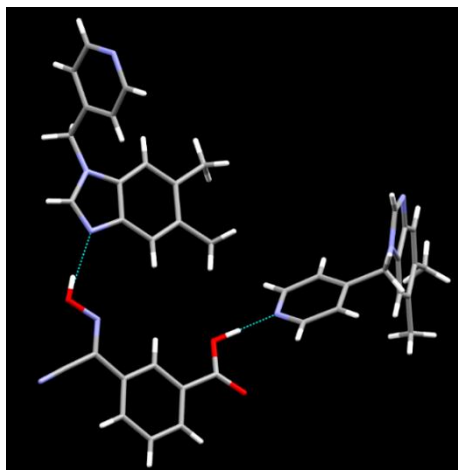


**Figure 4.14** The primary hydrogen-bond interactions in the crystal structure of 3BAOx:4MPB

The crystal structure determination of **3BAOx:4MPB** shows that in the resulting 1:1 co-crystal the cyanooxime, the best donor prefers to bind to the best acceptor, the benzimidazole site, (O47A...N13A 2.6641(14) Å) the second best donor, the carboxylic acid binds to the pyridine, the second best acceptor. O49...N21 2.5823(13) Å (Figure 4.14)

4.3.1.8. *Crystal structure of 4BAOx:PzO*

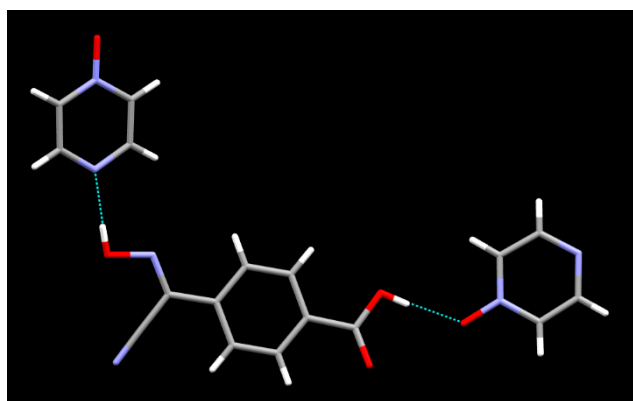


**Figure 4.15** The primary hydrogen-bond interactions in the crystal structure of 4BAOx:PzO

The crystal structure determination of **4BAOx:PzO** yields an unexpected result where the best donor, the cyanooxime forms a hydrogen-bond with the second best acceptor, pyrazine

nitrogen (O17···N24 2.674(2) Å) and the second best donor, carboxylic acid picks up the best acceptor, N-oxide group. (O19···N21 2.684(2) Å) forming a one dimensional chain.(Figure 4.15)

#### 4.3.1.9. *Crystal structure of 4BAOx:MPzO*

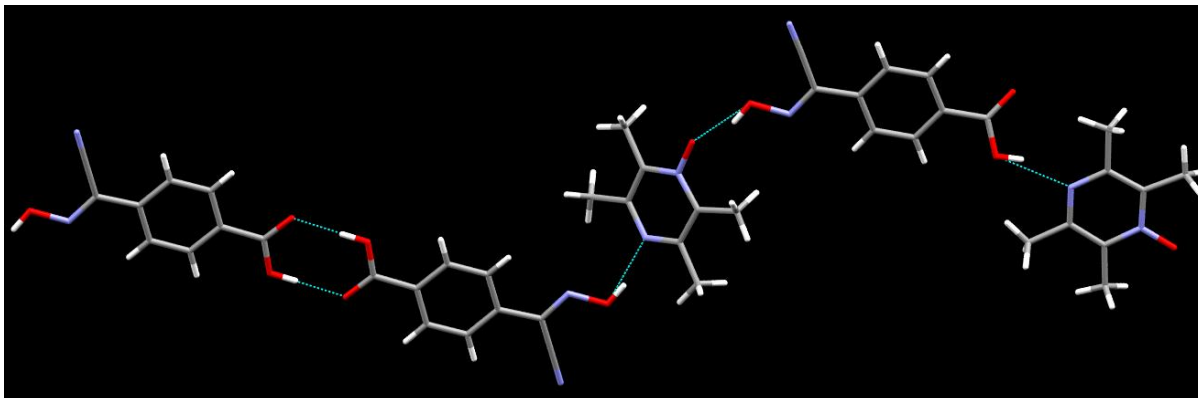


**Figure 4.16** The primary hydrogen-bond interactions in the crystal structure of **4BAOx:MPzO**

The asymmetric unit of **4BAOx:MPzO** has many different interactions, the best donor, cyanooxime group forms a hydrogen bond to the N-oxide (O27A···O34 2.533(2) Å), the second best acceptor, the pyrazine nitrogen atom also forms a hydrogen bond to a cyanooxime group (O17···O31 2.746(2) Å). The second best donor, acid group forms a hydrogen bond to the pyrazine nitrogen atom. (O29···N54 2.716(2) Å) an acid group also forms an acid-acid dimer (O19···N20 2.618(2) Å) (Figure 4.16)

### 4.3.2. Calculation of pairing energies for possible supramolecular outcomes

**Table 4.3 pairing energy calculations for 4-Phenolcyanooxime**

Acceptor	Self pairing of the donor	Self pairing of the acceptor	Phenol win	Cyanooxime win	Difference between The two outcomes
PzO	34.417	15.935	4.145	3.934	0.211
MPzO	34.417	10.174	9.009	8.617	0.392
BPO	34.417	21.827	10.291	10.096	0.195
3PI	34.417	19.097	20.582	20.235	0.347
1PB	34.417	19.813	13.181	13.138	0.043
3PB	34.417	23.718	14.951	14.565	0.386
4PB	34.417	23.343	13.794	13.488	0.306
3PMB	34.417	24.592	17.705	17.246	0.459
4PMB	34.417	23.942	15.937	15.548	0.389

**Table 4.4 pairing energy calculations for 4-acidcyanooxime**

Acceptor	Self-pairing of the donor	Self-pairing of the acceptor	Cyanooxime win	Acid win	Difference between The two outcomes
PzO	38.259	15.935	-0.591	-0.869	0.278
MPzO	38.259	10.174	3.421	2.904	0.516
BPO	38.259	21.827	5.392	5.135	0.257
3PI	38.259	19.097	14.717	14.260	0.457
1PB	38.259	19.813	7.812	7.755	0.057
3PB	38.259	23.718	9.784	9.277	0.507
4PB	38.259	23.343	8.443	8.040	0.403
3PMB	38.259	24.592	12.370	11.766	0.604
4PMB	38.259	23.942	10.444	9.932	0.512

**Table 4.5 pairing energy calculations for 3-Acidcyanooxime**

Acceptor	Self pairing of the donor	Self pairing of the acceptor	Cyanooxime win	Acid win	Difference between The two outcomes
PzO	37.904	15.935	4.145	3.934	0.211
MPzO	37.904	10.174	9.009	8.617	0.392
BPO	37.904	21.827	10.291	10.096	0.195
3PI	37.904	19.097	20.582	20.235	0.347
1PB	37.904	19.813	13.181	13.138	0.043
3PB	37.904	23.718	14.951	14.565	0.386
4PB	37.904	23.343	13.794	13.488	0.306
3PMB	37.904	24.592	17.705	17.246	0.459
4PMB	37.904	23.942	15.937	15.548	0.389

In the case of all three donors large pairing energies observed suggest a high susceptibility for co-crystallization. The energy difference between the predicted outcome and the alternative are less than 2 kJ/mol.

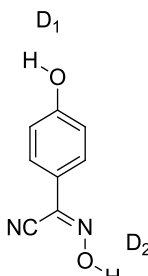
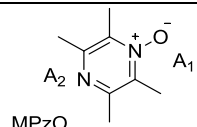
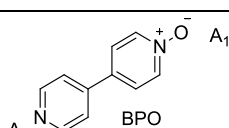
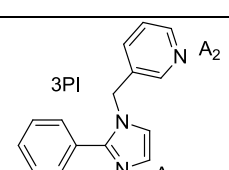
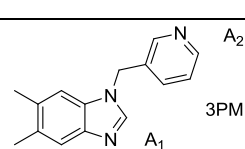
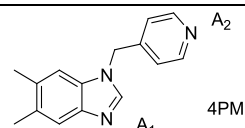
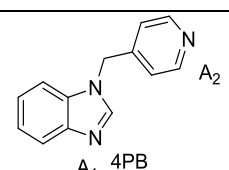
#### 4.4. Discussion

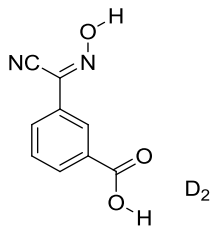
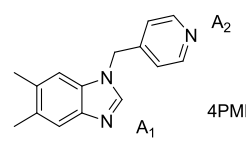
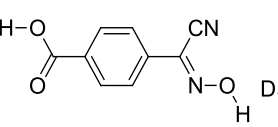
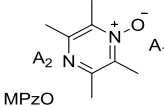
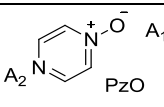
A few optimizations were made to the reported synthetic methods<sup>13</sup> in order to increase yields and reduce reaction time. For the conversion of the acetonitrile groups to cyanooximes, using a solution of NaOH in methanol instead of sodium in isopropanol did not have any adverse effect on the yield and it reduced the preparation time for the reaction as the tedious preparation of a sodium isopropoxide solution was not required. p-toluic acid and m-toluic acid were used as starting material instead of their more expensive chloromethyl analogues.

According to the MEP calculations the cyanooxime group is stronger than the carboxylic acid group and weaker than the phenol. All five structures obtained with 4-hydroxycyanooxime follow the preferences predicted by MEP calculations where, the best donor, phenol selectively hydrogen-bonded to the best acceptor and the cyanooxime which is the second best donor picked up the second best acceptor. Therefore the hierarchy between the phenol and cyanooxime was successfully predicted based on the calculated MEP values (table 4.6)

In the cases of 3 and 4-acidcyanooxime MEP calculations show the cyanooxime to be the better donor compared to the acid. Out of the four structures obtained, two exhibit the behavior predicted where the cyanooxime binds to the best acceptor and the acid group picks up the second best acceptor. Out of the remaining structures, in the asymmetric unit of 4-Acidcyanooxime:MPzO we observe two instances of the cyanooxime binding to the N-oxide group which is the best acceptor, the acid picks up the pyrazine nitrogen in one case and forms a two point acid-acid dimer in the other. Even though the exact predicted interactions were not observed in this case the cyanooxime appears to dominate as the stronger donor picking up the best acceptor and the second best acceptor. In the case of 4-acid cyanooxime and PzO however, the cyanooxime group picks up the pyrazine nitrogen ( $D_1 \cdots A_2$ ) and the carboxylic acid binds to the N-oxide site ( $D_2 \cdots A_1$ ) which contradicts the predictions made based on MEP calculations (Table 4.6)

**Table 4.6 Outcomes for the nine co-crystals obtained**

Donor	Acceptor	$D_1 \cdots A_1$	$D_1 \cdots A_2$	$D_2 \cdots A_1$	$D_2 \cdots A_2$
	 MPzO	✓	✗	✗	✓
	 BPO	✓	✗	✗	✓
	 3PI	✓	✗	✗	✓
	 3PMB	✓	✗	✗	✓
	 4PMB	✓	✗	✗	✓
	 4PB	✓	✗	✗	✓

$D_1$  $D_2$	 $A_2$ $A_1$ 4PMB	✓	✗	✗	✓
$D_2$  $D_1$	 $A_2$ $A_1$ MPzO	✓	✓	✗	✓
	 $A_2$ $A_1$ PzO	✗	✓	✓	✗

A survey of the Cambridge structure database on molecules containing the same combinations of donors yielded a the 1:1 binary co-crystal for 4BaOx:4PMB where the as predicted the best donor, cyanooxime group binds to the benzimidazole, the best acceptor and the acid group which is the second best donor picks up the pyridine.

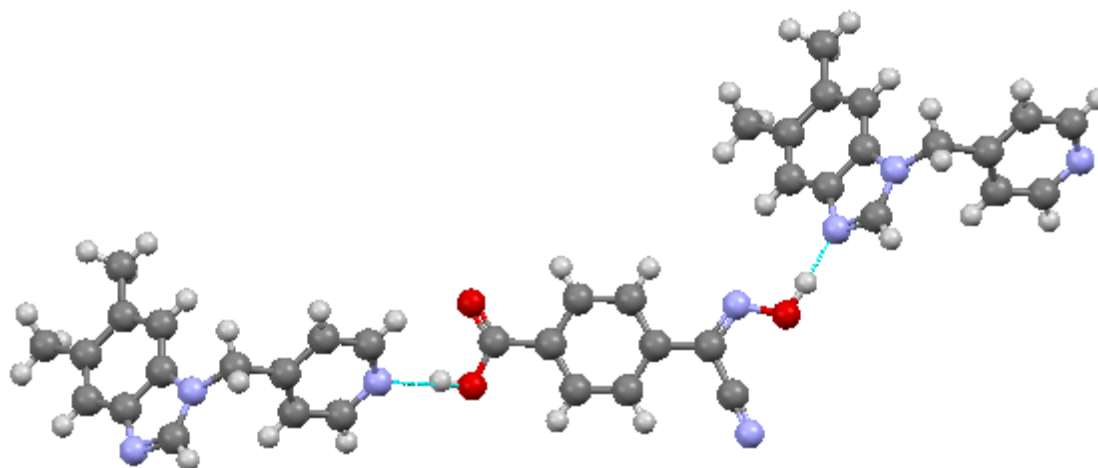


**Figure 4.17** The published structure of the 1:1 co-crystal of 4BaOx and 4PMB<sup>14</sup>

In total out of the ten asymmetric ditopic acceptors containing the cyanooxime functionality nine showed the supramolecular selectivity predicted by the ranking based on calculated MEP values.

The calculated pairing energies in many of the cases give values around and above 11 kJ/mol predicting co-crystal formation. However the energy differences between the predicted



outcome and the possible alternative to be less than 2 kJ/mol . Therefore predictions on possible supramolecular outcomes cannot be made using this method.

In this chapter we have shown that even in the case of weak and reversible supramolecular interactions nine out of ten times, the outcome was predicted using calculated MEP values with the cyanooxime group. This further proves that predicted MEP values can be used to predict the supramolecular outcomes over a variety of systems

## References

---

- <sup>1</sup> F. Tellier, R. Fritz, L. Kerhoas, P. Ducrot, A. Carlin-Sinclair, J. Einhornb and P. Leroux, *Pest Manag Sci.* **2009**, *65*, 129–136
- <sup>2</sup> K. Oberdorf, U. Kardorff, H. Theobald, A. Harreus, H. Koenig and V. Harries, US Patent 5,489,605, 1996.
- <sup>3</sup> N. Gerasimchuk, A. Gamian, G. Glover, and B. Szponar, *Inorganic Chemistry*, **2010**, *49*, **21**, 9863-9874
- <sup>4</sup> H. A Charlier, A. Gerasimchuk, , US Patent 7,727,967, June 1, 2010
- <sup>5</sup> A. A. Espenbetov, Yu. T. Struchkov, L. V. Rybakova, *J.Struct.Chem.* **1986**, *27*, 180-181
- <sup>6</sup> D. Musumeci, C.A. Hunter, R. Prohens, S. Scuderi and J. F. McCabe, *Chem. Sci.*, **2011**, *2*, 883-890.
- <sup>7</sup> M.C. Etter, *J. Phys. Chem.* **1991**, *95*, 4601
- <sup>8</sup> M. C.,Etter, G. M. Frankenbach, *Chem. Mater.* **1989**, *1*, 10.
- <sup>9</sup> D. J. Combs and R. S. Lokey, *Tetrahedron Lett.*, **2007**, *48*, 2679-2682
- <sup>10</sup> Thesis, Michelle Smith
- <sup>11</sup> Y. Sako, S. Ichikawa, A. Osada, A. Matsuda, *Bioorganic & Medicinal Chemistry*, **2010**, *18*, **22**, 7878-7889
- <sup>12</sup> E. Takagi, Y. Yokoi, M. Mangyo, Assignee: Mitsubishi Chemical Industries Ltd.; JP 32005565 B4 1957
- <sup>13</sup> D. Robertson, C. Barnes, N. Gerasimchuk, *J. Coord. Chem.* **2004**, *57*, 1205
- <sup>14</sup> C. B. Aakeroy, J. Desper, M. M. Smith, *Chem. Commun.* **2007**, *38*, 3936.

## Chapter 5. Exploring the structural landscape of 1-deazapurine

### 5.1. Tautomerism

Tautomerism is a form of isomerism where two versions of the same molecule are readily interconvertible<sup>1</sup>. For two isomers to be considered as tautomers, the free energy difference between the tautomers should be below 25 kcal/mol and both tautomers should be present in the system<sup>2</sup>. The migrating group X (Figure 5.1) can either be an electrofuge or a nucleofuge. Where the electrofuge is the proton, the resulting tautomerism is called prototropism or protontopic tautomerism.

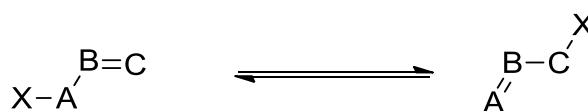


**Figure 5.1 A pair of tautomers where the group X acts as either an electrofuge or a nucleofuge during isomerization<sup>1</sup>**

Prototropic tautomerism differs from other types of tautomerism. Due to the small size of protons, sterics have little effect on this type of tautomerism and since protons can engage in hydrogen bonding, the hydrogen bonding environment can have a significant effect on the rate and equilibrium. Tautomeric forms of a molecule differ in shape, functional groups<sup>3</sup>, and hydrogen-bonding pattern<sup>4</sup>(Figure 5.2)

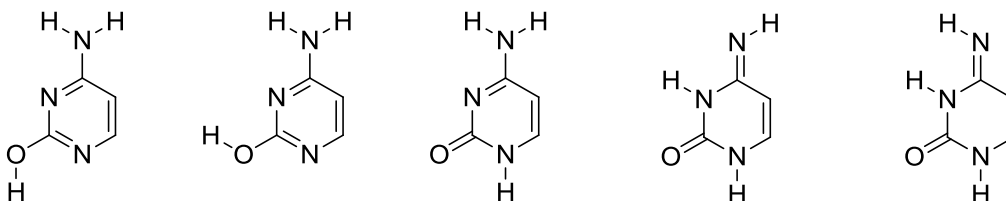


**Figure 5.2 The five most stable tautomeric forms of cytosine<sup>3</sup>.**

The presence of multiple tautomers presents a challenge in covalent synthesis as shown in Figure 5.3, as different tautomers can yield different constitutional isomers.

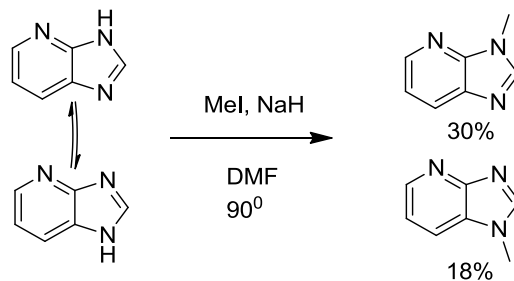


**Figure 5.3** Each tautomer of 1-deazapurine leads to a different isomeric product<sup>5</sup>.

## 5.2. Purines and deazapurines

Purines are vital components of nucleic acids that are essential for all known forms of life. In addition purines are the main functionalities in some pharmaceuticals<sup>6</sup> and organometallics<sup>7</sup>. This family of compounds also exhibit prototropic tautomerism. In the case of purines the two major tautomers (N(7)H and N(9)H) are observed<sup>8</sup> that have very different hydrogen-bonding environments<sup>9</sup>(Figure 5.4).

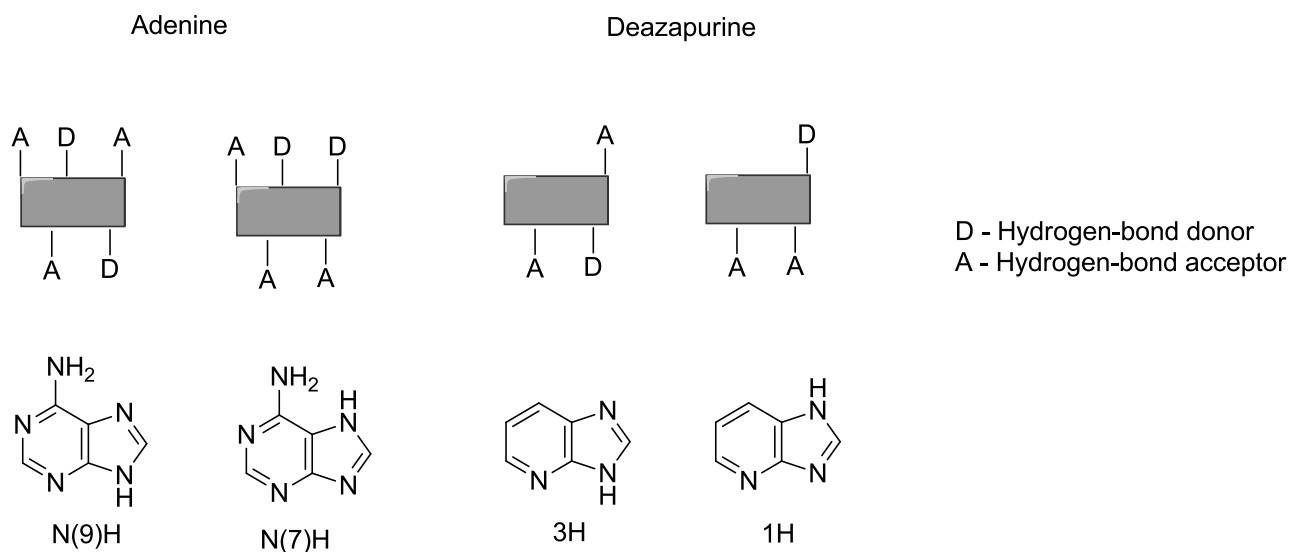


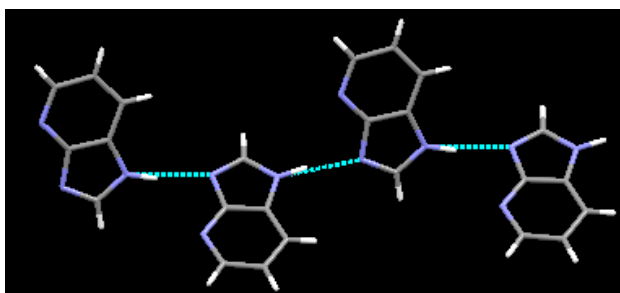
**Figure 5.4** Different hydrogen bonding environments of adenine (left) and 1-deazapurine (right)

Deazapurine exhibits the same type of tautomerism as adenine but has fewer donor and acceptor sites and better aqueous solubility compared to purines making them ideal model molecules for studying prototropism. In addition, 1-deazapurine (imidazo[4,5-b]pyridine) derivatives are used as algesics<sup>10</sup>, antidepressants<sup>11</sup>, antiviral agents<sup>12</sup> and cytotoxins<sup>13</sup>. DFT

calculations show that in the gas phase there is a 11.15 kJ/mol energy difference between the two tautomers favoring the 3H tautomer but in the aqueous phase this difference falls below 1 kJ/mol. Both the 1H and 3H tautomers are observed in aqueous solutions<sup>14</sup>.

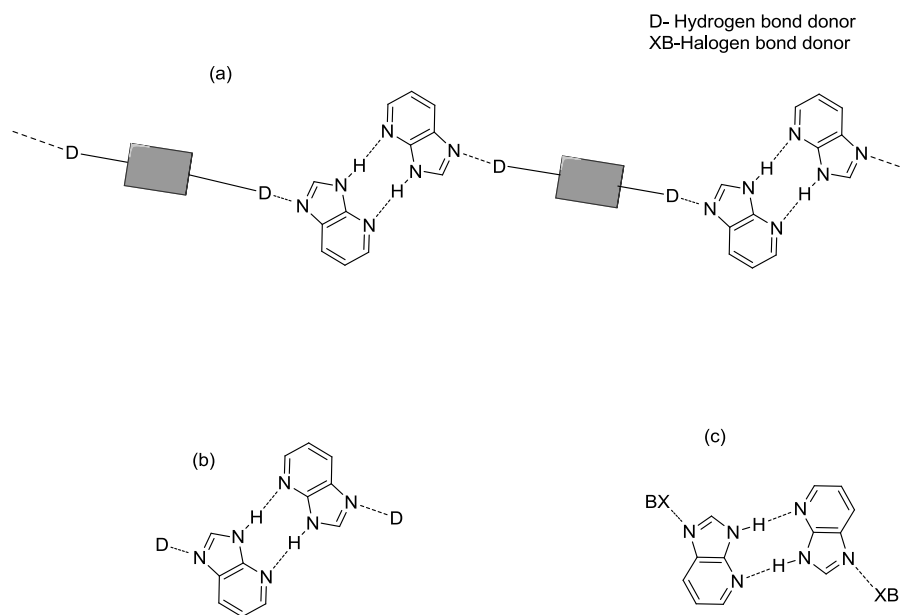
### 5.3. Supramolecular control of tautomerism

As equilibrium of prototropic tautomers can be affected by the local hydrogen bonding environment, it should in principle be possible to use supramolecular reagents to change the distribution of tautomers and even to isolate a desired tautomer in the solid state. In the case of deazapurine, the reported structure<sup>15</sup> in the solid state shows the 1H tautomer forming a one dimensional chain formed by the N-H group on the imidazole ring picking up the aromatic nitrogen atom on the imidazole ring (Figure 5.5)



**Figure 5.5 The primary hydrogen-bonding interactions in the crystal structure of 1-deazapurine**

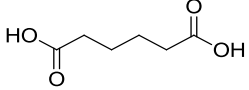
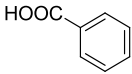
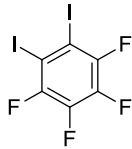
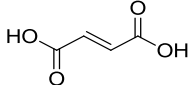
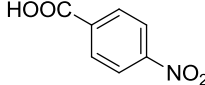
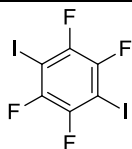
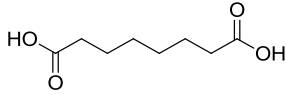
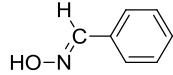
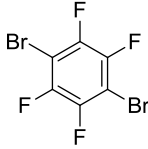
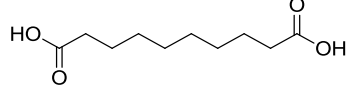
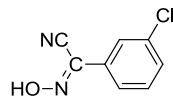
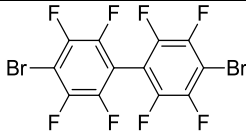
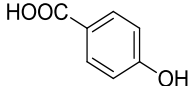
In the case of the 3H, tautomer we would expect it to form a self-complementary dimer involving the imidazole N-H group and the pyridyl N atom. In order to facilitate the formation of this dimer we could introduce a strong hydrogen-bond donor which can pick up the imidazole nitrogen atom.



**Figure 5.6 Possible synthons for stabilizing the possible supramolecular outcome for the 3H tautomer**

Table 5.1 shows the selected hydrogen and halogen bond donors that were used to stabilize and isolate the 3H tautomer, which we have separated in to three groups, symmetric ditopic hydrogen-bond donors which can form one dimensional chains incorporating the desired tautomer of 1-deazapurine (Figure 5.6 a). Monotopic hydrogen-bond donors that can stabilize the dimers as tetramers (Figure 5.6 b). Since 1-deazapurine has more than one acceptor site it is possible that strong hydrogen-bond donors could disrupt the dimer. Halogen bond donors might prove to be a suitable alternative (Figure 5.6 c).

**Table 5.1 Selection of hydrogen and halogen bond donors**

Ditopic hydrogen-bond donors	Monotopic hydrogen-bond donors	Halogen bond donors
		
		
		
		
		

The goals for this chapter are to:

- Synthesize and characterize 1-deazapurine;
- Perform DFT calculations on the donors and acceptors;
- Attempt to isolate the 3H tautomer of 1-deazapurine by co-crystallizing with hydrogen and halogen bond donors;
- Synthesize co-crystals of deazapurine with selected donors.

## 5.4.Experimental

### 5.4.1. Synthesis

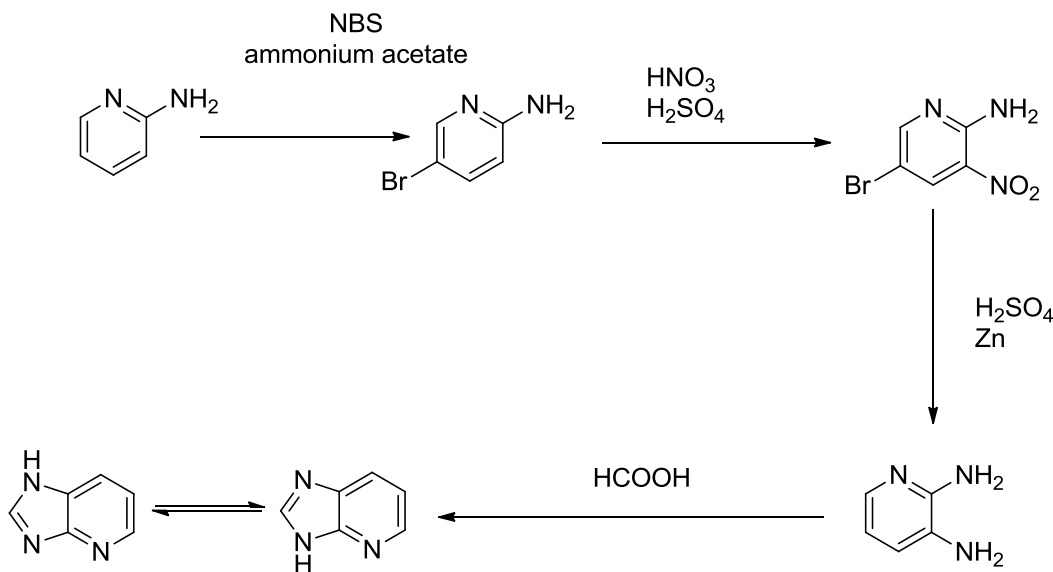
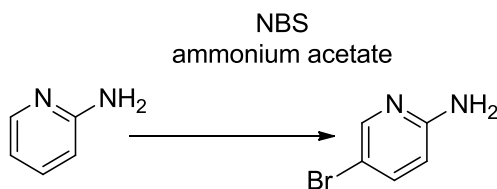


Figure 5.7 Synthetic scheme for 1-deazapurine.

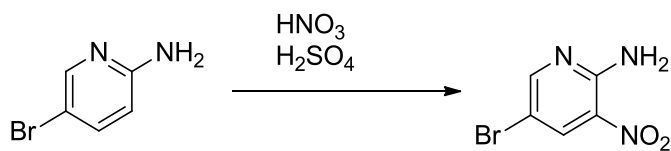
#### 5.4.1.1. Synthesis of 2-amino-5-bromopyridine



2-Aminopyridine (5 g, 53 mmol) was dissolved in 150 ml of acetonitrile. 20 g of ammonium acetate was added to it. NBS (9.9g, 53 mmol) was slowly added to the stirring suspension dropwise. The absence of starting material was confirmed via TLC in about 15 minutes. The acetonitrile was removed under reduced pressure. The solid was dissolved in ethyl acetate, washed with water and brine and dried over MgSO<sub>4</sub>. Ethyl acetate was removed under reduced pressure yielding a light brown crystalline solid. (8.2 g, 90% ) m.p. 115-120 °C, <sup>1</sup>H NMR (400 MHz, CDCl<sub>3</sub>-d) δ ppm 6.42 (1 H, d, *J*=8.98 Hz), 7.50 (1 H, dd, *J*=8.59, 2.34 Hz), 8.11 (1 H, d, *J*=2.34 Hz)

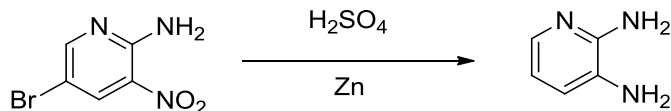


#### 5.4.1.2. *Synthesis of 2-amino-3-nitro-5-bromopyridine*



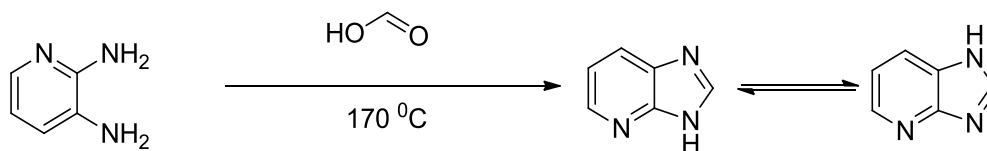
2-Aminopyridine-5-bromopyridine (2 g, 11.6 mmol) was carefully dissolved in 30 ml of H<sub>2</sub>SO<sub>4</sub>. The mixture was cooled to 0 °C. HNO<sub>3</sub> (0.8 ml, 11.6 mmol) was added dropwise to the stirring solution. The solution was stirred at 0 °C for two hours and heated to 50 °C for another two hours. The yellow liquid was poured on to 10 g of crushed ice and a yellow precipitate was filtered (2.25 g, 88.9%) m.p. 192-198 °C. <sup>1</sup>H NMR (400 MHz, DMSO-*d*<sub>6</sub>) δ ppm 8.07 (2 H, s), 8.49 (1 H, d, *J*=2.34 Hz), 8.52 (1 H, d, *J*=2.34 Hz)

#### 5.4.1.3. *Synthesis of 2,3-diaminopyridine*



2-Amino-3-nitro-5-bromopyridine (0.5 g, 2.30 mmol) and Zn dust (0.83g, 12.6 mmol) were added to 8 ml of water and 5 ml of methanol. Conc. H<sub>2</sub>SO<sub>4</sub> (0.733 ml 13.76 mmol) was added to the suspension and heated at 90 °C for 48 hours. The absence of reactants was confirmed by TLC. An excess of Na<sub>2</sub>CO<sub>3</sub> was added to the suspension and any solvent present was removed under reduced pressure. The product was extracted in methanol. The methanol was removed under reduced pressure and the solid obtained was extracted with ethyl acetate. The ethyl acetate was dried over MgSO<sub>4</sub> and removed under reduced pressure to obtain the product (0.05 g, 20%). m.p. 92-95 °C <sup>1</sup>H NMR (400 MHz, DMSO-*d*<sub>6</sub>) δ ppm 4.61 (2 H, br. s.), 5.29 (2 H, br. s.), 6.36 (1 H, d, *J*=4.69 Hz), 6.67 (1 H, d, *J*=7.42 Hz), 7.26 (1 H, d, *J*=5.08 Hz)

#### 5.4.1.4. *Synthesis of 1-deazapurine*

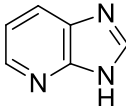
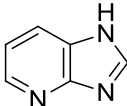
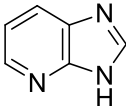
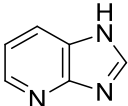


2,3-Diaminopyridine (1.0 g, 9.16 mmol) was mixed with formic acid (0.5 ml, 13.2 mmol). The resulting mixture was heated at 170 °C for 48 hours. The excess formic acid was removed under reduced pressure and the remaining solid was dissolved in 100 ml water. The product was

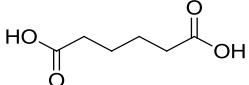
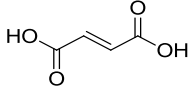
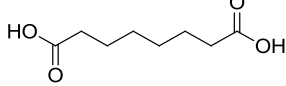
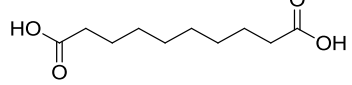
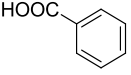
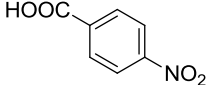
extracted to ethyl acetate 100 ml X 4. The ethyl acetate was removed under reduced pressure to yield the pure product. (0.33g, 30%) m.p. 125-130 °C <sup>1</sup>H NMR (400 MHz, DMSO-d<sub>6</sub>) δ ppm 7.23 (1 H, dd, J=7.81, 4.69 Hz), 8.02 (1 H, d, J=7.81 Hz), 8.35 (1 H, d, J=4.90 Hz), 8.43 (1 H, s), 12.91 (1 H, br. s.).

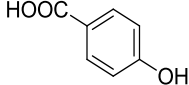
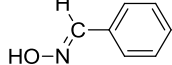
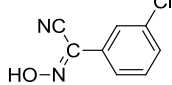
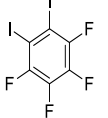
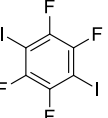
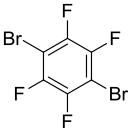
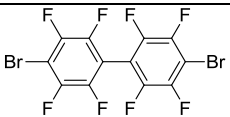
#### 5.4.2. MEP calculations on the donors and acceptors

##### 5.4.2.1. Calculated MEP values for the 1H and 3H tautomers of 1-Deazapurine

	AM1/ kJmol <sup>-1</sup>		DFT 6-31+G*/kJmol <sup>-1</sup>	
	3H 	1H 	3H 	1H 
Py - N	-242	-306	-153	-226
Im - N	-283	-305	-184	-227
N-H	183	203	259	288

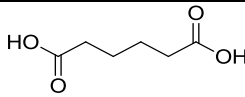
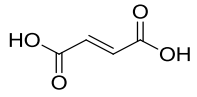
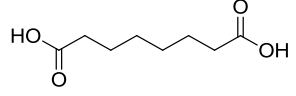
##### 5.4.2.2. Calculated MEP values for the hydrogen-bond and halogen bond donors

Hydrogen-bond donors	AM1/ kJmol <sup>-1</sup>	DFT 6-31+G*/kJmol <sup>-1</sup>
	144	276
	163	295
	140	267
	137	262
	134	267
	170	309

	191(OH) 138 (COOH)	305(OH) 244(COOH)
	134	244
	176	296
	--	175
	--	182
	--	141
	--	143

### 5.4.3. Solvent-drop grinding experiments

The deazapurine (10 mg 0.083 mmol) was mixed with hydrogen or halogen bond donors (0.083 mmol). Two drops of methanol (Hydrogen bond donors) or dichloromethane (halogen bond donors) was added to the mixture and ground for two minutes. The solid obtained was analyzed by FTIR.

		C=O	930-960 cm <sup>-1</sup>	Co-crystal
DA1		1708	953	YES
DA2		1688	-	YES
DA3		1693	-	YES

DA4		1693	-	YES
A1		1684	950	YES
A2		1687	-	YES
A3		1675	951,933	YES
O1		NA	942	YES
O2		NA	952	YES
I1		NA	950	YES
I2		NA	-	YES
I3		NA	953	No
I4		NA	954	No

#### 5.4.4. Determination of the tautomer based on IR spectroscopy

Based on the IR spectra of the co-crystals of which the structure has been determined it was observed that the stretch at around  $950\text{ cm}^{-1}$  in the deazapurine shifts to around  $930\text{ cm}^{-1}$  in all of the structures with the 1H tautomer. No such shift was observed with the structures with the 3H tautomer.

#### **5.4.5. Syntheses for obtained co-crystals**

##### **5.4.5.1. Synthesis of 1-deazapurine, 1,2-diiodotetrafluorobenzene (1:1), DP:I1**

1-Deazapurine (2.96 mg, 0.025 mmol) and 1,2-diiodotetrafluorobenzene (10 mg, 0.025 mmol) were dissolved in 2 ml dichloromethane with heat. The solution was allowed to stand at room temperature for slow evaporation. Colourless plates were observed in 10 days (m.p. 78 – 82 °C).

##### **5.4.5.2. Synthesis of 1-deazapurine, 1,4-diiodotetrafluorobenzene (1:1), DP:I2**

1-Deazapurine (5 mg, 0.04 mmol) and 1,4-diiodotetrafluorobenzene (16.9 mg, 0.04 mmol) were dissolved in methanol with heat. The solution was allowed to stand at room temperature for slow evaporation. Bronze prisms were observed in two weeks. (m.p. 145 – 149 °C).

##### **5.4.5.3. Synthesis of 1-deazapurine, adipic acid (1:1), DP:DA1**

1-Deazapurine (10 mg, 0.08 mmol) and adipic acid (12.2 mg, 0.08 mmol) were ground together with a drop of methanol. The resulting solid was allowed to crystallize under slow evaporation at room temperature. Brown prisms were observed in one week. (m.p. 100 - 104 °C).

##### **5.4.5.4. Synthesis of 1-deazapurine, sebacic acid (1:1), DP:DA4**

1-deazapurine (10 mg, 0.08 mmol) and sebacic acid (17.0 mg, 0.08 mmol) were ground together with a drop of methanol. The resulting solid was allowed to crystallize under slow evaporation at room temperature. Colorless prisms were observed in 15 days. (m.p. 80 - 84 °C).

##### **5.4.5.5. Synthesis of 1-deazapurine, 4-hydroxybenzoic acid (1:1), DP:A4**

1-Deazapurine (10 mg, 0.08 mmol) and 4-hydroxybenzoic acid (11.6 mg, 0.08 mmol) were ground together with a drop of methanol. The resulting solid was allowed to crystallize under slow evaporation at room temperature. Brown rods were observed in three weeks. (m.p. 165 -170 °C)

#### 5.4.6. Structure descriptions

##### 5.4.6.1. Crystal structure of 1-deazapurine , 1,2-diiodotetrafluorobenzene (1:1), DP:I1

Structure determination of **DP:I1** shows that in the resulting 1:1 co-crystal the deazapurine exists in the 3H tautomeric form. The N-H group on the deazapurine picks up the pyridine site of another deazapurine molecule forming a homodimer (N13-H13...N15 1.97 Å, N13...N15 2.843(4) Å). The imidazole nitrogen forms a halogen bond to the iodine site on **I1** (I1...N11 2.800(4) Å) resulting in a zero dimensional tetramer. (Figure 5.8)

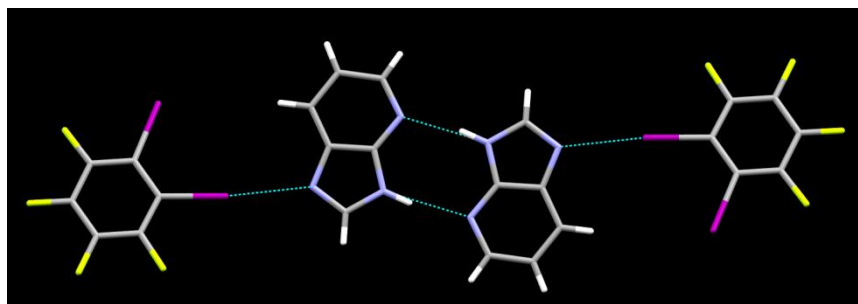
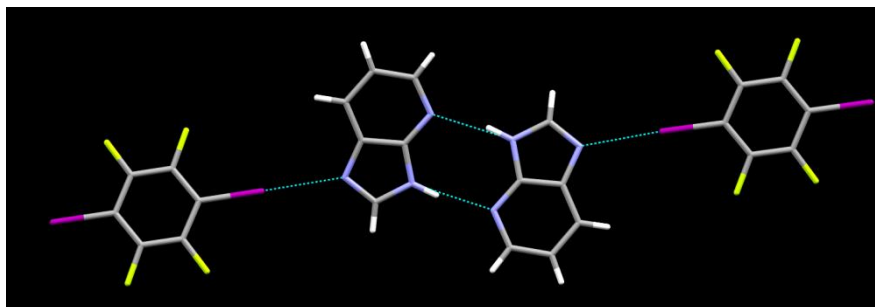


Figure 5.8 The primary hydrogen-bond interactions in the crystal structure of DP:I1

##### 5.4.6.2. Crystal structure of 1-deazapurine , 1,4-diiodotetrafluorobenzene (1:1), DP:I2

Structure determination of **DP:I2** shows that in the resulting 1:1 co-crystal the deazapurine exists in the 3H tautomeric form. The N-H group on the deazapurine picks up the pyridine site of another deazapurine molecule forming a homodimer (N13-H13...N25 1.96 Å, N13...N25 2.828(7) Å and N23-H23...N15 1.99 Å, N15...N23 2.848(7) Å). The imidazole nitrogen forms a halogen bond to the iodine site (I1...N11 2.777(5) Å, I3...N21 2.769(5) Å) on **I2** forming a one dimensional chain.(Figure 5.9)



**Figure 5.9** The primary hydrogen-bond interactions in the crystal structure of DP:I2

#### 5.4.6.3. *Crystal structure of 1-deazapurine , adipic acid (1:1), DP:DA1*

Structure determination of DP:DA1 shows that in the resulting 1:1 co-crystal the deazapurine exists in the 3H tautomeric form. The N-H group on deazapurine picks up the pyridine site of another deazapurine molecule forming a homodimer (N13-H13 $\cdots$ N15 1.97(2) Å, N13 $\cdots$ N15 2.854(18) Å). The imidazole nitrogen atom is picked up by the carboxylic acid group (O21-H21 $\cdots$ N11 1.70(3) Å, O21 $\cdots$ N11 2.666(15) Å) resulting in a one dimensional chain. (Figure 5.10)

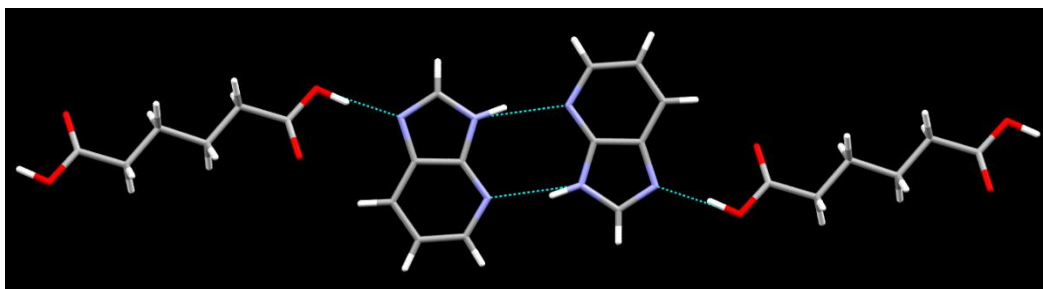


**Figure 5.10** The primary hydrogen-bond interactions in the crystal structure of DP:DA1.

#### 5.4.6.4. *Crystal structure of 1-deazapurine , sebacic acid (2:1), DP:DA4*

In the case of sebacic acid, a 2:1 co crystal was obtained where the deazapurine exists in the 3H tautomer. Instead of the homodimer, the pyridyl nitrogen atom and the N-H group deazapurine form a two point interaction with one of the acid groups (N13-H13 $\cdots$ O22 2.063(19) Å, N13 $\cdots$ O22 2.8624(16) Å) and (O21-H21 $\cdots$ N15 1.84(2) Å, O21 $\cdots$ N15 2.6845(16) Å) the second acid group picks up the imidazole nitrogen atom of a second deazapurine molecule forming a single point interaction. (O30-H30 $\cdots$ N11 1.86(2) Å, O30 $\cdots$ N11 2.7603(16) Å) resulting in a one dimensional chain.(Figure 5.11)

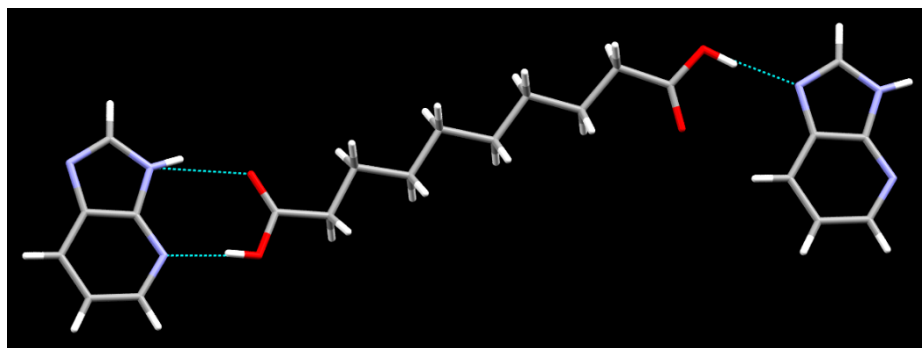


**Figure 5.11** The primary hydrogen-bond interactions in the crystal structure of DP:DA4

**5.4.6.5. Crystal structure of 1-deazapurine , 4-hydroxybenzoic acid (1:1), DP:A4**

Structure determination of DP:A4 shows that in the resulting 1:1 co-crystal the 1H tautomer is observed where the carboxylic acid group forms a hydrogen-bond to the imidazole nitrogen atom (O21-H21 $\cdots$ N13 1.72(3) Å, O21 $\cdots$ N13 2.6322(15) Å) and the N-H group on the deazapurine hydrogen bonds to a pyridyl nitrogen atom (N11-H11 $\cdots$ N15 1.97(2) Å, N11 $\cdots$ N15 2.8506(16) Å). The phenol group forms a hydrogen-bond to the carbonyl group on a carboxylic acid group (O24-H24 $\cdots$ O22 1.84(3) Å O24 $\cdots$ O22 2.5961(15) Å) resulting in 2D sheets.(Figure 5.12)

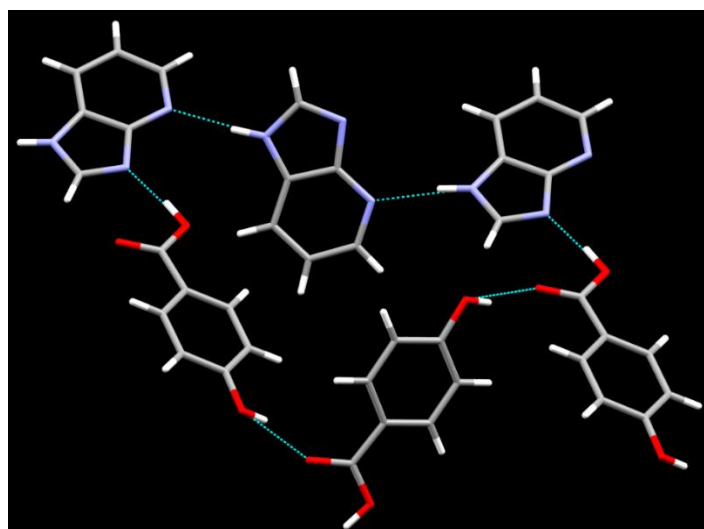


**Figure 5.12** The primary hydrogen-bond interactions in the crystal structure of DP:A4



## 5.5. Discussion

The synthetic steps for making 1-deazapurine were based on published synthetic methods. The bromination of the 5 position of 2-aminopyridine was required as direct nitration almost completely yielded 2-amino-5-bromopyridine. Only by blocking the 5 position using the bromo group as a protecting group on the pyridine, were we able to obtain the 3-nitro species in significant yields. We also combined the reduction of the nitro group and the removal of the Br protecting group by hydrodehalogenation in to a single step using Zn as the catalyst and generating H<sub>2</sub> in-situ using H<sub>2</sub>SO<sub>4</sub>. The low yield was due to the photosensitivity of 2,3-diaminopyridine. At the end of the reaction no starting material or byproducts were detected by TLC or NMR. This reaction was carried out in a closed system under dark conditions.

The structural data shows that four out of the five structures obtained was of the 3H tautomeric form out of which, three formed the deazapurine dimer with the donor group interacting with the imidazole nitrogen atom (Figure 5.13 (a)) thus stabilizing the dimer formed between 3H tautomer molecules.

With sebacic acid however, instead of the intended complementary deazapurine dimer a similar two- point interaction was observed between the acid and the deazapurine in addition to the usual acid imidazole nitrogen interaction (Figure 5.13 (b)).

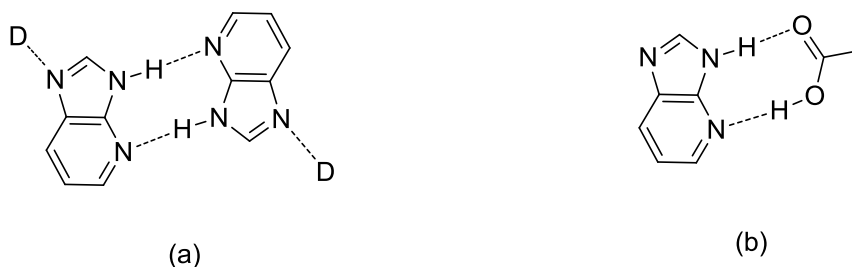


**Figure 5.13 The two supramolecular motifs observed with the 3H tautomer**

The former interaction can be expected as the acid and the 3H tautomer as shown in Figure 5.14 the two sites are geometrically compatible and the donor site on the acid has a stronger hydrogen-bond donating ability compared to the N-H group on the deazapurine. Therefore, sebacic acid, which has a higher MEP value, has picked up both acceptor sites on the deazapurine.

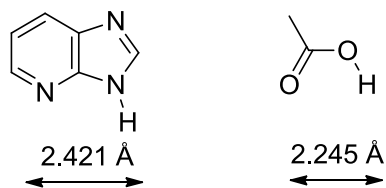


**Figure 5.14** The 3H tautomer of the deazapurine and the acid are geometrically compatible

IR spectroscopy was used to characterize the formation of co-crystals. Upon comparing IR spectra it was observed that the peak at around  $930\text{ cm}^{-1}$  was not found in the IR spectra of any of the structures containing the 3H tautomer (Figure 5.15). Although this cannot be observed in all cases as some of the donors have broad peaks in the same area, but frequently can be used to identify the tautomer present without growing single crystals.

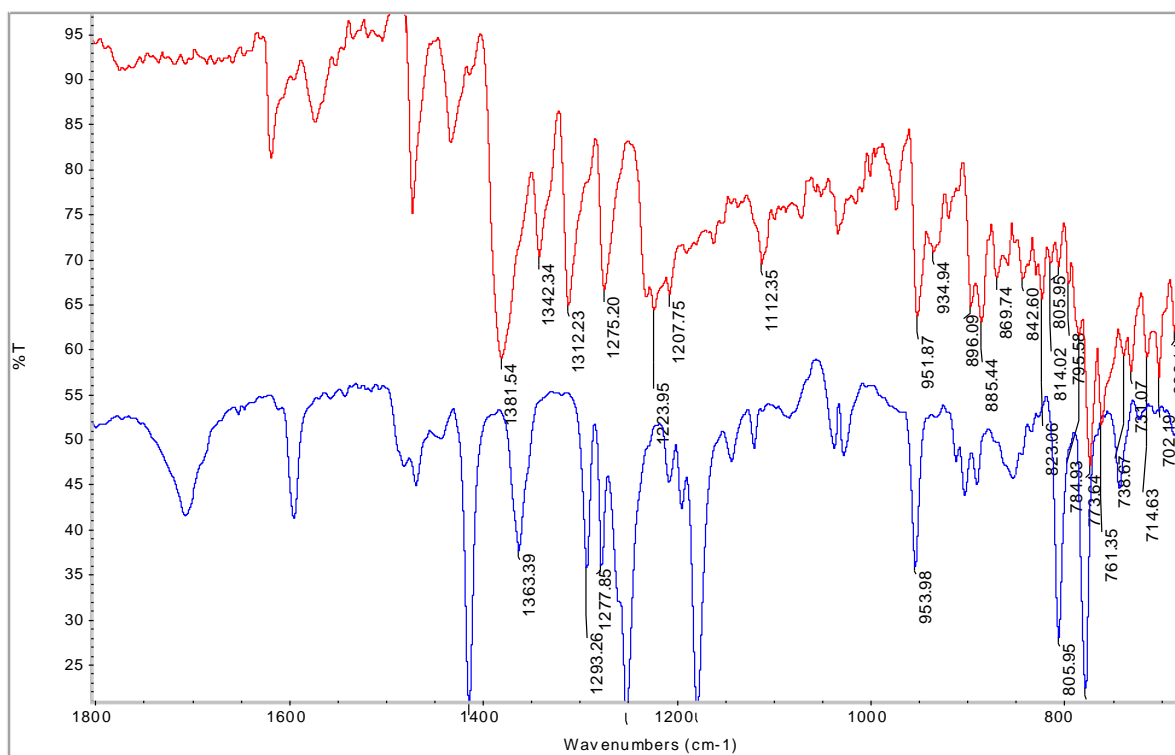


**Figure 5.15** IR spectra of 1-deazapurine (red) and the 1:1 co-crystal of 1-deazapurine:acetic acid (blue)

Based on calculated MEP values, the hydrogen-bond donor ability of the carboxylic acids are greater than that of the N-H group on the deazapurine. The structures obtained with sebacic acid and adipic acid (**DP:DA3** and **DP:DA1**) show that using strong two point donor systems like carboxylic acids can effectively isolate the 3H tautomer but it can prevent the formation of the homomeric deazapurine dimer by forming a heteromeric two-point interaction with the

deazapurine (Figure 5.13 (b)). Therefore, even though the desired tautomer is isolated there is no structural consistency due to synthon crossover<sup>16</sup>. In the case of halogen bond donors, the weaker halogen bond donors<sup>17</sup> are unable to compete with the two point hydrogen bonded dimer and as observed in the two structures **DP:I1** and **DP:I2**, will pick up the imidazole nitrogen atom thereby stabilizing the self-complementary deazapurine dimer. Therefore halogen bond donors can be used stabilize the 3H tautomer without any possibility for synthon crossover.

## 5.6. Conclusions

In conclusion, 1-deazapurine can exist in two prototropic tautomeric forms in aqueous solution. Using a selection of hydrogen and halogen bond donors we have successfully isolated the 3H tautomer four out of five times by stabilizing complementary dimer formed between the deazapurine molecules by forming a hydrogen-bond to the remaining imidazole site on the deazapurine. Carboxylic acids have stronger donor group compared to the deazapurine N-H site and this can result in it competing for the geometrically compatible pyridine site resulting in synthon crossover. This can be prevented by using weaker halogen bond donors that does not possess the strength or the geometric bias to compete with the self-complementary homomeric deazapurine interaction. Therefore, single-point halogen bond donors can be used to isolate the 3H tautomer while maintaining structural consistency.

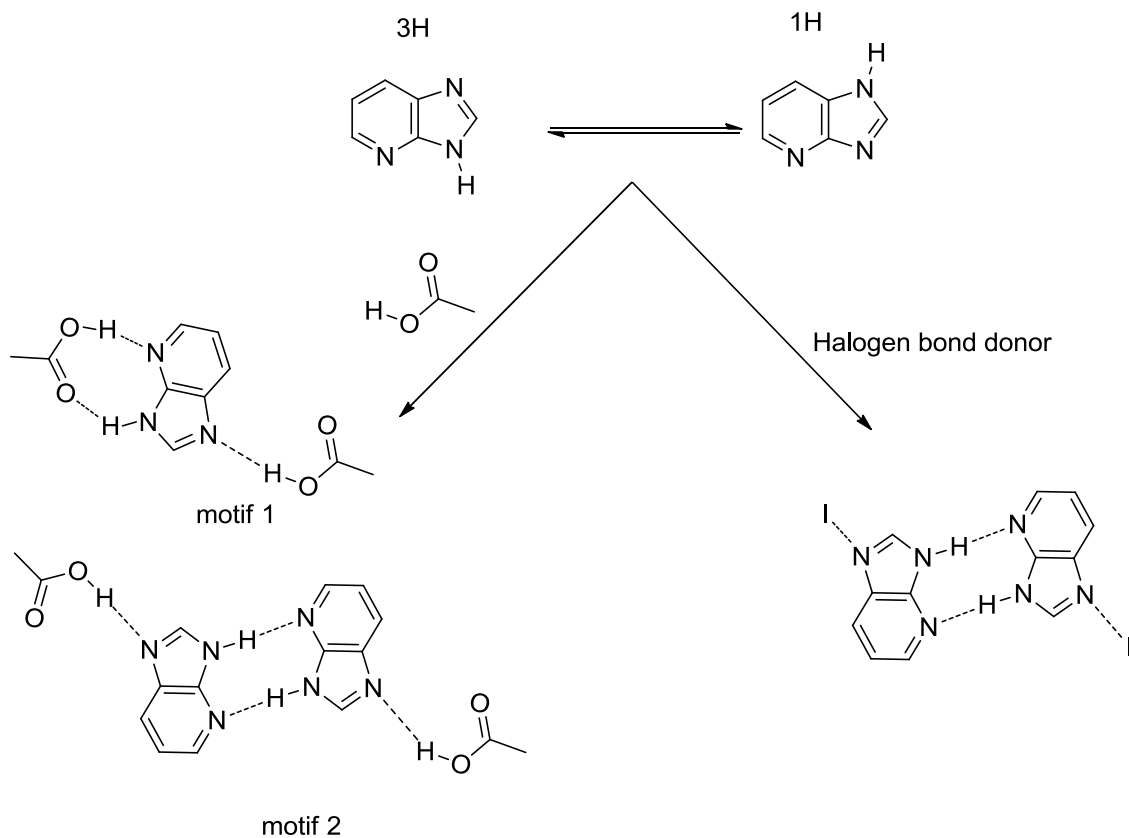


**Figure 5.16 Both hydrogen and halogen bond donors can be used to isolate the 3H tautomer of 1-deazapurine.**

## References

---

- <sup>1</sup> IUPAC. Compendium of Chemical Terminology, 2nd ed. (the "Gold Book"). Compiled by A. D. McNaught and A. Wilkinson. Blackwell Scientific Publications, Oxford (1997). XML on-line corrected version: <http://goldbook.iupac.org> (2006-) created by M. Nic, J. Jirat, B. Kosata; updates compiled by A. Jenkins. ISBN 0-9678550-9-8. doi:10.1351/goldbook.
- <sup>2</sup> J. Elguero, A. R. Katritzky, O. V. Denisko, *Adv. Heterocycl. Chem.* **2000**, 1-84
- <sup>3</sup> J. L. Alonso, V. Vaquero, I. Peña, J. C. López, S. Mata and W. Caminati, *Angew. Chem. Int. Ed.*, **2013**, 52, 2331–2334.
- <sup>4</sup> F. R. Llansola and E. W. Meije. *J.Am.Chem.Soc.* **2013**, 135, 6549–6553
- <sup>5</sup> J. Müller, F. Polonius, M. Roitzsch, *Inorg. Chim. Acta* **2005**, 4, 1225-1230
- <sup>6</sup> T. G. Davies, J. Bentley, C. E. Arris, F. T. Boyle, N. J. Curtin, J. A. Endicott, A. E. Gibson, B. T. Golding, R. J. Griffin and I. R. Hardcastle, *Nature Structural & Molecular Biology*, **2002**, 9, 745-749
- <sup>7</sup> J. Schütz and W. A. Herrmann, *Journal of organometallic chemistry*, **2004**, 689, 2995-2999
- <sup>8</sup> P. D. Lawley. "Fused Pyrimidines", Part 11, "Purines", D. J. Brown, Ed., Wiley-Interscience, New York, N.Y., **1971**, 439.
- <sup>9</sup> M. Dreyfus, G. Dodin, Bensaude, and J. E. Dubois *J Am Chem Soc.* **1975** 97, **9**, 2369-76
- <sup>10</sup> R. L. Clark, A. A. Pessolano, T. Y. Shen, D. P. Jacobus, H. Jones, V. J. Lotti, and L. M. Flataker, *J. Med. Chem.*, **1978**, 21, 965
- <sup>11</sup> M. M. Robinson and N. Finch, US Pat. 3719683.
- <sup>12</sup> J. P. Babbar and B. L. Chowdhury, *J. Sci. Ind. Res.*, **1962**, 21C, 312
- <sup>13</sup> J. A. Montgomery and K. Hewson, *J. Med. Chem.*, **1966**, 9, 105
- <sup>14</sup> J. Elguero, A. Fruchier, S. Mignonac-Mondon, *Bull. Soc. Chim. Fr.* **1972**, 7, 2916
- <sup>15</sup> L. Dymińska, A. Gağor, M. Mączka, Z. Węgliński and J. Hanuza, *J. Raman Spectrosc.*, **2010**, 41, 1021-1029
- <sup>16</sup> C. B. Aakeröy, P. D. Chopade, and J. Desper, *Cryst. Growth Des.* **2011**, 11, 5333–5336
- <sup>17</sup> C. B. Aakeröy, S. Panikkattu, P. D. Chopade and J. Desper, *CrystEngComm*, **2013**, 15, 3125-3136

## Chapter 6. Can urea be used to isolate the 1H tautomer of 1-deazapurine?

### 6.1. Introduction

#### 6.1.1. Deazapurines

As discussed in Chapter 5, 1-deazapurine exists in two main tautomeric forms which have different supramolecular environments. The 1H tautomer has two donor sites on the same side of the molecule and one acceptor site at the opposite end. A CSD search for possible geometrically compatible cofomers yielded one promising contender, N,N disubstituted urea with two donor sites and a single acceptor site is geometrically compatible to the 1H tautomer of 1-deazapurine. Figure 6.1

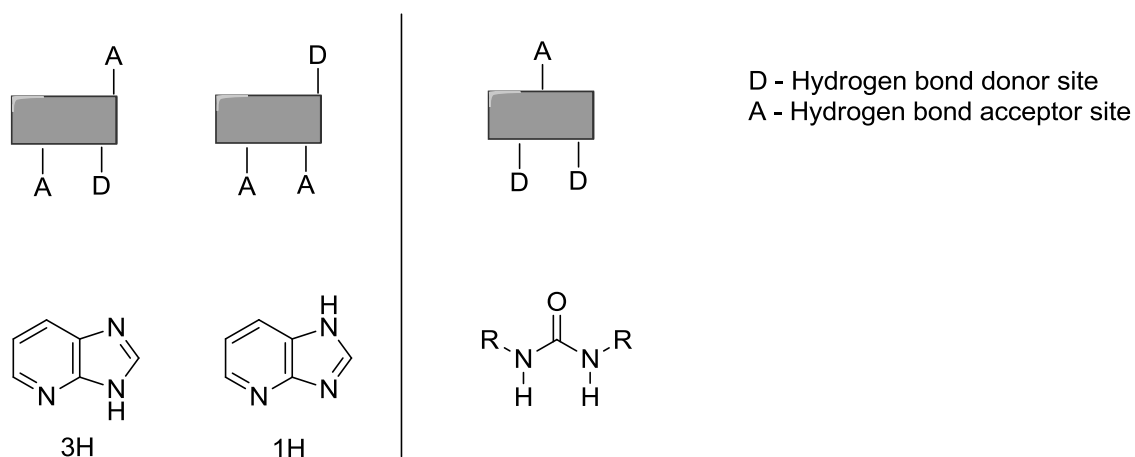


**Figure 6.1** The 1H tautomer of 1-deazapurine is compatible with urea.

#### 6.1.2. Urea

The urea functionality has shown considerable importance in pharmaceuticals<sup>1,2,3</sup>, organocatalysts<sup>4</sup> self-healing polymers<sup>5</sup>, supramolecular polymers<sup>6</sup> and as selective ion sensors<sup>7,8</sup>. It is also a functional group that has received a great deal of attention in the field of crystal engineering<sup>9,10,11</sup>.

In almost all of the above cases the functionality and importance of these molecules is directly related to the supramolecular behavior of the urea moiety. For example, urea based p38 MAP kinase inhibitors, which have potential as treatment for Crohn's disease<sup>1</sup> and rheumatoid arthritis<sup>1</sup>, binds to its substrate through a two point hydrogen bond interaction between the urea

hydrogen atoms and the carboxylate oxygen atoms of a glutamate group on the substrate, incorporation of triurea groups in polydimethylsiloxane polymers results in a self-healing material<sup>5</sup> (Figure 6.2 (a)) and in a florescent anion sensor, urea groups act as binding sites for the anion<sup>7</sup> (Figure 6.2 (b)).

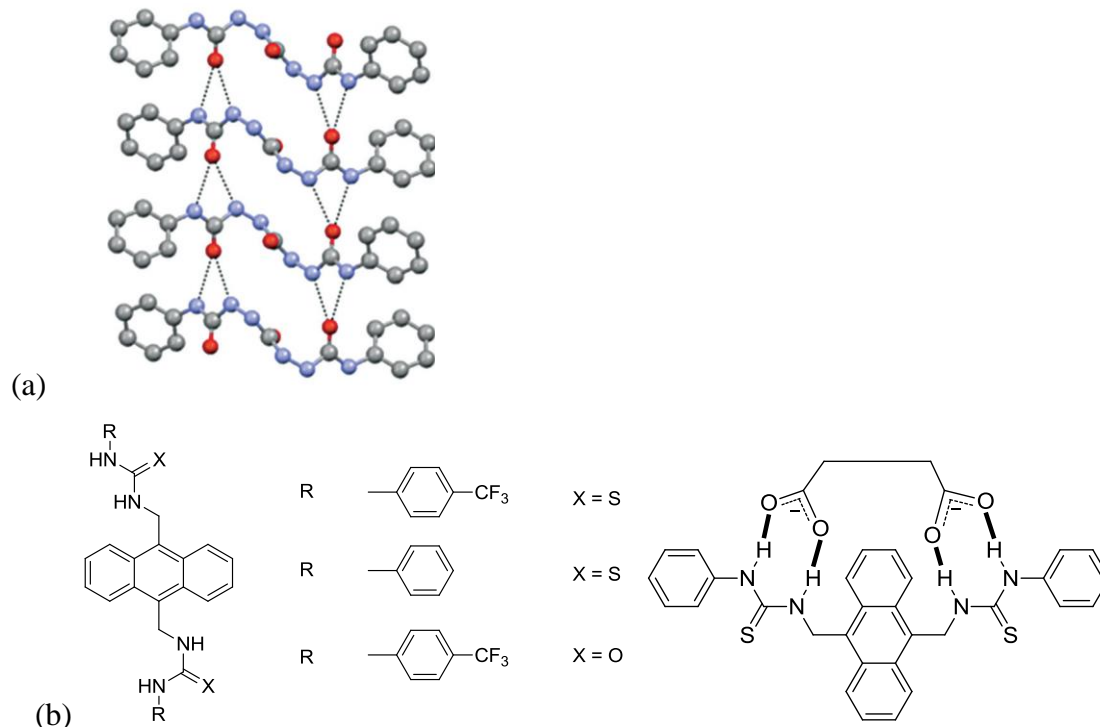


**Figure 6.2 (a) homomeric interaction of triurea<sup>5</sup> (b) urea based carboxylate sensor<sup>7</sup>**

In the solid state, N,N-disubstituted ureas form a tape-like network that involves both N-H groups forming bifurcated hydrogen bonds to the carbonyl group. This robust synthon, known as the  $\alpha$  network or  $\alpha$  tape is observed in a majority of crystal structure of N,N-disubstituted ureas. It has been reported that this synthon persists even in the presence of strong donor groups such as carboxylic acids and amides.<sup>12</sup>

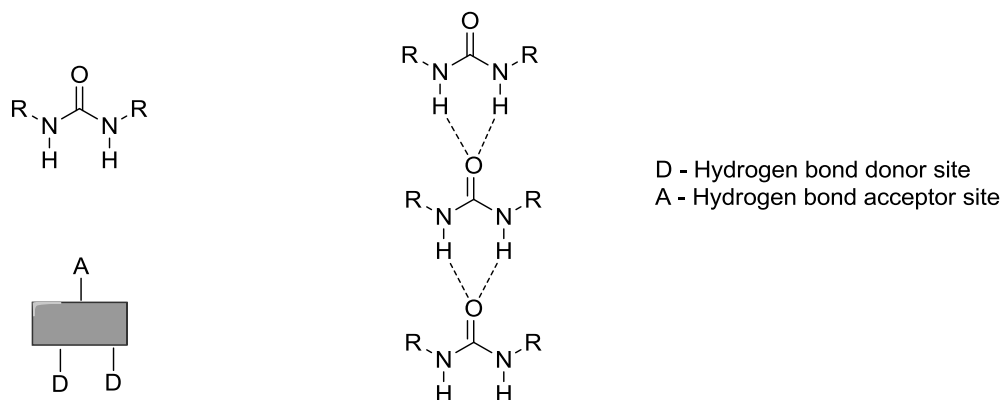


### Figure 6.3 Donors, acceptors and the $\alpha$ tape motif of N,N-disubstituted urea

However, the formation of the  $\alpha$  tape can be prevented by steric crowding<sup>13</sup>. In some cases such as pyridyl ureas, the urea N-H hydrogen atoms do not form the  $\alpha$  tape synthon. Instead, the two N-H groups form hydrogen bonds to the pyridyl nitrogen<sup>14</sup> (the better acceptor).

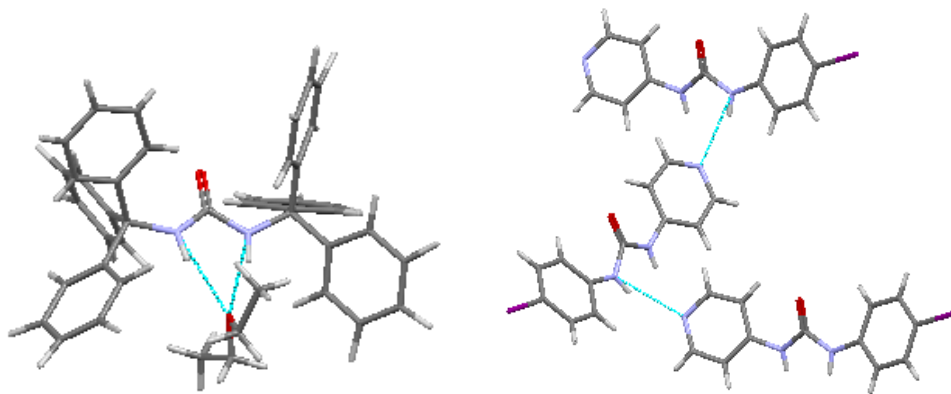


**Figure 6.4 (a) N,N-bistritylurea forms solvates due to steric crowding (b) 1-(4-chlorophenyl)-3-pyridyl urea forms a N-H...N interaction instead of the  $\alpha$  tape synthon.<sup>15</sup>**

Therefore, it is conceivable that this type of interaction can be used to control the formation of the persistent  $\alpha$  tape synthon in a multi-component system by controlling the electronic and steric environment on the ureas by covalent modification.

#### 6.1.3. Hypothesis

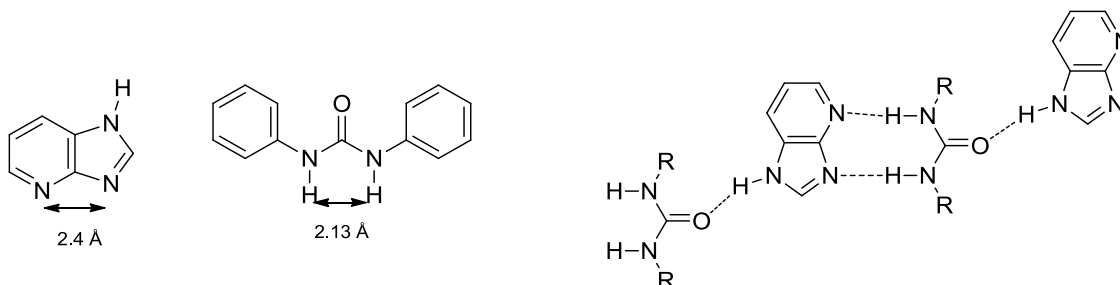


**Figure 6.5 Suggested motif for the co-crystal of the 1H tautomer of 1-deazapurine and urea**

In this chapter, we explore possibility isolating the 1H tautomer of 1 deazapurine with the geometrically compatible urea functionality and the effects of changing the electronic and steric environment on co-crystal formation (Table 6.1).



**Table 6.1 Family of ureas with varying donor and acceptor strengths.**

	EDG		EWG		both
U2		U3		U1	
U6		U4		U5	
U9		U14		U8	
U11		U10		U12	
		U13		U15	
		U7			

The goals for this chapter are to,

- Synthesize 1,3-diphenyl urea.
- Carry out MEP calculations on the deazapurines and the library of ureas.
- Screen the library of ureas (Table 6.1) against 1-deazapurine.
- Analyze the screens with IR spectroscopy and X-ray diffraction to detect the formation of co-crystals.
- Isolate the 3H tautomer through co-crystallization.

## 6.2. Experimental

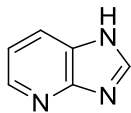
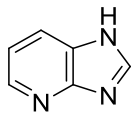
### 6.2.1. Synthesis of ureas

#### 6.2.1.1. Synthesis of diphenylurea U1

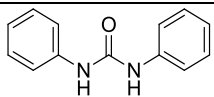
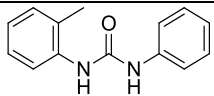
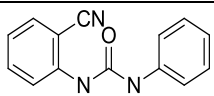
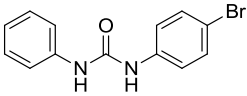
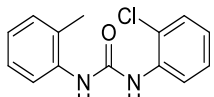
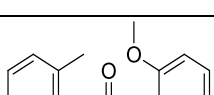
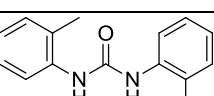
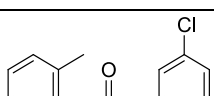
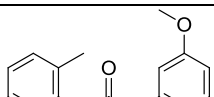
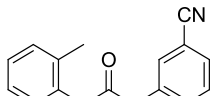
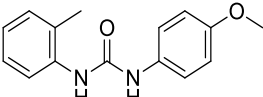
Phenylisocyanate (2.14 ml, 19.5 mmol) was dissolved in 10 ml of hexane. Aniline (1.82 ml, 19.7 mmol) was added dropwise very slowly. The mixture was stirred for one hour. A white precipitate was filtered out. (3.90 g, 95%) m.p. 235-239 °C <sup>1</sup>H NMR (400 MHz, DMSO-*d*<sub>6</sub>) δ ppm 6.92 - 7.01 (2 H, m), 7.22 - 7.31 (4 H, m), 7.44 (4 H, d, *J*=8.59 Hz), 8.66 (2 H, s)

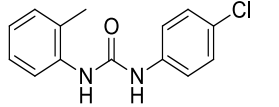
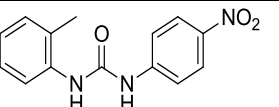
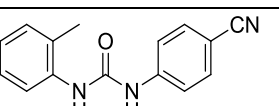
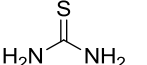
### 6.2.2. MEP calculations

**Table 6.2 AM1 and DFT values for the 1H tautomer of 1-deazapurine.**

	AM1/ kJmol <sup>-1</sup>	DFT 6-31+G*/kJmol <sup>-1</sup>
	1H 	1H 
Py - N	-306	-226
Im - N	-305	-227
N-H	+203	+288

**Table 6.3 AM1 and DFT values for the library of ureas**

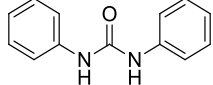
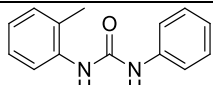
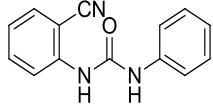
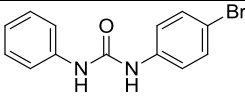
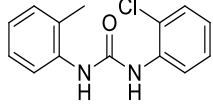
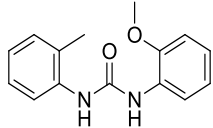
		AM1/ kJmol <sup>-1</sup>		DFT 6-31+G*/kJmol <sup>-1</sup>	
		C=O	N-H	C=O	N-H
U1		-287	198	-162	296
U2		-308	179	-194	260
U3		-300	182	-185	269
U4		-270	215	-148	312
U5		-326	157	-209	237
U6		-310	158	-210	226
U7		-310	186	-203	262
U8		-306	189	-187	274
U9		-305	183	-188	260
U10		-297	198	-177	290
U11		-312	174	-198	253

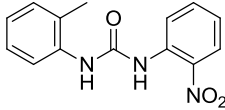
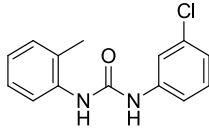
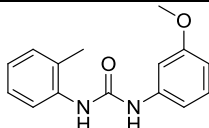
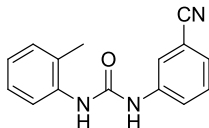
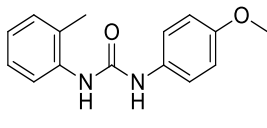
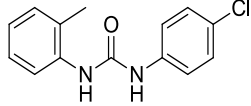
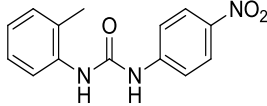
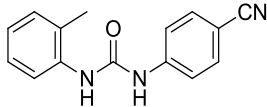
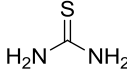
U12		-299	192	-184	273
U13		-270	231	-179	311
U14		-283	211	-165	300
U15		-269	204	-146	253

### 6.2.3. Solvent-drop grinding experiments

The deazapurine (10 mg 0.083 mmol) was mixed with the urea (0.083 mmol). Two drops of acetone were added to the mixture and ground for two minutes. The solid obtained was analyzed by FTIR.

### 6.2.4. IR data from solvent drop grinding experiments

		C=O	930-960 cm <sup>-1</sup>	Co-crystal
U1		1678	939	YES
U2		1632	953	NO
U3		1673	942	YES
U4		1675	935	YES
U5		1642	950	NO
U6		1640	951	NO

U7		1681	938	YES
U8		1637	935 (U8)	NO
U9		1632	952	NO
U10		1643	952	NO
U11		1640	942	NO
U12		1633	952	NO
U13		1682	942	YES
U14		1681	942	YES
U15		1614	937	YES

Formation of co-crystals was determined by the shifting of the carbonyl peaks of urea. It was observed that the stretch at around  $950\text{ cm}^{-1}$  in deazapurine is absent in all cases where the IR spectrum of the co-crystals and the stretch at around  $930\text{ cm}^{-1}$  is prominent.

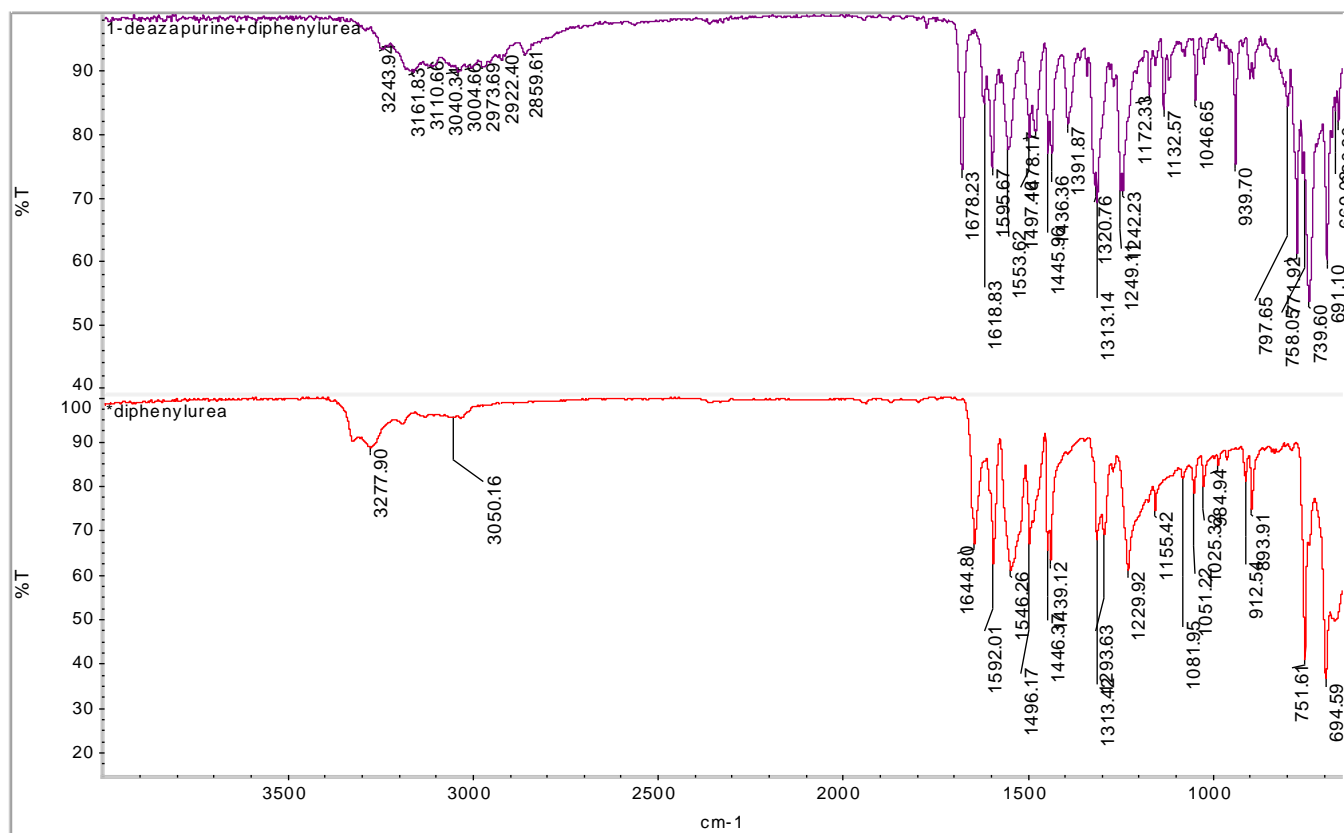


**Figure 6.6 Co-crystals were identified by the shifting carbonyl peak on the urea(1644 – 1678 cm<sup>-1</sup> for diphenylurea).**

## 6.2.5. Syntheses of co-crystals

### 6.2.5.1. Synthesis of 1-deazapurine diphenylurea (1:1), DP:U1

1-Deazapurine (10 mg, 0.08 mmol) and diphenylurea were dissolved in 3 ml of acetone with heat. The solution was allowed to stand at room temperature for slow evaporation. Colourless needles were observed in three days. (m.p. 170 – 174 C<sup>0</sup>)

### 6.2.5.2. Synthesis of 1-deazapurine 1-(2-cyanophenyl)-3-phenylurea (1:1), DP:U3

1-Deazapurine (10 mg, 0.08 mmol) and 1-(2-cyanophenyl)-3-phenylurea (8.91 mg 0.04 mmol) were ground together with a drop of acetone and dissolved in 3 ml methylethylketone with heat. The solution was allowed to stand at 0<sup>0</sup>C for slow evaporation. Bronze prisms were observed in a week. (m.p.120 – 125<sup>0</sup>C)

#### 6.2.5.3. *Synthesis of 1-deazapurine 1-(4-bromophenyl)-3-phenylurea (1:1), DP:U4*

1-Deazapurine (10 mg, 0.08 mmol) and 1-(4-bromophenyl)-3-phenylurea (24.4 mg, 0.08 mmol) were dissolved in 3 ml acetone and a drop of DMSO with heat. The solution was allowed to stand at room temperature for slow evaporation. Colourless plates were observed in two weeks (m.p. 165-173 C<sup>0</sup>)

#### 6.2.5.4. *Synthesis of 1-deazapurine 1-(4-nitrophenyl)-3-(2-tolyl)urea (1:1), DP:U14*

1-Deazapurine (10 mg, 0.08 mmol) and 1-(4-nitrophenyl)-3-(2-tolyl)urea (10.19 mg 0.04 mmol) were ground together with a drop of acetone and dissolved in a mixture of 3 ml acetone, 1 ml methanol and 1 ml chloroform with heat. The solution was allowed to stand at 0 °C for slow evaporation. Yellow prisms were observed in a week (m.p. 155 -160 C<sup>0</sup>)

#### 6.2.5.5. *Synthesis of 1-deazapurine thiourea (1:1), DP:U15*

1-Deazapurine (10 mg, 0.08 mmol) and thiourea (6.09 mg, 0.025 mmol) were dissolved in 2 ml of methanol with heat. The solution was allowed to stand at room temperature for slow evaporation. Gold prisms were observed in two weeks. (m.p. 167 -170 C<sup>0</sup>)

### 6.2.6. *Structure descriptions*

#### 6.2.6.1. *Crystal structure of 1-deazapurine diphenylurea (1:1), DP:U1*

The structure determination of **DP:U1** shows that in the resulting 1:1 co-crystal, deazapurine exists in the 1H tautomeric form. The two N-H groups of the urea form hydrogen bonds to the imidazole (N41-H41...N19 1.974(18) Å, N41...N19 2.8942(19) Å) and pyridyl (N31-H31...N13 2.196(19) Å, N31...N13 3.061(2) Å) nitrogen atoms. The N-H group on the deazapurine picks up the carbonyl group (N17-H17...O21 Å, 1.81(2) N17...O21 2.7508(18) Å) on the urea forming a one dimensional chain.(Figure 6.7)

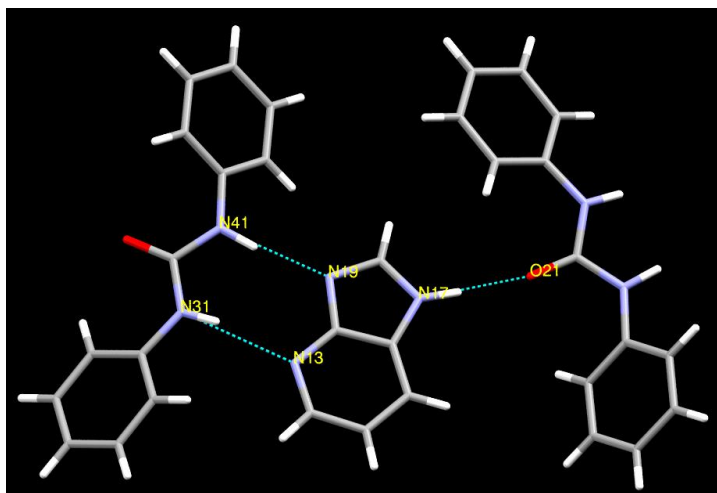


**Figure 6.7** The primary hydrogen-bond interactions in the crystal structure of DP:U1

**6.2.6.2.** *Crystal structure of 1-deazapurine 1-(2-cyanophenyl)-3-phenylurea (1:1), DP:U3*

In the resulting 1:1 co-crystal of DP:U3 deazapurine exists in the 1H tautomeric form. The two N-H groups of the urea form hydrogen bonds to the imidazole (N41-H41 $\cdots$ N13 2.13(2) Å, N41 $\cdots$ N13 3.040(2) Å) and pyridyl (N31-H31 $\cdots$ N15 1.98(2) Å, N31 $\cdots$ N15 2.902(2) Å) nitrogen atoms. The N-H group on the deazapurine picks up the carbonyl group on the urea (N11-H11 $\cdots$ O21 1.87(2) Å, N11 $\cdots$ O21 2.799(2) Å) resulting in a one dimensional chain. (Figure 6.8)

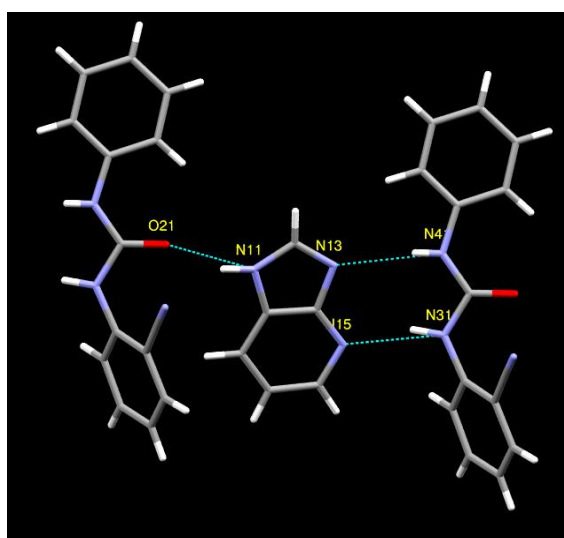


**Figure 6.8** The primary hydrogen-bond interactions in the crystal structure of DP:U3



**6.2.6.3. Crystal structure of 1-deazapurine 1-(4-bromophenyl)-3-phenylurea (1:1), DP:U4**

The structure determination of **DP:U4** shows a 1:1 co-crystal, where deazapurine exists in the 1H tautomeric form. The two N-H groups of the urea form hydrogen bonds to the imidazole (N31-H31...N13 2.17(7) Å, N31...N13 2.857(6) Å) and pyridyl (N41-H41...N15 2.16(7) Å, N41...N15 3.023(6) Å) nitrogen atoms. The N-H group on the deazapurine picks up the carbonyl group on the urea. (N11-H11...O21 1.99(7) Å, N11...O21 2.701(5) Å) resulting in a one dimensional chain.(Figure 6.9)

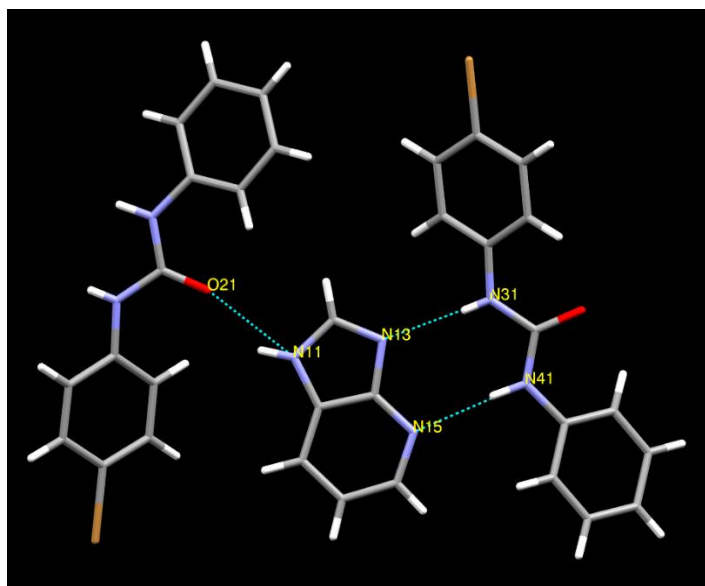


**Figure 6.9 The primary hydrogen-bond interactions in the crystal structure of DP:U4**

**6.2.6.4. Crystal structure of 1-deazapurine 1-(4-nitrophenyl)-3-(2-tolyl)urea (1:1), DP:U13**

Structure determination of **DP:U13** shows that in the resulting 1:1 co-crystal deazapurine exists in the 1H tautomeric form. In the two resulting symmetrically inequivalent chains, the two N-H groups of the urea form hydrogen bonds to the imidazole (N31\_1-H31\_1...N13\_1 2.02(4) Å, N31\_1...N13\_1 2.978(4) Å, N31\_2-H31\_2...N13\_2 2.08(3) Å, N31\_2...N13\_2 3.005(4) Å) and pyridyl (N41\_1-H41\_1...N15\_1 Å, 2.02(4) N41\_1...N15\_1 2.994(4) Å, N41\_2-H41\_2...N15\_2 2.08(3) Å, N41\_2...N15\_2 3.024(4) Å) nitrogen atoms. The N-H group on the deazapurine picks up the carbonyl group on the urea (N11\_1-H11\_1...O21\_2 Å, 1.77(4) N11\_1...O21\_2 2.794 (4) Å N11\_2-H11\_2...O21\_1 1.85(3) N11\_2...O21\_1 2.803(3) Å). (Figure 6.10)

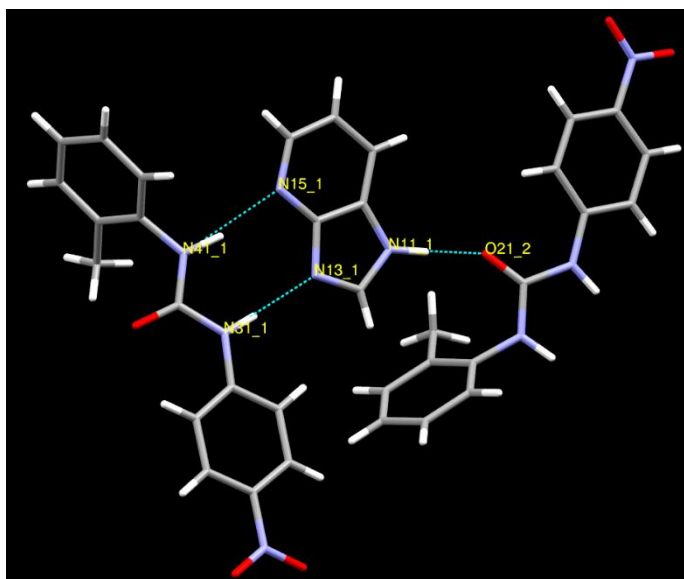


**Figure 6.10** The primary hydrogen-bond interactions in the crystal structure of DP:U13

**6.2.6.5. Crystal structure of 1-deazapurine thiourea (1:1), DP:U15**

In the 1:1 co-crystal of DP:U5 deazapurine exists in the 1H tautomeric form. In this structure however, the two N-H groups form bifurcated hydrogen bonds to the imidazole nitrogen atom N31-H31A $\cdots$ N19 2.295(15) Å N31 $\cdots$ N19 3.0378(12) Å, N41-H41A $\cdots$ N19 2.239(16) Å N41 $\cdots$ N19 3.0437(12) Å the N-H group on the deazapurine picks up the pyridyl nitrogen atom N17-H17 $\cdots$ N13 1.980(15) Å N17 $\cdots$ N13 2.8396(11) Å forming a one dimensional chain.(Figure 6.11)

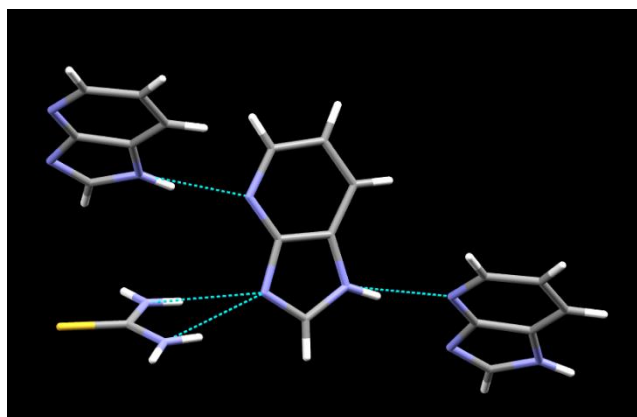


**Figure 6.11** The primary hydrogen-bond interactions in the crystal structure of DP:U15

### 6.3. Discussion

All the ureas used in the study were synthesized in a method similar to that shown for 1,3-diphenyl urea, where the anilines and phenylisocyanates with the desired functional groups were combined as shown in section 6.2.1.1. One of the main difficulties experienced in this study was in the synthesis of co-crystals as the solubilities of the ureas were significantly lower than that of deazapurine, resulting in precipitation of the ureas during slow evaporation. Using asymmetrically substituted ureas resulted in slightly improved solubility. Best results were observed with acetone and methy ethyl ketone and mixtures of these solvents.

The infrared spectra of the co-crystals obtained with urea (Figure 6.12) show that unlike the co-crystals containing the 3H tautomer, where out of two possible peaks at around  $930\text{ cm}^{-1}$  and  $950\text{ cm}^{-1}$  only the peak at around  $950\text{ cm}^{-1}$  was observed, in the cases where the 1H tautomer is present, only the peak at around  $930\text{ cm}^{-1}$  is present. Both peaks are observed in the synthesized 1-deazapurine. Even though few data points exist, these peaks maybe useful in predicting which tautomer is present without obtaining single crystal data.

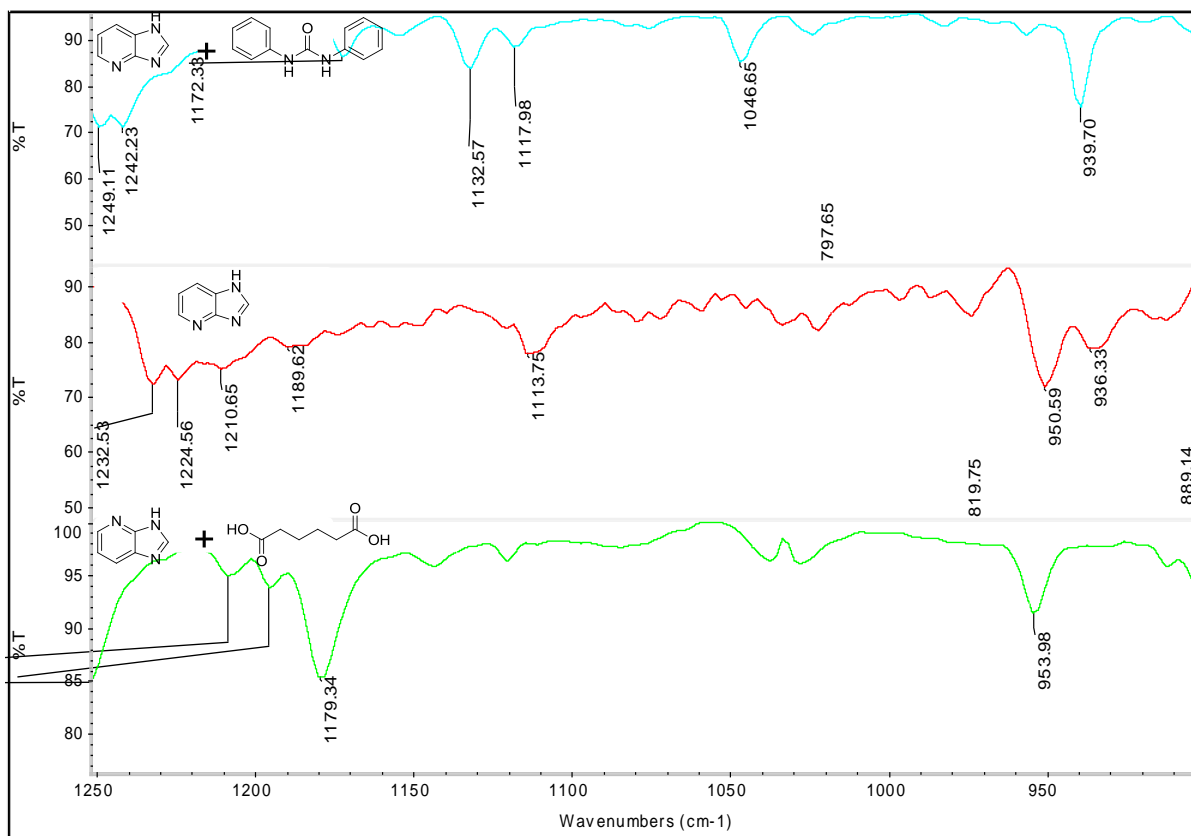
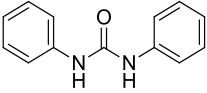
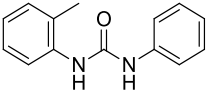
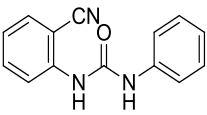
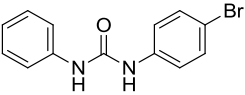
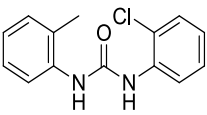
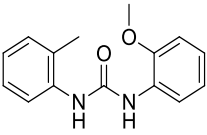
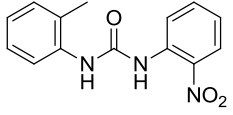
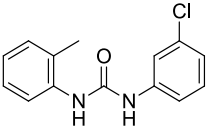
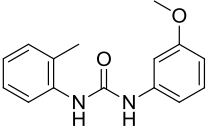
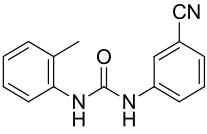
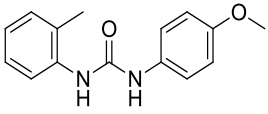
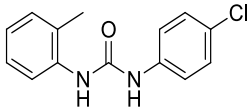
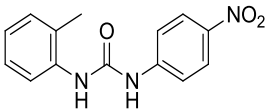
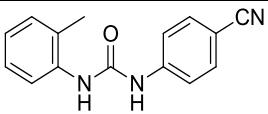
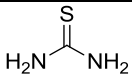


Figure 6.12 Comparing IR spectra of the two tautomers of 1-deazapurine.

As seen on Table 6.4, seven out of the fourteen ureas analysed showed evidence of co-crystal formation. Out of the seven cases where co-crystal formation has been confirmed by IR spectroscopy, five show that the MEP values on the carbonyl group on the urea are significantly lower than the value on the 1H tautomer of 1-deazapurine. In addition, all four ureas containing strong electron donating groups showed no evidence of co-crystal formation. Out of the six ureas with strong electron withdrawing functionalities five formed co-crystals.

**Table 6.4 Correlating MEP values with synthesized outcomes**

		AM1		DFT		Co-crystal
		C=O	N-H	C=O	N-H	
U1		-287	198	-162	296	YES
U2		-308	179	-194	260	NO
U3		-300	182	-185	269	YES
U4		-270	215	-148	312	YES
U5		-326	157	-209	237	NO
U6		-310	158	-210	226	NO
U7		-310	186	-203	262	YES
U8		-306	189	-187	274	NO

U9		-305	183	-188	260	NO
U10		-297	198	-177	290	NO
U11		-312	174	-198	253	NO
U12		-299	192	-184	273	NO
U13		-270	231	-179	311	YES
U14		-283	211	-165	300	YES
U15		-269	204	-146	253	YES

The calculated MEP values are consistent with the observed supramolecular outcomes. The fact that unsubstituted diphenylurea forms a co-crystal with 1H tautomer of 1-deazapurine tells us that the geometric bias of 1H tautomer. Electron-withdrawing substituents enhance co-crystallization whereas electron-donating substituents prevent co-crystal formation. This is in agreement with data published by Etter et. al<sup>16,17</sup> where only the ureas with electron withdrawing groups except 1,3-di(o-nitrophenyl)ureas resulted in the formation of various co-crystals and solvates while the rest of the diarylureas with various substituents consistently formed the urea  $\alpha$  tape synthon (Table 6.5). This has been explained via a stabilizing intramolecular hydrogen bond between the C-H groups *ortho* to the urea and the carbonyl group.

**Table 6.5 Only the diarylureas with electron-withdrawing substituents form co-crystals<sup>17</sup>**

Compd	A	B	C	D	E	F
Class I: Diarylureas that will not complex guest acceptors						
1	H	H	H	H	H	H

3 $\alpha,\beta$	H	H	OCH <sub>3</sub>	OCH <sub>3</sub>	H	H
6	OCH <sub>3</sub>	H	H	H		OCH <sub>3</sub>
7	OCH <sub>3</sub>	H	H	H	H	H
8	H	H	OCH <sub>3</sub>	H	H	H
9	H	H	NO <sub>2</sub>	NO <sub>2</sub>	H	H
11	H	CH <sub>3</sub>	H	H	CH <sub>3</sub>	H
Class II: Diarylureas that complex the strong guest acceptors TPPO and/ or DMSO						
4	H	NO <sub>2</sub>	H	H	H	H
5	H	NO <sub>2</sub>	H	H	H	NO <sub>2</sub>
10	NO <sub>2</sub>	H	H	H	H	NO <sub>2</sub>
12	H	CF <sub>3</sub>	H	H	CF <sub>3</sub>	H
Class III: Diarylureas that complex strong and moderate acceptors (Ketones, Ethers, Nitroanilines)						
2	H	NO <sub>2</sub>	H	H	NO <sub>2</sub>	H

In all four structures we obtained with the diphenylureas, the two NH groups on the urea pick up the pyridyl and imidazole nitrogen atoms on the deazapurine. The N-H group on the deazapurine picks up the carbonyl group on the urea. Out of the 14 ureas screened, in five the AM1 charge on the carbonyl group was significantly smaller than the charges on the acceptor sites on the deazapurine all five of these molecules resulted in co-crystals (Table 6.4). Therefore this system too is consistent with Etter's rules based on calculated AM1 MEP values.

## 6.4. Conclusion

Urea is geometrically compatible with the 1H tautomer of 1-deazapurine and therefore is capable of forming co-crystals with this family of molecules disrupting the very robust urea-urea  $\alpha$ -tape synthon. This is mainly due to the acceptor sites on the deazapurine being significantly stronger than the carbonyl group on the urea. Electron donating substituents on the urea increase the acceptor ability on the carbonyl group preventing co-crystal formation and electron donating groups on the urea further weaken the carbonyl as an acceptor facilitating co-crystal formation.

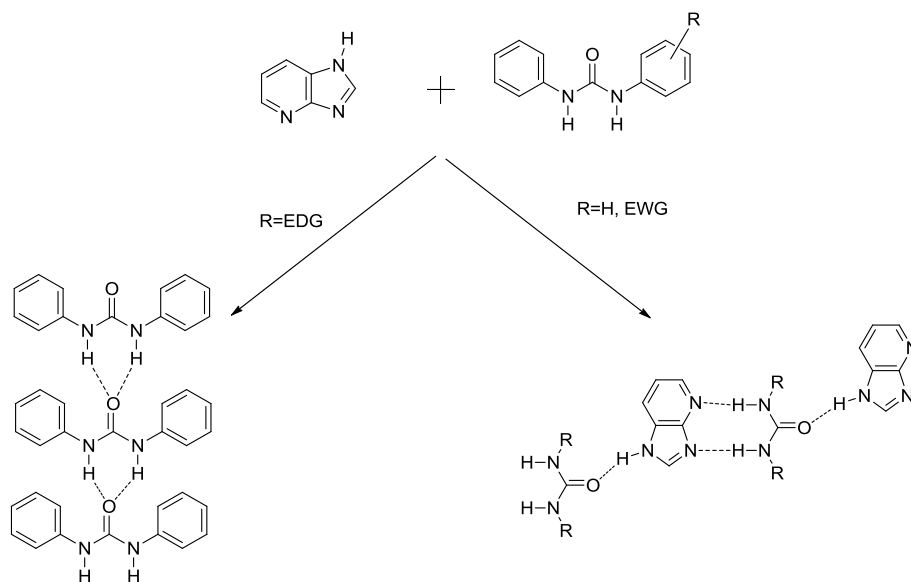


**Figure 6.13 Geometrically compatible urea was successfully used to isolate the 1H tautomer of 1-deazapurine.**

## References

---

- <sup>1</sup> J. Regan, S. Breitfelder, P. Cirillo, T. Gilmore, A. G. Graham, E. Hickey, B. Klaus, J. Madwed, M. Moriak, N. Moss, C. Pargellis, S. Pav, A. Proto, A. Swinamer, L. Tong, C. Torcellin, *J. Med. Chem.* **2002**, *45*, 2994-3008
- <sup>2</sup> Wilson, L. J.; Morris, T. W.; Wu, Q.; Renick, P. J.; Parker, C. N.; Davis, M. C.; McKeever, H. D.; Hershberger, P. M.; Switzer, A. G.; Shrum, G. *Bioorg. Med. Chem. Lett.* **2001**, *9*, 1149-1152.
- <sup>3</sup> J. Baldwin, C. H. Michnoff, N. A. Malmquist, J. White, M. G. Roth, P. K. Rathod and M. A. Phillips, *J. Biol. Chem.*, **2005**, *280*, 21847-21853
- <sup>4</sup> A. Berkessel, F. Cleemann, S. Mukherjee, and T. N. Müller, *J. Lex, Angew. Chem. Int. Ed.*, **2005**, *44*, 807-811
- <sup>5</sup> N. Roy, E. Buhler and J. Lehn, *Chemistr A European Journal*, **2013**, *19*, 8814-8820
- <sup>6</sup> V. Simic, L. Bouteiller, and M. Jalabert *J. Am. Chem. Soc.*, **2003**, *125*, **43**, 13148-13154
- <sup>7</sup> T. Gunnlaugsson, A. P. Davis, J. E. O'Brien and M. Glynn, *Org. Biomol. Chem.*, **2005**, *3*, 48-56
- <sup>8</sup> R. Kumar, V. Bhalla and M. Kumar, *Tetrahedron*, **2008**, *64*, 8095-8101
- <sup>9</sup> C. B. Aakeröy and K. R. Seddon, *Chem. Soc. Rev.*, **1993**, 397
- <sup>10</sup> M. D. Hollingsworth, *Science*, **2002**, *295*, 2410.
- <sup>11</sup> G. R. Desiraju, *Nature*, **2001**, *412*, 397
- <sup>12</sup> X. Zhao, Y.-L. Chang, F. W. Fowler and J. W. Lauher, *J. Am. Chem. Soc.*, **1990**, *112*, 6627
- <sup>13</sup> H. Hart, L. T. W. Lin, D. L. Ward, *J. Chem. Soc., Chem. Commun.* **1985**, 293-294
- <sup>14</sup> L. S. Reddy, S. Basavoju, V. R. Vangala, and A. Nangia *Cryst. Growth Des.*, **2006**, *6*, 161-173,
- <sup>15</sup> S. K. Chandran, N. K. Nath, S. Cherukuvada, A. Nangia, *Journal of Molecular Structure*, **2010**, *968*, 99-107
- <sup>16</sup> M. C. Etter and T. W. Panunto *J. Am. Chem. Soc.* **1988**, *110*, 5897-5898
- <sup>17</sup> M. C. Etter, Z. Urbakzyk-Lipkowska, S. M. Zia-Ebrahimi, and T. W. Panunto *J. Am. Chem. Soc.* **1990**, *112*, 8415-8426



## Appendix A - NMR Spectra

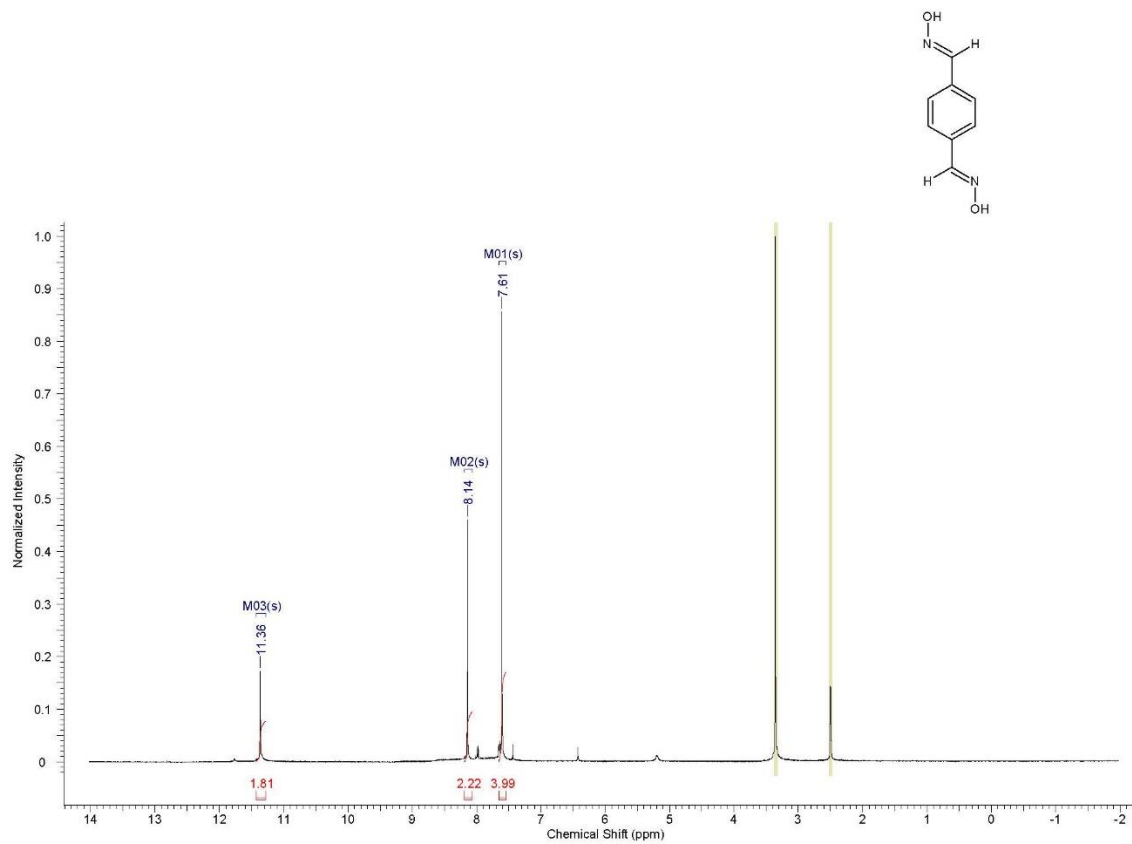


Figure A.1  $^1\text{H}$ NMR spectrum of di(H)ox

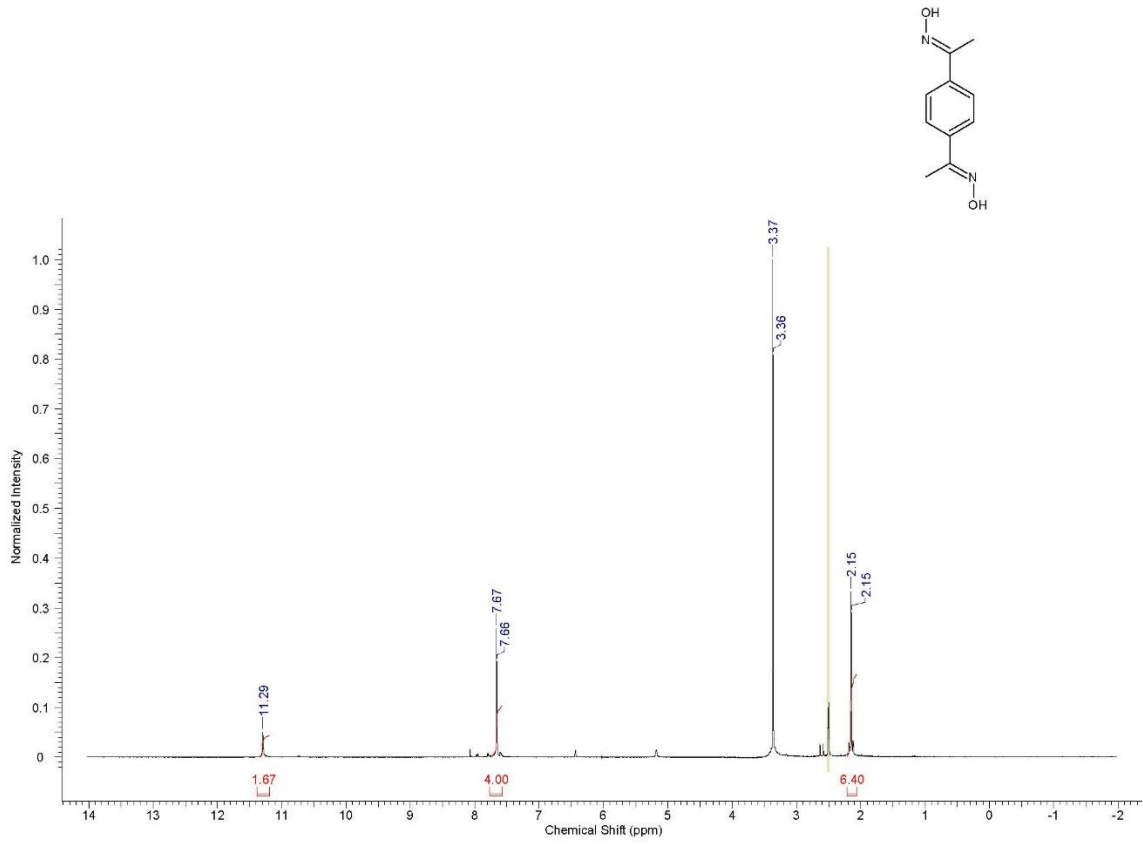


Figure A.2 <sup>1</sup>H NMR spectrum of di(CH<sub>3</sub>)ox

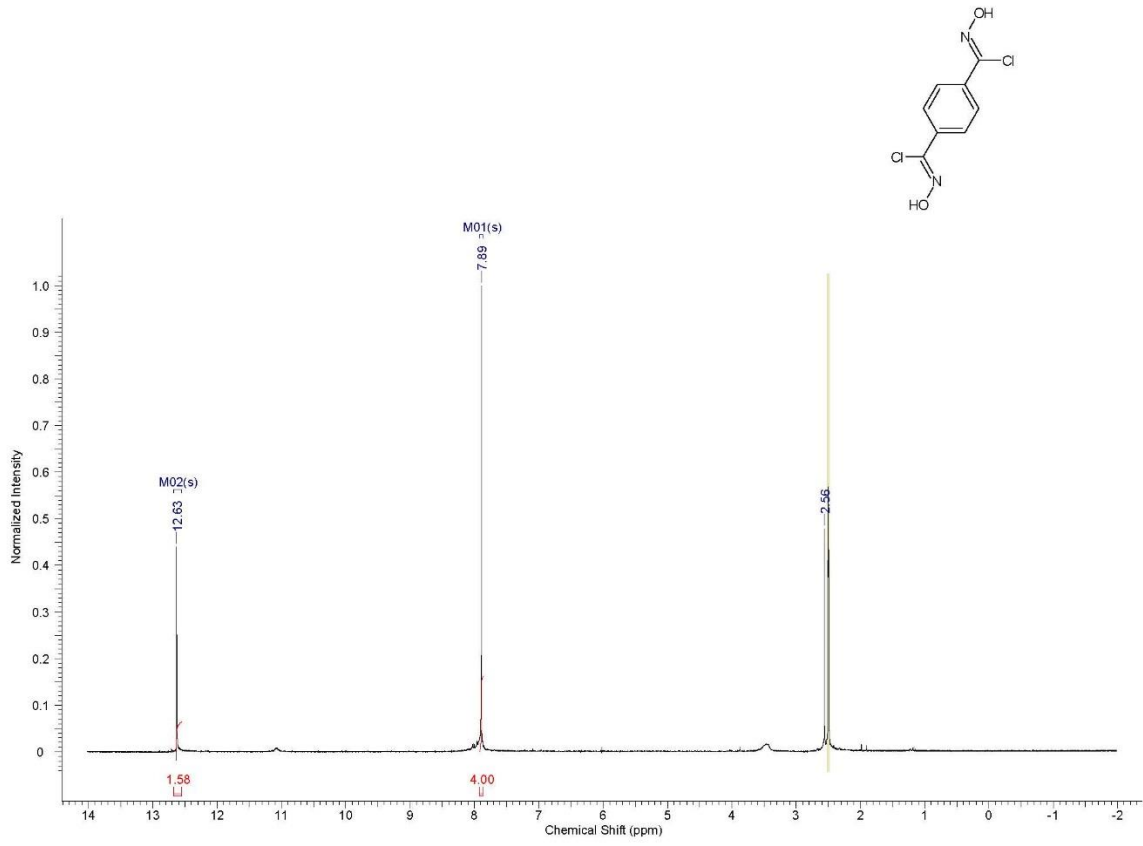
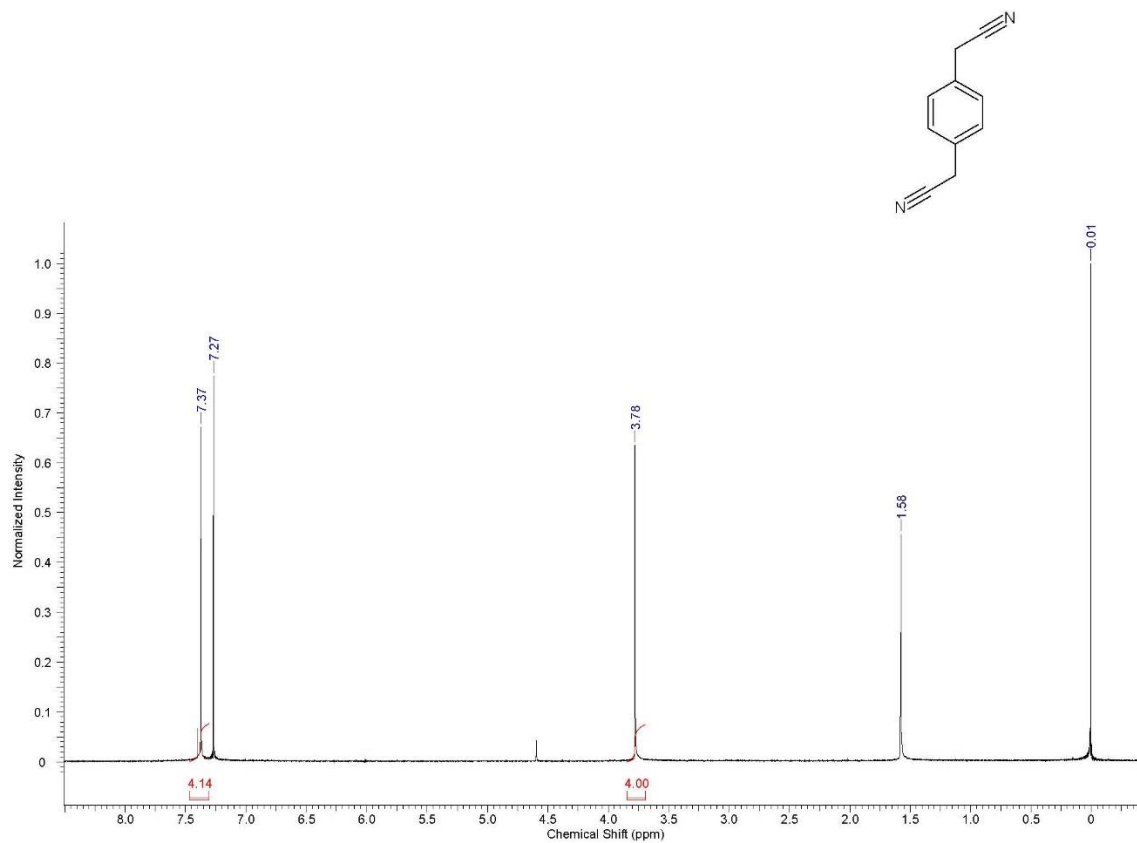
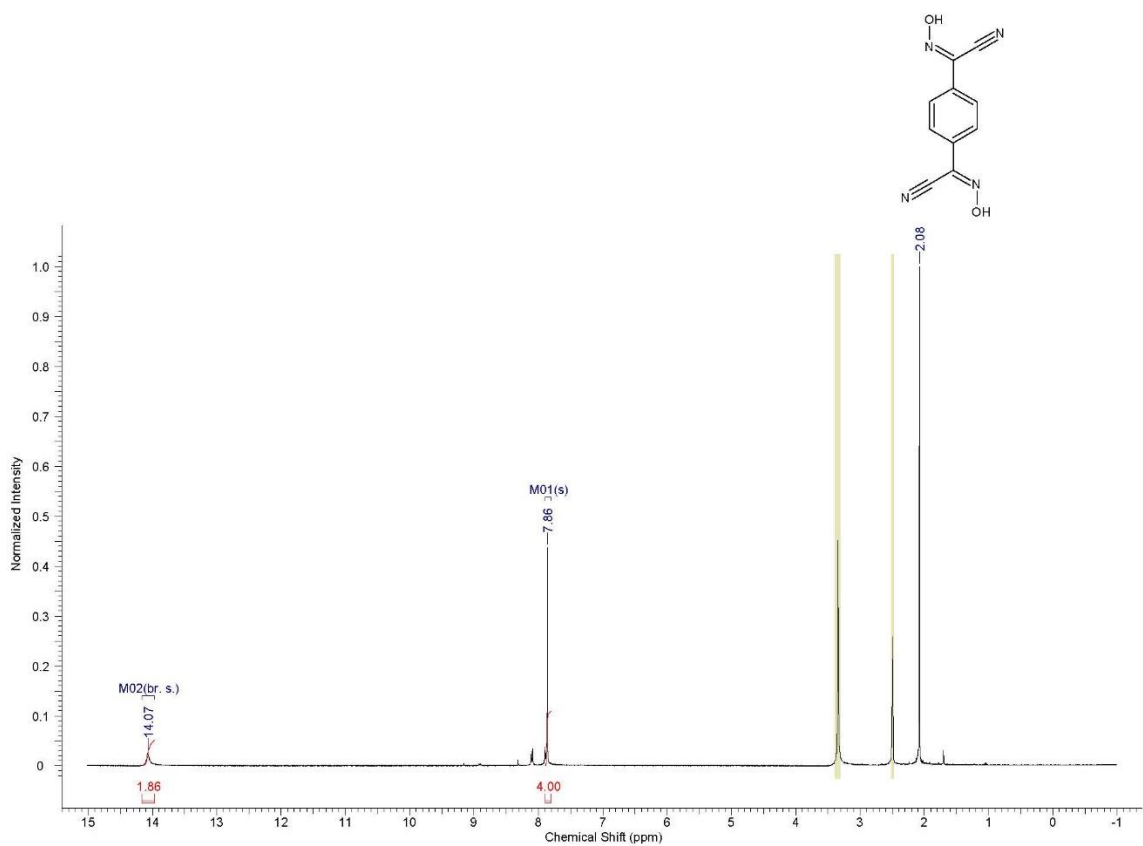


Figure A.3  $^1\text{H}$ NMR spectrum of di(Cl)ox



**Figure A.4** <sup>1</sup>H NMR spectrum of 1,4-dicyanomethylbenzene



**Figure A.5** <sup>1</sup>H NMR spectrum of di(CN)ox

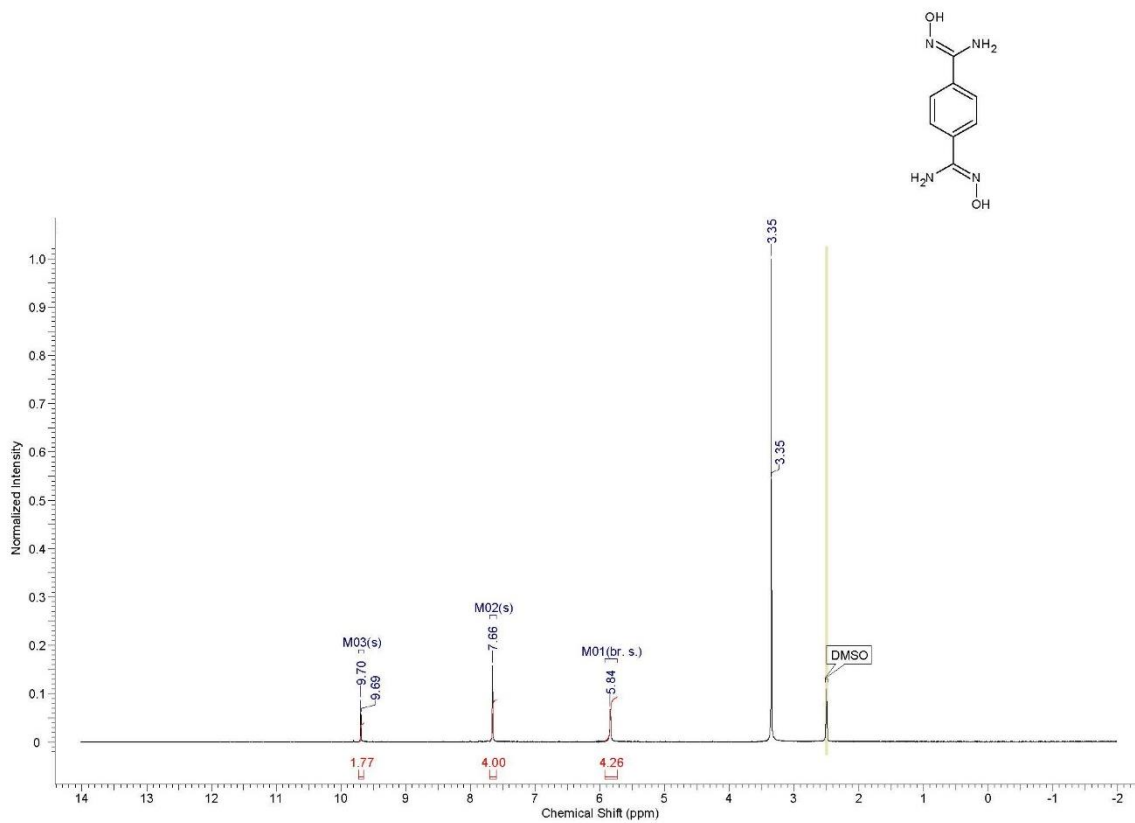


Figure A.6 <sup>1</sup>H NMR spectrum of di(NH<sub>2</sub>)ox

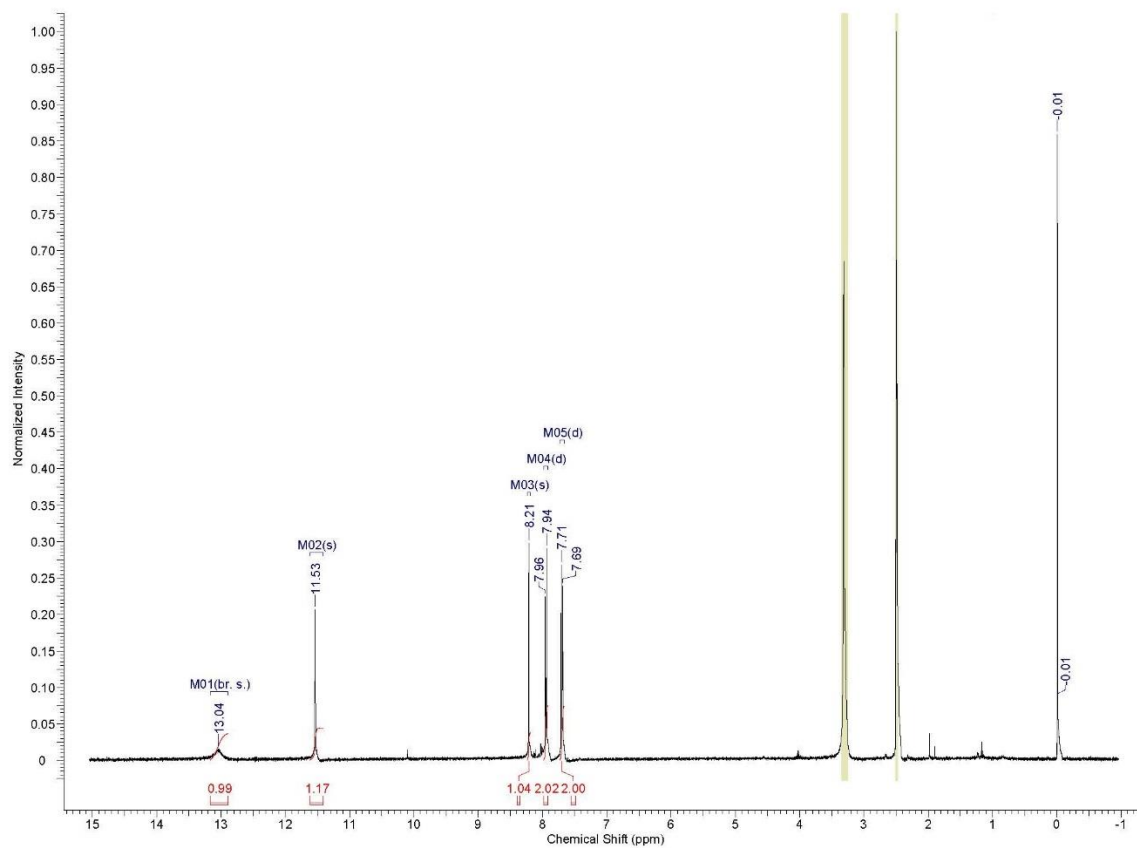
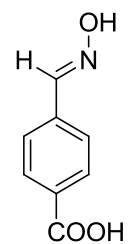


Figure A.7 <sup>1</sup>H NMR spectrum of ABA

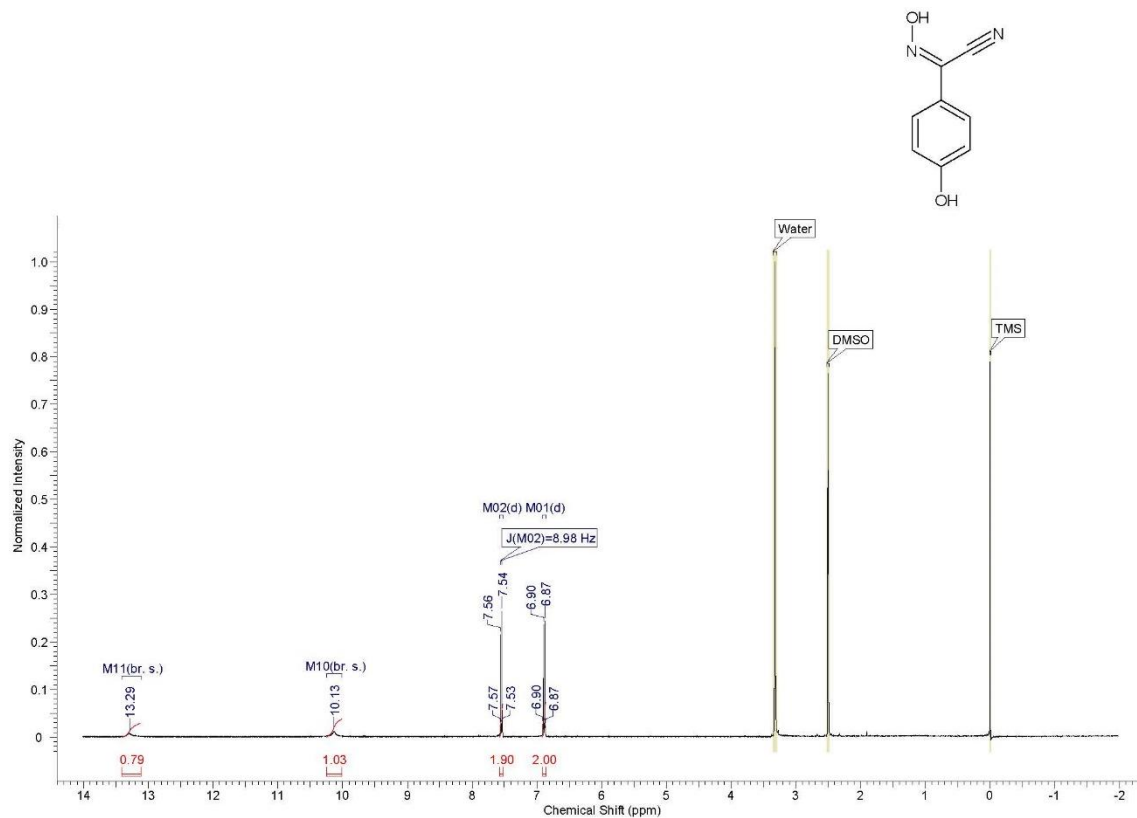


Figure A.8  $^1\text{H}$ NMR spectrum of PhOx



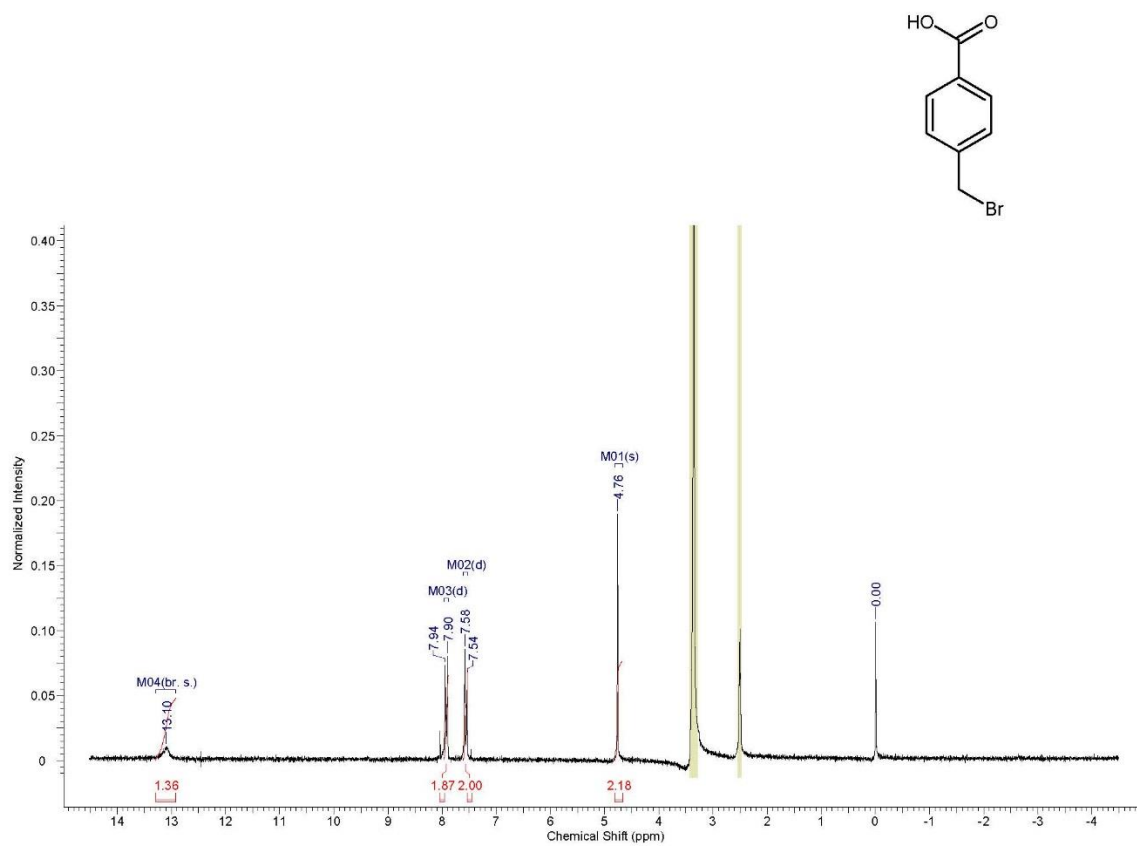


Figure A.9 <sup>1</sup>H NMR spectrum of 4-bromomethylbenzoic acid

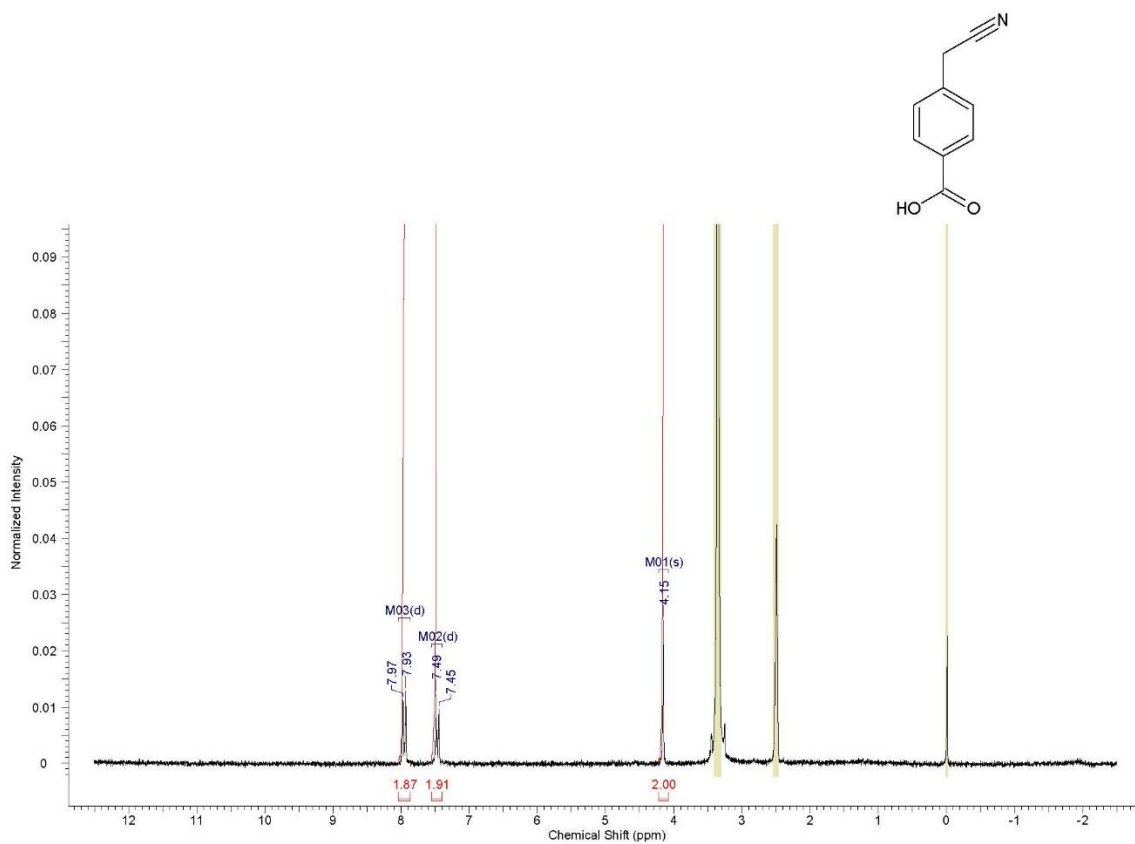


Figure A.10  $^1\text{H}$ NMR spectrum of 4-cyanomethylbenzoic acid

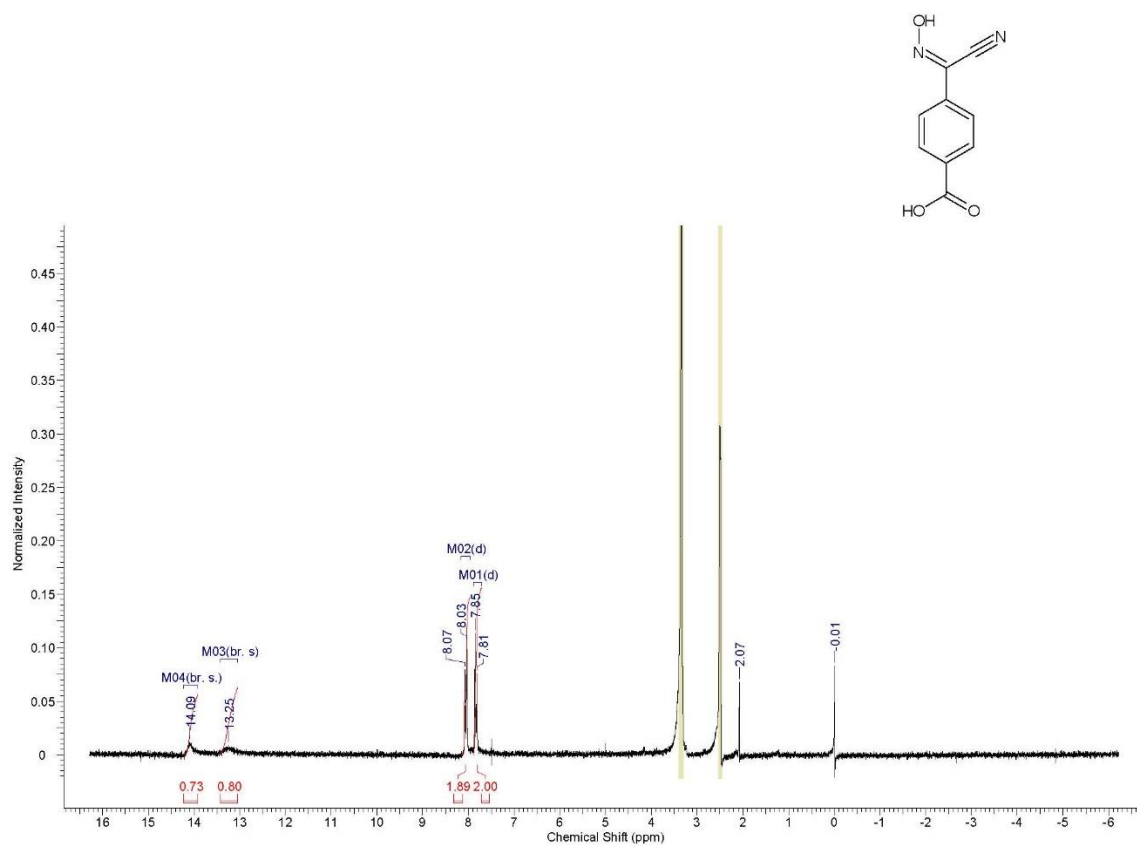
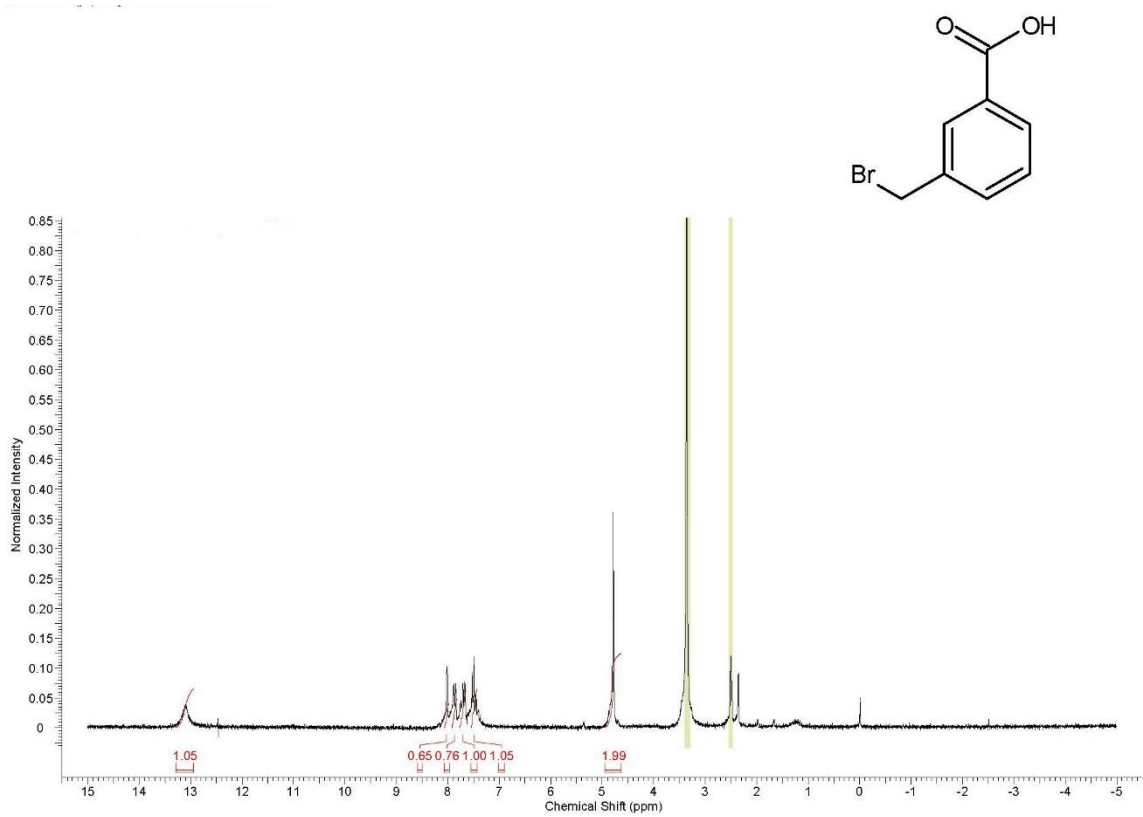
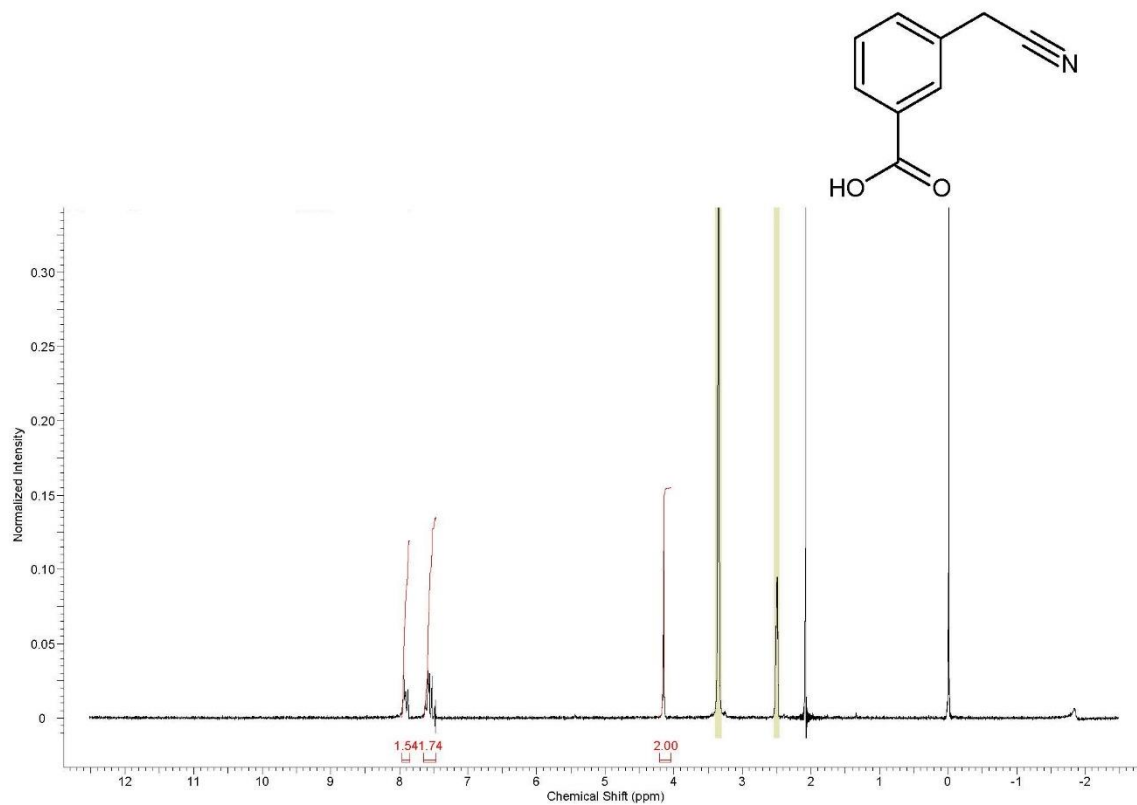


Figure A.11  $^1\text{H NMR}$  spectrum of 4BaOx



**Figure A.12** <sup>1</sup>H NMR spectrum of 3-bromomethylbenzoic acid



**Figure A.13** <sup>1</sup>H NMR spectrum of 3-cyanomethylbenzoic acid

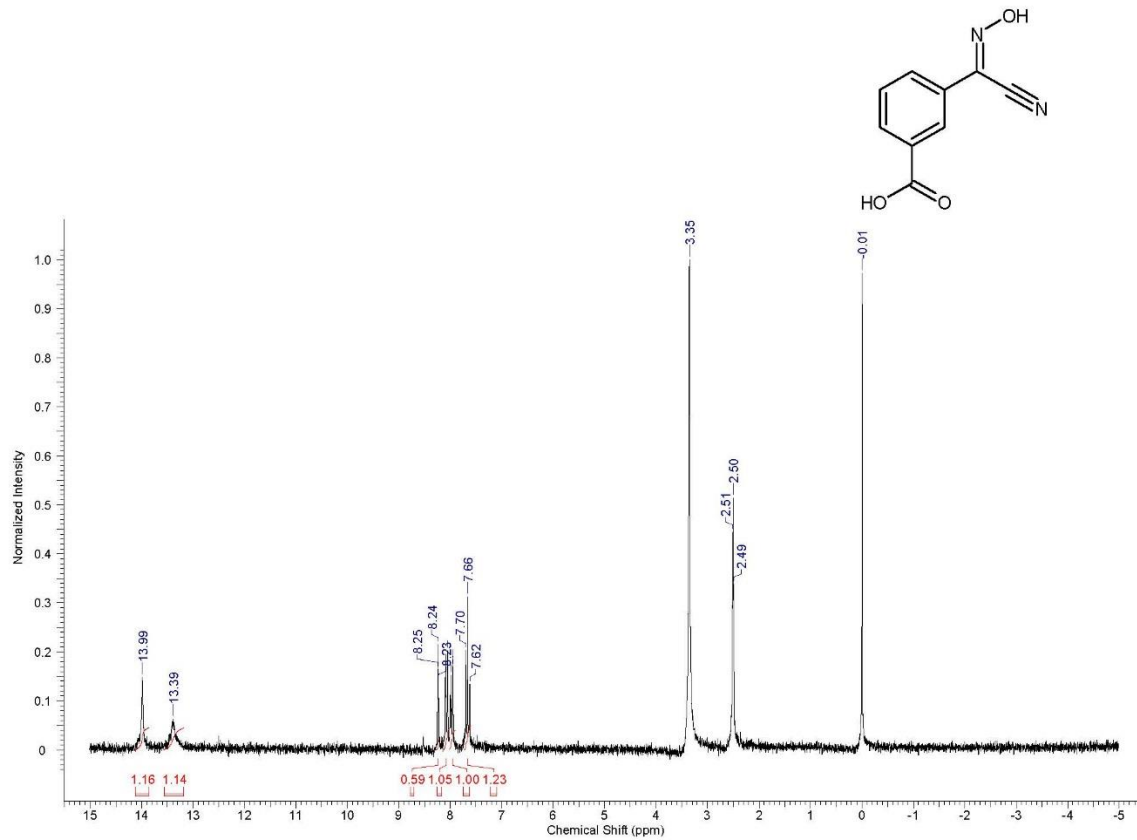
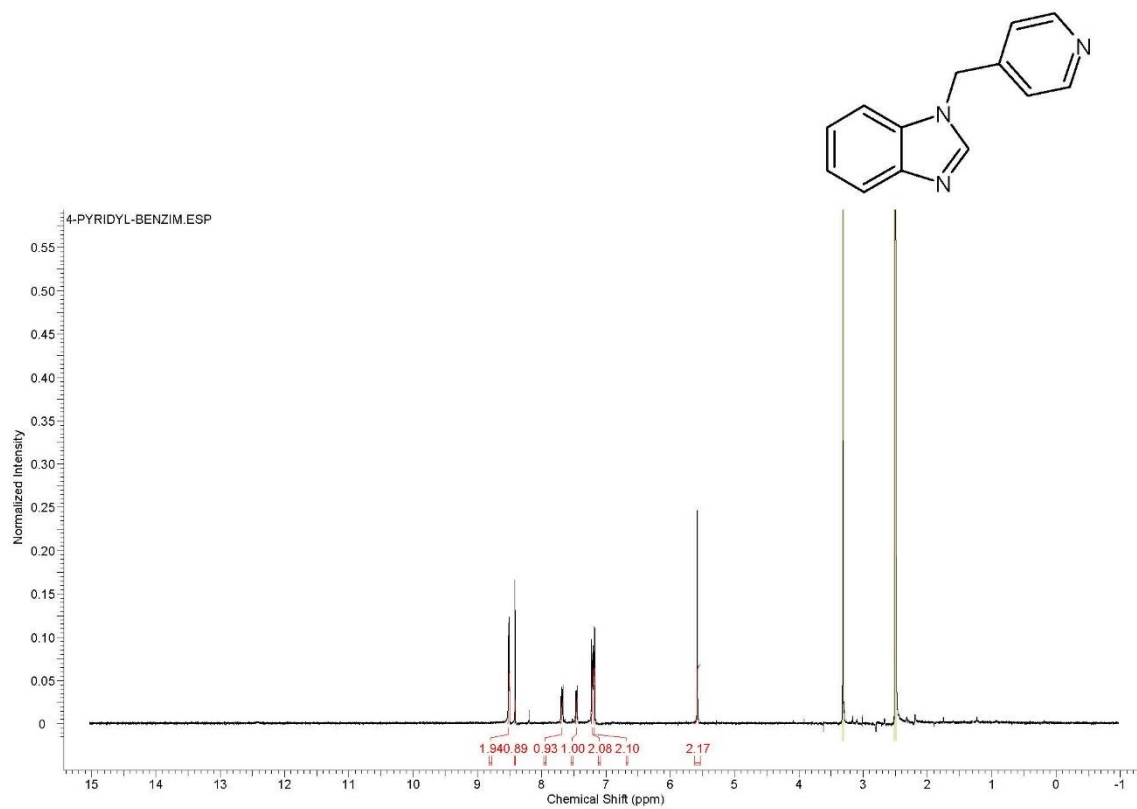


Figure A.14  $^1\text{H}$ NMR spectrum of 3BaOx



**Figure A.15** <sup>1</sup>H NMR spectrum of 4PB

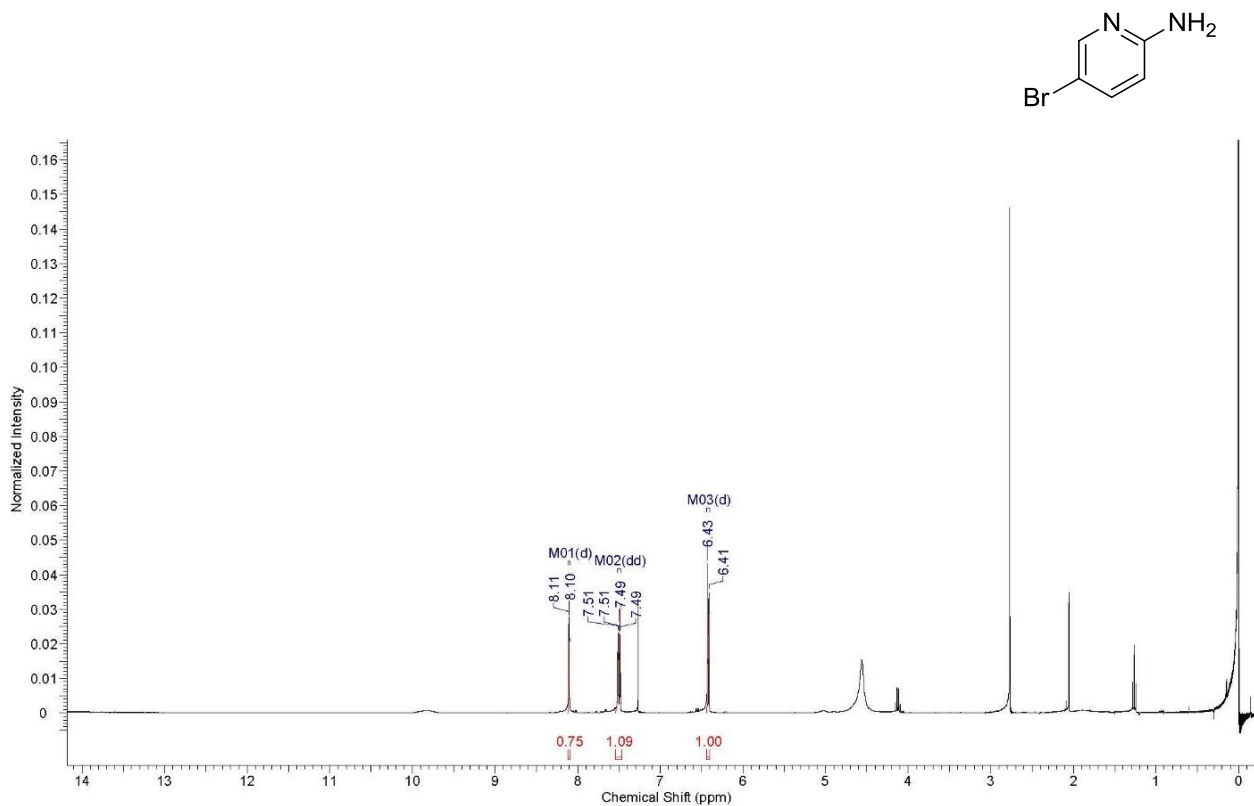


Figure A.16  $^1\text{H}$ NMR spectrum of 2-amino-5-bromopyridine



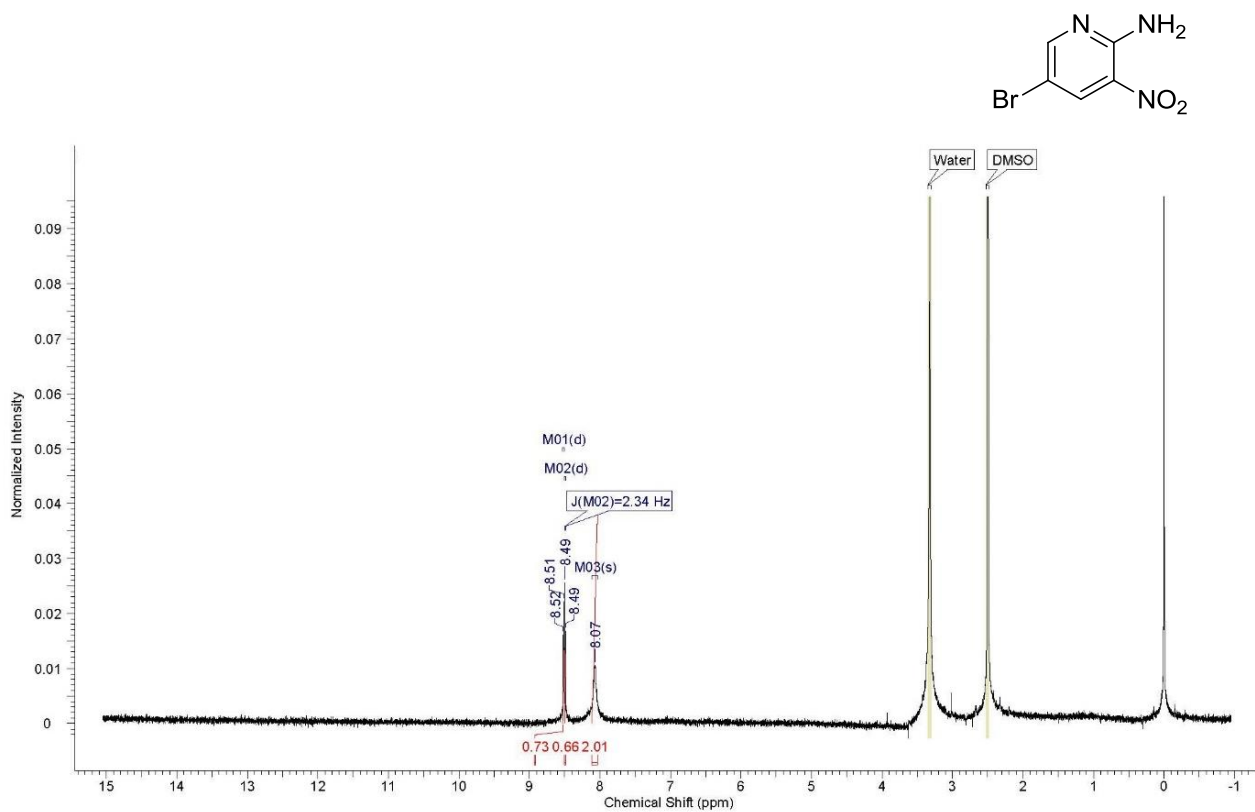


Figure A.17 <sup>1</sup>H NMR spectrum of 2-amino-3-nitro-5-bromopyridine

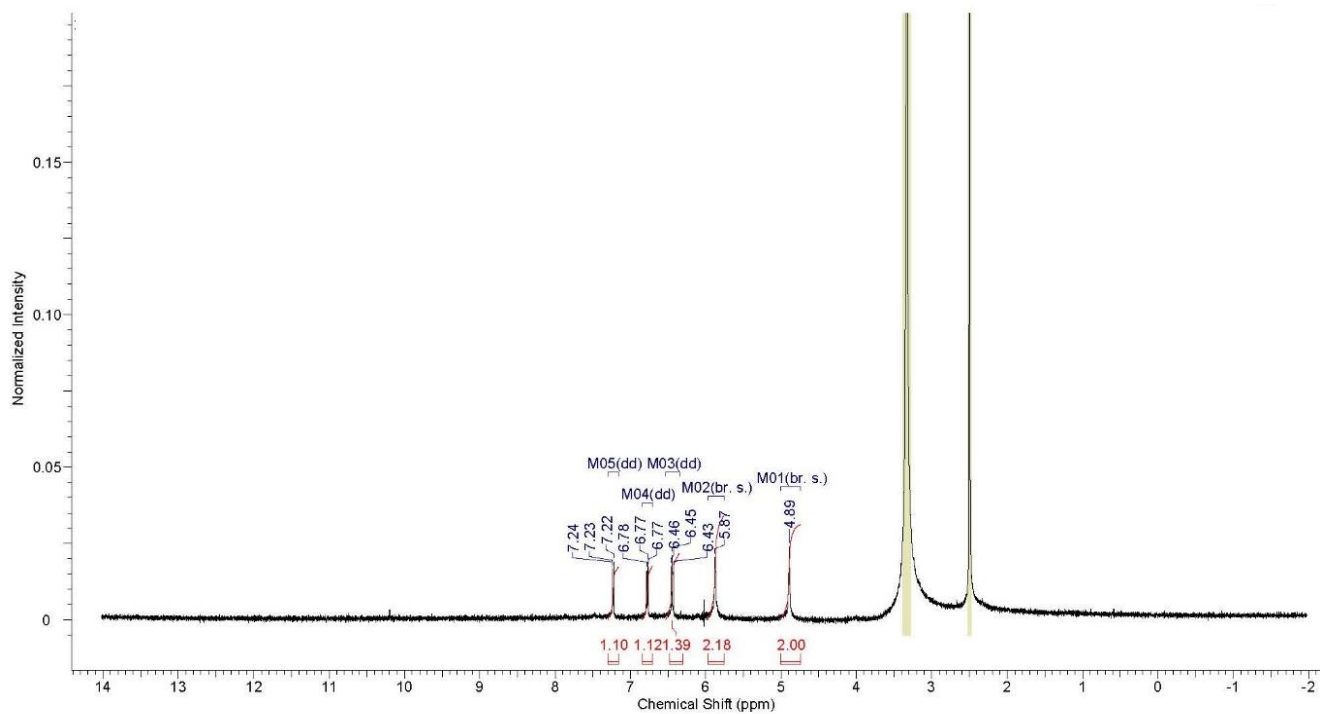
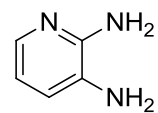
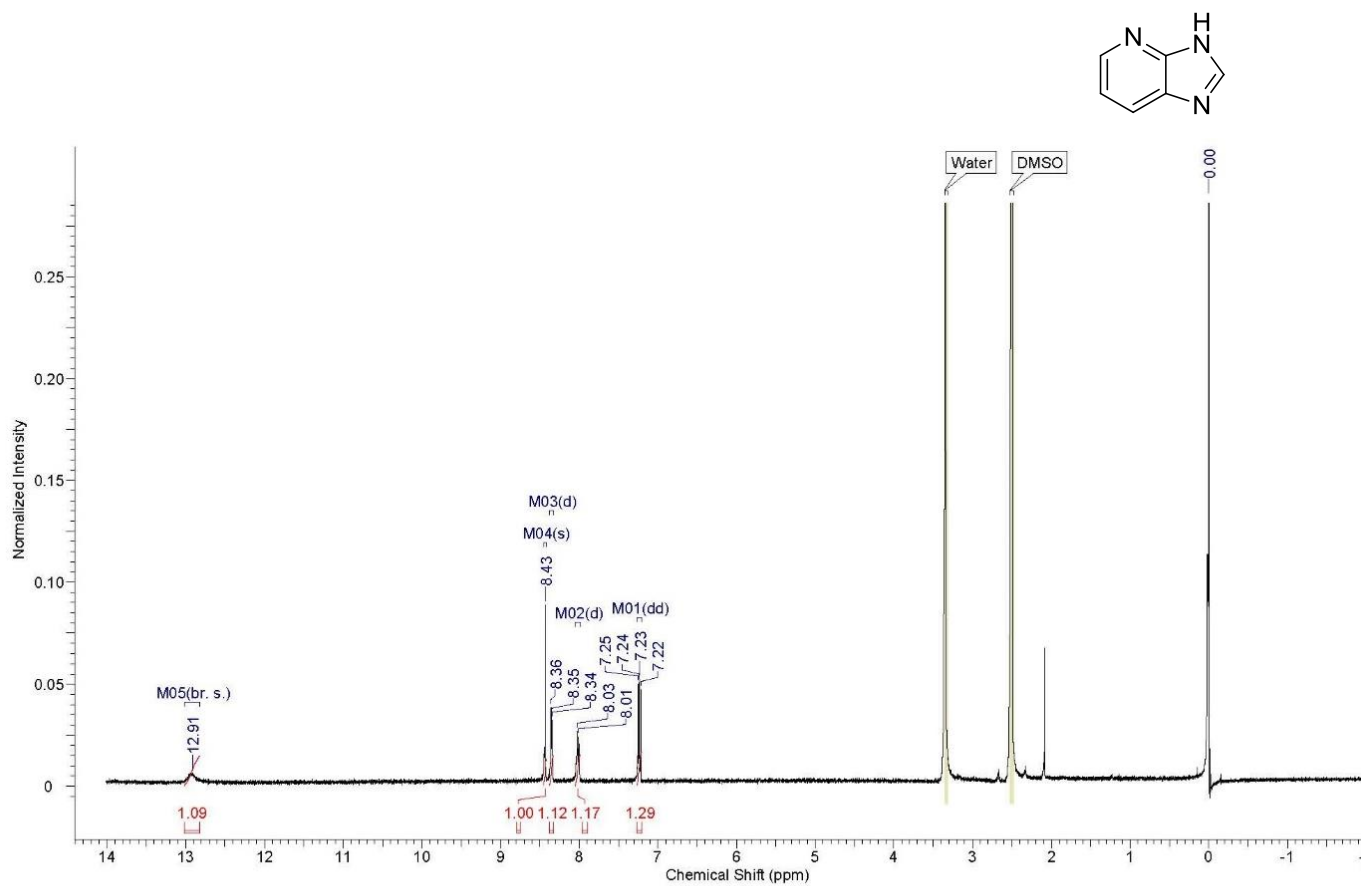


Figure A.18  $^1\text{H}$ NMR spectrum of 2,3-diaminopyridine.



**Figure A.19**  $^1\text{H}$ NMR spectrum of 1-deazapurine.

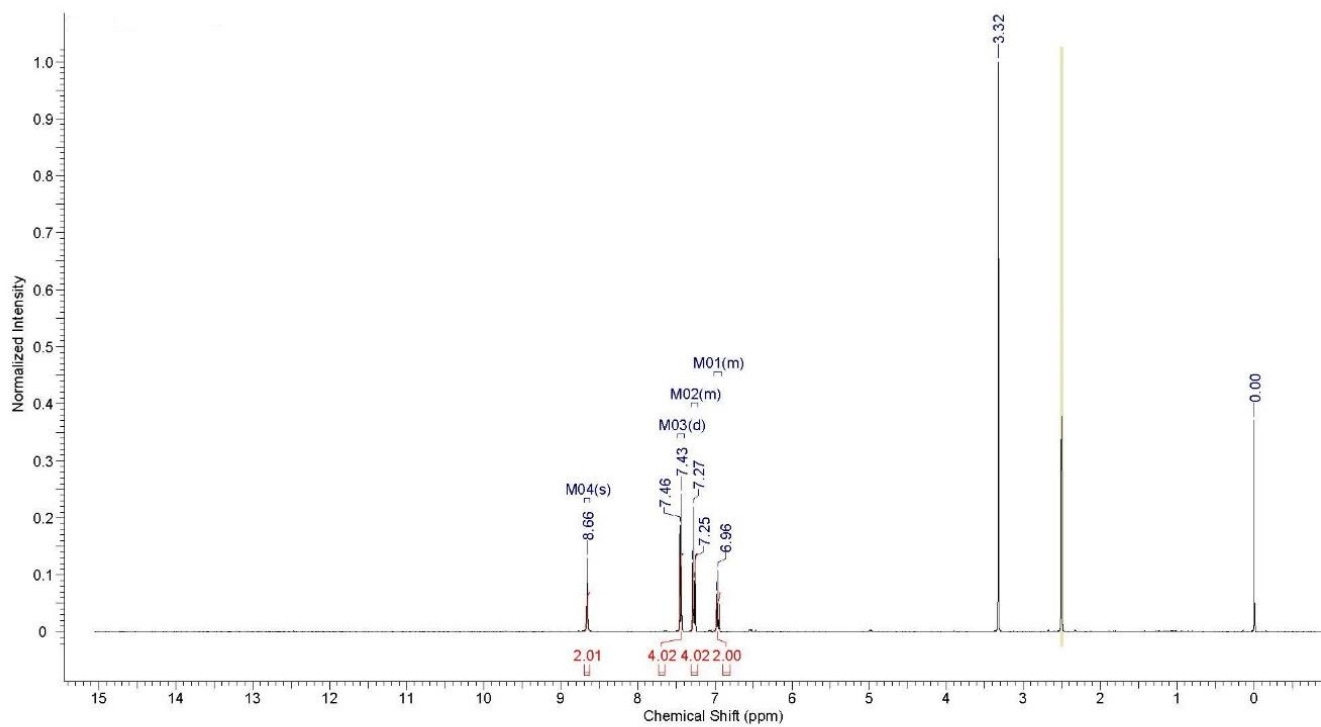
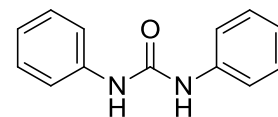


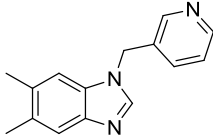
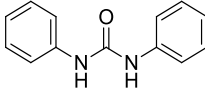
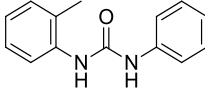
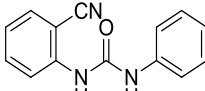
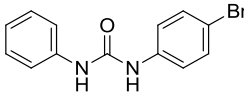
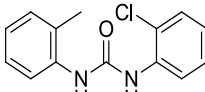
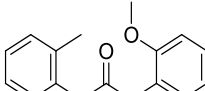
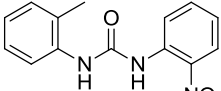
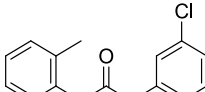
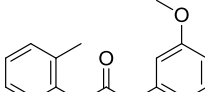
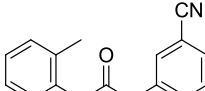
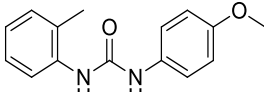
Figure A.20 <sup>1</sup>H NMR spectrum of diphenylurea(U1)

## Appendix B - Index of abbreviations

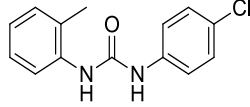
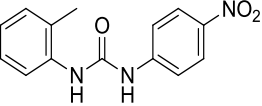
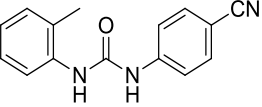
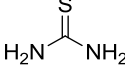
Abbreviation	Structure	Name
di(NH <sub>2</sub> )ox		(1Z,4Z)-N'1,N'4-dihydroxyterephthalamidamide
di(CH <sub>3</sub> )ox		(1E,1'E)-1-(4-((E)-1-(hydroxyimino)ethyl)phenyl)ethanone oxime
di(H)ox		(1E,1'E)-4-((E)-(hydroxyimino)methyl)benzaldehyde oxime
di(Cl)ox		(1Z,4Z)-N'1,N'4-dihydroxyterephthalamidoyl dichloride
di(CN)ox		(1Z,4Z)-N'1,N'4-dihydroxyterephthalamidoyl cyanide
Pz		pyrazine
Mpz		2,3,5,6-tetramethylpyrazine
Bp		4,4'-bipyridine
Bpe		1,2-di(pyridin-4-yl)ethane
bpe2		(E)-1,2-di(pyridin-4-yl)ethene
dpp		1,3-di(pyridin-4-yl)propane
bpo		[4,4'-bipyridine] 1,1'-dioxide
dbim		1,4-bis((1H-benzo[d]imidazol-1-yl)methyl)benzene

tbim		1,3,5-tris((1H-benzod[imidazol-1-yl)methyl)benzene
mdpy		1,4-bis((3,5-dimethyl-1H-pyrazol-1-yl)methyl)benzene
bdpy		1,4-bis((4-bromo-3,5-dimethyl-1H-pyrazol-1-yl)methyl)benzene
dpy		1,4-bis((1H-pyrazol-1-yl)methyl)benzene
4pp		4-phenylpyridine
3bp		phenyl(pyridin-3-yl)methanone
4bp		phenyl(pyridin-4-yl)methanone
dcp		3,5-dichloropyridine
4po		4-methylpyridine 1-oxide
3po		3-methylpyridine 1-oxide
35dpb		2,5-dibromopyridine
3HBA		3-hydroxybenzoic acid
4HBA		4-hydroxybenzoic acid
4ABA		(E)-4-((hydroxyimino)methyl)benzoic acid

4BaOx		(Z)-4-(cyano(hydroxyimino)methyl)benzoic acid
3BaOx		(Z)-3-(cyano(hydroxyimino)methyl)benzoic acid
4PhOx		(Z)-N,4-dihydroxybenzimidoyl cyanide
PzO		pyrazine 1-oxide
MpzO		2,3,5,6-tetramethylpyrazine 1-oxide
BPO		4,4'-bipyridine 1-oxide
4PI		4-((2-phenyl-1H-imidazol-1-yl)methyl)pyridine
3PI		3-((2-phenyl-1H-imidazol-1-yl)methyl)pyridine
1PB		1-methyl-2-(pyridin-4-yl)-1H-benzo[d]imidazole
4PB		1-(pyridin-4-ylmethyl)-1H-benzo[d]imidazole
3PB		1-(pyridin-3-ylmethyl)-1H-benzo[d]imidazole
4MPB		5,6-dimethyl-1-(pyridin-4-ylmethyl)-1H-benzo[d]imidazole

3MPB		5,6-dimethyl-1-(pyridin-3-ylmethyl)-1H-benzo[d]imidazole
U1		1,3-diphenylurea
U2		1-phenyl-3-(o-tolyl)urea
U3		1-(2-cyanophenyl)-3-phenylurea
U4		1-(4-bromophenyl)-3-phenylurea
U5		1-(2-chlorophenyl)-3-(o-tolyl)urea
U6		1-(2-methoxyphenyl)-3-(o-tolyl)urea
U7		1-(2-nitrophenyl)-3-(o-tolyl)urea
U8		1-(3-chlorophenyl)-3-(o-tolyl)urea
U9		1-(3-methoxyphenyl)-3-(o-tolyl)urea
U10		1-(3-cyanophenyl)-3-(o-tolyl)urea
U11		1-(4-methoxyphenyl)-3-(o-tolyl)urea



U12		1-(4-chlorophenyl)-3-(o-tolyl)urea
U13		1-(4-nitrophenyl)-3-(o-tolyl)urea
U14		1-(4-cyanophenyl)-3-(o-tolyl)urea
U15		Thiourea